TWO-STAGE SIMULATION-BASED OPTIMIZATION FOR OPTIMAL DEVELOPMENT OF WIND FARMS CONSIDERING WIND UNCERTAINTY

By

QING LI

A dissertation submitted to the

School of Graduate Studies

Rutgers, The State University of New Jersey

In partial fulfillment of the requirements

For the degree of

Doctor of Philosophy

Graduate Program in Industrial and Systems Engineering

Written under the direction of

David W. Coit

And approved by

_____

_____

_____

_____

_____

New Brunswick, New Jersey

May, 2020

ABSTRACT OF THE DISSERTATION

TWO-STAGE SIMULATION-BASED OPTIMIZATION FOR OPTIMAL DEVELOPMENT OF WIND FARMS CONSIDERING WIND UNCERTAINTY

By QING LI

Dissertation Director:

David W. Coit

As one of the most promising renewable energy sources, wind power provides clean and carbon free energy and becomes more economically viable with significant environmental benefits. To feed the rapidly expanding energy market and to provide alternatives for the consumption of traditional non-renewable energy sources such as fossil fuel, wind farms have been developed to meet the ever-expanding growth of energy consumption. In the meantime, wind farm development and turbine manufacturing technology still need to address the challenges of high installation and operation costs, production stability, electricity capacity and economic efficiency. To enable economic feasibility of large-scale wind energy generation, optimal development of wind farms appears to be crucial for viable wind energy systems. This research presents stochastic models and optimization methods for optimal development of wind farms in different applications.

In this research, wind uncertainty is quantified using probabilistic models for stochastic wind speeds and directions. The two-stage optimization framework is developed to sequentially determine the optimal number of turbines and their most-productive placement. In the first stage of optimization, possible turbine locations are predefined at a number of candidate locations. A binary variable is associated with each location to determine whether a turbine is installed there. The first stage of global search optimization finds the optimal number of turbines needed and their corresponding locations. In the second stage of optimization, the solution from the previous stage is relaxed into a continuous solution space. The local search algorithm is then applied to further improve the locations of turbines identified by the optimization solution from the previous stage. With the two-stage optimization framework, the optimization procedure can determine the optimal number of turbines and refine the turbine placement for the most-productive layout design.

To minimize the objective function - Cost per Expected Power Production (CEPP), five different applications of wind farm models have been studied, in terms of geometric shape of wind farm, site selection and energy sources collaborations. First, the common rectangular wind farm model is studied with pre-defined cells, where the center of each cell represents a candidate turbine location. Next, more-realistic arbitrary-shaped wind farms are considered with engineering constraints, which fits flexibly in various surface conditions, applied to both onshore and offshore wind farm cases. Additionally, a wind farm model in Energy Storage Integrated Wind Energy System (ESIWES) is designed within a micro-grid. With energy storage functioning as backup supply, the wind farm generates electricity in order to meet the demand of the micro-grid community, and at the

same time, maintain the minimal CEPP cost by leveraging storage of excess wind energy. The fifth application expands the renewable energy system to include biorefinery – the waste-to-energy recovery pipeline. With biorefinery, the Hybrid Wind, Biorefinery, Energy-storage based Renewable Energy System (HWBRES) is developed to generate more sustainable energy, and at the same time, tackle environmental risk problems caused by waste.

Last but not the least, an advanced scheduling and maintenance model is developed on top of the HWBRES system, in which the turbine operation scheduling and periodic inspection are both taken into consideration to save energy from excess production while maintaining the reliability of each turbine. Additionally, opportunistic maintenance is scheduled occasionally for the cluster of switched-off turbines, by implementing this model it ensures the reliable energy production with limited maintenance costs.

ACKNOWLEDGEMENT

They say ‘Knowledge is power’, but I say there is no knowledge that is more powerful than taking a great risk on yourself, exploring your potential and creating your own future. I wish I could say that I had this grand plan, some vision that carried me to this day, but I cannot. I am old enough to know sometimes life comes at you fast, unpredictable, and not always in pleasant ways. Reflecting back on what I have done, who I have become, I cannot be more certain that I am head to toe, sideways but always grateful to those who took a chance on me, who guide me through to the light at the end of tunnel.

First, I would like to express my deepest gratitude to my former advisor, Dr. Honggang Wang, for his inspiration, guidance and unconditional support. He has taught me not only the knowledge, but also how to be a good researcher and thinking broadly.

I would also like to give thanks to Prof. Gal Hochman, Prof. Mohsen Jafari, and Prof. Hoang Pham, for serving on my dissertation committee and providing valuable suggestions along the way. Additionally, my sincere gratitude to Prof. Elsayed A. Elsayed, who initiated my research, supported me through school years and continued to extend his support in my career.

Especially I am grateful to my dissertation director Prof. David Coit, who was the first faculty invited me to the campus tour years ago, and now under his supervision I conclude my chapter as Ph.D. student at Rutgers University. Among these years he provided invaluable lessons on researches, careers, and mentored me through many aspects of my life, the completion of this dissertation would not have been possible without his support.

Last but most definitely not the least, to my husband Zelin. Throughout my journey there have been ups and downs, you were the only constant in my life, encouraging and

supporting me unconditionally. For that, I am grateful. As B. Brown once said ‘when we make the choice to dare greatly, we sign up to get our asses kicked. We can choose courage, or we can choose comfort, but we can’t have both.’ As I chose courage, you fight alongside with me. Zell, this work is for you.

TABLE OF CONTENTS

LIST OF FIGURES

LIST OF TABLES

Chapter 1 INTRODUCTION

The worldwide demand for renewable energy is increasing rapidly due to the limited resources of non-renewable energy, i.e. fossil fuels, as well as the rising awareness in climate change. In 2015, it is estimated that 147 GW of renewable capacity were added globally and reached the total 439 GW at year's end. About 23.7% of the total consumption worldwide was from renewable power generation [1], comparing to 18.8% in 2013 [2]. Non-renewable energy sources such as fossil fuels, still play a significant role in the global energy supply. However, more and more public concern, including reduced deposits of fossil fuel, competitive price of alternative renewable sources and negative climate consequences etc., causes the continuous increasing replacement of fossil fuels with renewable energy. The limitation of oil sources brings the energy dependency, while the stable growth of renewable energy installations, such as wind, solar PV and biofuel, reduces a nation's energy dependency and mitigates environmental impact from burning fossil fuels.

Per UCSUSA in 'Benefits of Renewable Energy Use' [3], the significant amount of carbon-dioxide emissions per natural gas (0.6-2 CO_2E/kWh) and coal (1.4-3.6 CO_2E/kWh) still contributes as the major cause of global warming. Sustainable energy resources, such as wind power (0.02-0.04 CO_2E/kWh), solar PV (0.07-0.2 CO_2E/kWh), geothermal (0.1-0.2 CO_2E/kWh) and hydroelectric (0.1-0.5 CO_2E/kWh), on the other side, have low carbon footprint, which can improve public health and environmental quality by replacing carbon-intense energy sources. Therefore, alternative renewable energy sources have seized increasing public support and growing energy market.

1.1 Wind Energy Overview

Recently wind energy has been cost competitive compared to fossil fuels even without accounting for externalities [1]. The increasing deployment is also driven by wind energy's environmental and other benefits. Wind power provides clean and carbon free energy without carbon emissions and straining water supply. It is a domestic source of energy where the supply is inexhaustible, and wind farms can be built on land (onshore) or in ocean water (offshore). Even without government subsidies, wind power is the least-cost renewable energy technology for new power generating capacity in the U.S. With these benefits, today wind energy becomes one of the most promising renewable energy technologies to feed the rapidly growing energy market and to displace the consumption of traditional non-renewable energy sources.

As of 2014, the market volume for new wind projects was 40% greater than in 2013 [4]. In 2015, more than 63 GW wind power was added – about an 22% increase over the 2014 market – for a total of 433 GW global wide. Wind energy production is rapidly growing not only in the top three producer countries – China, U.S. and Germany, but also in those with large capacities such as India, Spain, Brazil, etc. Based on the 2016 report by Renewable Energy Policy Network [1], China led in both new installations and largest capacity of wind power, followed by U.S., Germany and India; these countries were named as the top countries for global wind energy addition and capacity in 2015, as shown in Table 1-1. New markets were expanded across Africa, Asia, the Middle East and South America. Guatemala, Jordan and Serbia developed their first large scale wind farms.

In Europe and U.S., wind is the leading source of new power generation. Particularly in Europe, including both onshore and offshore projects, wind represented over 44% of new power capacity in 2015. During the same year wind energy generation reached another

record year in annual installations. Among them, Germany accounted for half of European wind energy market. At the end of 2015, the leading countries for total wind power capacity per person were Denmark, Sweden, Germany, Ireland and Spain [1].

	TOTAL END-2014	ADDED 2015	TOTAL END-2015
		GW	
TOP COUNTRIES BY ADDITIONS			
China[1]	97.3/114.6	33/30.8	129.3/145.4
United States	65.4	8.6	74
Germany[2]	39.2	6	45
Brazil	6	2.8	8.7
India	22.5	2.6	25.1
Canada	9.7	1.5	11.2
Poland	3.8	1.3	5.1
France	9.3	1.1	10.4
United Kingdom	12.6	1	13.6
Turkey	3.7	1	4.7
TOP COUNTRIES BY TOTAL CAPACITY			
China[1]	97.3/114.6	33/30.8	129.3/145.4
United States	65.4	8.6	74
Germany[2]	39.2	6	45
India	22.5	2.6	25.1
Spain	23	0	23
United Kingdom	12.6	1	13.6
Canada	9.7	1.5	11.2
France	9.3	1.1	10.4
Italy	8.7	0.3	9
Brazil	6	2.8	8.7
World Total	**370**	**63**	**433**

Table 1-1 Wind power global capacity and additions, top 10 countries, 2015 [1]

In the United States, wind power, mainly onshore wind, is a $10 billion per year industry. It led global wide wind power generation (190.9 TWh [1]) by the end of 2015, with the potential to generate 20% of national electricity by 2030. In 2012, 42% of all new electricity generation capacity was from wind. About 80% of the wind power generation facilities were located in twelve states, including Texas, Iowa, California, and Oklahoma. Wind energy generation and consumption in Texas, Iowa, and South Dakota reached 25%

or more of their total energy consumption. By 2014, more than 46,000 utility-scale wind turbines were installed [5]. Per Renewable Energy Policy Network [1], during 2015, wind energy was the top energy source for new installation capacity, accounting for over 40% in total. More installations were added in the fourth quarter of 2015 alone than in the whole year of 2014. The cost competitiveness of wind energy attracted more public attention, making 2015 the first year with half of the known US purchase agreements being contributed by independent power producer. By the year end, an additional 9.4 GW of capacity was scheduled under construction.

1.2 Wind Farms Overview

Wind power generation facilities include onshore and offshore wind farms. The power is typically generated by large scale wind farms that are located either on mainland or close to shoreline, where they are able to connect and transmit to the power grid, and then to further distribute to consumers. While offshore wind development is still at an early stage in the U.S., onshore wind farms has matured and gained the majority share of renewable energy market. The cost competitiveness of wind power generation reflects mainly on onshore wind farms. In 2015 the global weighted average levelized cost of electricity (LCOE) of onshore wind power generation was about $0.06/kWh. Estimated based on its technology improvement and reduced installation costs, worldwide wind farms were expected to deliver electricity in between $0.04/kWh to $0.09/kWh without government subsides. Power purchase agreement (PPA) assessed cost of wind energy in both 2015 and 2016, which could be as low as $0.04/kWh for further delivery, competing with fossil fuels cost where lay between $0.045/kWh and $0.14/kWh [1].

Onshore wind farms are located in areas with constant flow of non-turbulent wind. In the U.S. they are mainly located in the vast plains or near ridgeline of mountains and most

of them are located in western U.S. The most commonly used wind turbines are three-bladed, horizontal axis machine operating at near-fixed rotational speed, with turbine sizes of 1.5 MW and 3 MW. Typical wind turbine starts generating electricity at 3-5 m/s, reaching maximum power at 15 m/s and cutting out at wind speed great than 25 m/s [6].

Similar to onshore wind development, offshore wind energy draws increasing attention due to its enormous potential in vast coast areas. Offshore wind is known to be intense, steady and abundant. Since offshore wind is stronger during the middle of the day and evening when energy is consumed most, offshore wind power can play a significant role for peak hour energy supply. Comparing to onshore wind, offshore wind power generation shows many advantages, such as higher wind speed, open coast areas without land use, less visual barriers and acoustic noise barriers for human life, etc.

Higher wind speed in coastline areas provides better power generation, which in turn offsets higher installation and operations & maintenance (O&M) costs. Offshore wind, with abundant location choice, allows turbine installations sufficiently far from a coastline to significantly eliminate its negative impact on human activities. On the other side, offshore wind power has its own challenges. The major ones are high capital costs, difficulty to maintain and repair, harsh environmental conditions. Because of higher investment costs in turbine foundation, cabling, towers and general installations, offshore wind energy generation is at least 1.5-2 times more expensive than onshore wind generation [7]. While some problems can be fixed relatively easily and cheaply onshore, offshore maintenance requires time consuming transportation methods which may potentially cause longer production interruptions. Such constraints on maintenance lead to lower productivity of offshore wind energy generation systems. Furthermore, the ocean

volatile weather conditions cause potential harsher environmental impact on offshore wind turbines, such as corrosion from sea water, higher wear-out rate due to wave and loading, lack of vessels for construction etc. One solution to address such technical risks is by using highly reliable components, this way it reduces the potential of damage at the expense of higher investment cost. Although there are different opinions on the trade-off between energy production versus higher capital, offshore wind development continues being a hot topic and attracting commercializing opportunities [8].

In Europe, offshore wind farms have been well developed and are steadily expanding. There have been more than 2,000 offshore wind turbines installed, providing thousands of Mega-watts of electricity each year. In 2015, world offshore energy capacity reached 12 GW, of which 3.4 GW offshore power was generated in Europe. In Denmark, 42% of electricity demand was satisfied by offshore wind farms. In Germany, more than 60% of electricity demand in four states was met by offshore wind farms. In Uruguay, offshore power supplied 15.5% of total national electricity [1].

Offshore wind projects in the U.S., however, are in the early stage. In 2014, the Department of Energy initiated three pilot offshore wind projects, including the on-going one in south New Jersey. The potential is promising and demonstrated. In Dec 2016, the first offshore wind farm began to run in Block Island, RI. Although the pioneer project has installed only five turbines, it is capable of powering about 17,000 homes. The areas of U.S. coast within a 50 nautical miles limit comprise a potential of 907 GW, which is close to the cumulative capacity in the country [7, 9]. In addition, there are the Great Lake and Gulf coast, with potential of gigawatt offshore power generation. As of 2017, about 30 wind projects totaling 24 GW of potential installed capacity were being planned.

1.3 Motivation of Research

As the wind energy becomes more economically viable with significant environmental benefits, advances in science and technology for wind turbine design and manufacturing continuously improve the power efficiency and reduce the costs. Modern wind turbines produce 10 times more electricity now than decades ago. Wind farm development, however, requires land and space to be preferably convenient for either transmission lines or consumers. The land is expensive, and the wind source is location dependent. To improve economic use of land, optimal wind farm layout for onshore installations is one of the most significant strategies. In regard to offshore wind farms, the layout design maintains critical for efficient energy production, consistent transmission and turbine protection.

Specifically, optimal development of wind farms, involving decisions on the number of turbines and their best placement, seeks to use the land more effectively and produce energy more efficiently. Previous research focuses on onshore wind farm layout design, mainly considering regular shaped farms. The most commonly used wind farm model is rectangular and divided into candidate cells, where the center of each cell represents the candidate turbine location. Such a model was originally developed by Mosetti [10] and Grady [11] on the basis of Jensen's analytical wake loss model with the objective to minimize cost per energy production. Once candidate locations are predefined, binary Genetic Algorithm is applied to find the optimal turbine installation layout.

In the past decades there have been extensive researches on optimizing regular-shaped wind farm layouts. In reality, due to the topology of mountains and the limitation of land space, wind farms are designated either on the ridgeline of mountains or surrounded by existing structures, such as forest, main road, reservoir, restriction zones, etc. Therefore, the wind farm site may not always be compatible with regular-shaped boundaries. To meet

site selection criterions, arbitrarily shaped wind farm can be taken into consideration and in need of further design.

Research on wind farm development has three outstanding challenges: (i) By the uncertain nature of wind and complex interaction between turbines, accurate evaluation of power generation of the farm becomes challenging and is subjected to various sources of noises; (ii) Determining the number of turbines in the wind farm is a major challenge, because the system performance (an energy production measure in the function of the number of turbines, turbine placement, and wind scenarios) is highly nonlinear and combinatorial. That being the case, in order to find the optimal development plan, variables of number of turbines and turbine placement need to be considered simultaneously under wind uncertainty; and (iii) A mixed integer stochastic programming (MISP) model needs to be developed to account for stochastic wind profiles, integer variables and continuous variables.

1.4 Research Contributions

In this research, a new optimization framework is developed to find the wind farm layout that optimizes the cost and production objectives. Such an optimization framework overcomes the computational difficulty that happened due to large number of decision variables and expensive function evaluations. With this framework, the optimization procedure can determine the optimal number of turbines and refine the turbine placement for most-productive layout design under complex wind uncertainty. As a general structure, this optimization method can be used for logistic, transportation, and facility planning problems under complex system uncertainty.

Second, with the proposed optimization framework, new heuristic algorithms are developed and implemented in the first stage, followed by a local search algorithm in the

second refining stage. It significantly simplifies the evolving steps by branching out using current existing information at each iteration, bypassing the computational challenge in the nature of solving combinatorial problems.

Third, wind uncertainty is considered by using probabilistic models for stochastic wind speeds and directions. Specifically, seasonal scenarios are taken into Monte Carlo simulation for wind data sampling. Both onshore and offshore wind farm models are based on real data captured in the country. Onshore wind data is collected from wind farms in Montezuma, Kansas. Offshore wind data is collected from a current wind project along the Atlantic shoreline in south New Jersey. By using real wind data, it reflects the real-time shift through date-time and seasons, which in turn is more practical to simulate the intermittent nature of wind power generation.

Finally, this study integrates important research aspects into one general project of wind farm development: from onshore to offshore wind farm models; from regular to arbitrary shaped wind farm designs; from uniform to complex terrain condition; from wind-grid-market energy components to wind-energy storage-biorefinery integrated systems in a micro-grid. All these topics are taken part and evaluated in the modeling and numerical studies.

Chapter 2 BACKGROUND AND LITERATURE REVIEWS

The wind farm layout design is often studied as combinatorial problems. There have been inspiring works in the area of wind farm development, which can be generally be categorized by wake loss models, wind farm models, wind uncertainty models, optimization models and algorithms, wind farm based renewable energy systems, renewable energy-based micro-grid applications, as well as scheduling and maintenance policies .

2.1 Wake Lose Models

To accurately evaluate wind energy generated from wind turbines, wake loss models have been widely applied to account for turbine interactions. For instance, a downwind turbine generates less power compared to its upwind turbines. The turbulence generated behind the rotor of a turbine is known as wake. Due to convection and counter effects, wind speeds captured by a downwind turbine in the wake region will be reduced, thus less energy will be generated from a downwind turbine. The wake effect decayed with distance can be quantified by wake loss models.

Generally speaking, wake loss models can be broadly classified into two categories: analytical wake loss models [10-27] and computational wake loss models [28-35]. Analytical wake loss models, known for their simplicity, characterize the speed in a wake by the use of analytical expressions. One of the most popular analytical models is developed by Jensen [36], which has been commonly adopted among literature. Jensen's wake loss model assumes that the momentum of wind is conserved in the wake and the vertex shedding is neglected. The wake expands linearly, and the speed of turbine in a wake region is modeled as a function of turbine distance. Because of its reliable prediction with

simplified turbulence measurements to quantify wind speed reduction at the downwind turbine, this is the most well-known wake loss model. Besides Jensen's model, there are other analytical wake loss models [12, 25, 27]. For instance, Ishihara's [25] considers turbulence's recovery rate. Ozturk's [12] develops a direction-based model, which considers linear reduction wake model in cross wind interference and quadratic reduction wake model in prevailing wind interference.

In the second category, most computational wake loss models apply Computational Fluid Dynamics (CFD) for the turbulence and wake effect. The common procedure is to average the Navier-Stokes equations to obtain the Reynolds-averaged Navier-Stokes (RANS) solver and the k-ε turbulence model. Crespo [30] conducts a comprehensive study in both analytical and computational wake loss models. Among several wake models, a parabolic model UPMWAKE is highlighted for estimating turbulence characteristics. The turbulence counter-effect is taken into account by imposing perturbation values of velocity, temperature, kinetic energy and dissipation at the turbine location [33]. Specifically, k-ε turbulence model is employed to simulate the turbulence transport terms in flow equations.

2.2 Wind Farm Models

The wind farm layout problem is often studied as combinatorial problems. Extensive research in wind farm layout design includes both onshore wind farms [10-14, 16-20, 22-24, 27] and offshore farms [37-50]. The difference between offshore wind farm models and onshore wind farm models mainly refers to the types of foundation during turbine installation, such as regular mono-piles, tripod, concrete gravity foundation and floating, etc. [6].

With respect to the wind farm topologies, there are two types of onshore wind farm models discussed in the recent literature: regular-shaped wind farm models in uniform terrain conditions [10, 11, 14, 16-24] and arbitrary-shaped wind farm models under complex terrain conditions [14, 27, 28, 34, 35, 48]. In 1994, Mosetti [10] first proposed a systematic position optimization scheme of wind farm layout with 10x10 candidate turbine locations. The objective is to minimize the total cost per energy production, which considers installation cost and overall energy production. Three scenarios of wind profiles are considered based on wind speed/direction variations. This work is further improved by Grady [11] in terms of programming accuracy and efficiency. Both Mosetti's and Grady's studies are based on discretizing fields with predefined square cells. This approach represents a classic turbine installation design, which has been adopted in literature [10-17, 20-24, 27]. Li's work [19] presents different discretization methods: instead of square cells the wind farm is discretized into equilateral triangular meshes. Kusiak [18] proposes circular-shaped wind farm model with the fixed turbine number and no pre-defined cell locations.

There are several other researches on the layout design for complex wind farms and heterogeneous turbines. Abbes [28] presents a real life wind development case in Tunisia. Song's work [34, 35] considers complex terrain scenarios with computational wake loss model by pre-determining turbine numbers. Gonzalez [27] uses similar models from Mosetti's to seek optimal development of a wind farm under complex terrain constraints such as main road, forbidden zones and load bearing capacity crossing farm. Frandersen's [26] wake loss model aims to maximize annual incomes. In the scheme of turbine-selection

related layout design to maximize power production, Chen [14] extends Mosetti's work by considering arrangement of turbines with three different hub heights.

For offshore wind energy, many studies use the similar wind farm model as the onshore's, however there are some other innovative models. Amaral et al. [42] develops a micro sitting model slightly different from the one introduced earlier where the center of each cell represents the candidate turbine location. Instead they further divide each cell into multiple sub-cells, this allows further improving turbine locations within the cells, and at the same time, maintain the advantages of the traditional method. Li et. al. [48] introduces a wind farm model in arbitrary shape with predefined 132 candidate turbine locations at an initial stage, and later relaxes the constraints so the turbines are able to move within the farm model for location selection. Rodrigues et al. [40] proposes an offshore wind farm model with floating turbines which allowed turbines to move after installation. In particular their research considers turbines with mobile anchoring position, promoting the movement in two directions.

2.3 Wind Uncertainty Models

Another thread of research in wind farm development is on wind uncertainty modeling. A valid wind uncertainty model is crucial for robust wind farm design. Due to the variation of wind direction, wake loss effects can change significantly. Typical approaches for wind modeling is to use probabilistic models for wind speeds and directions; specifically the Weibull distribution is widely used to model the wind speed variation [18, 22, 24, 27, 28]. For the Weibull probability distribution, the parameters of speed distribution may vary as a function of wind directions. In our study, historical data are fit into Weibull distributions to determine the distribution parameters. Daytime and seasonal factors are considered in different wind scenarios for more accurate wind prediction models.

2.4 Optimization Models and Algorithms

Exhaustive evaluations of all possible turbine placements in a wind field is not feasible for large-scale wind farm development problems. Mathematical optimization procedures using mixed integer programming (MIP) models can be employed to quickly search for optimal or practically good solutions in such problems. Methods developed can be classified by pre-defining either possible turbine locations [10, 11, 16, 17, 19-23], or the number of turbines [18, 24, 51]. For example, in Mosetti's [10] when the possible turbine locations are pre-defined (in the center of 10x10 discretized cells), the optimization process is applied to look through all possible layout solutions for the optimal number of turbines as well as their best placement. Once the number of turbines is determined, the optimization algorithm can be applied to further refine turbine locations and return with the best layout.

For placement optimization, evolution-based global search algorithms, such as Genetic Algorithm [10, 11, 14, 16, 19], Gaussian Particle Swarm [24], Mixed Discrete Particle Swarm [52], virus-based algorithm [17], bionic algorithm [34] are widely used to search for the optimal turbine layout. Wan [23] develops a two-stage Genetic Algorithm for wind farm development. In the first stage, it employs binary Genetic Algorithm to seek turbine locations for minimal cost per unit energy production. During the second stage, the positions of turbines are allowed to be adjusted within their cells to further improve the energy production. This method combines the global search with local refinement, but it lacks realistic constraints on turbine distance and the cell local refinement improves the solutions very little. Other optimization models include greedy algorithm [35], heuristic algorithm [12], etc.

2.5 Wind Farm Based Renewable Energy Systems

Due to the stochastic nature of wind, wind power generation is highly fluctuating and intermittent which affect the stability of energy generation and cause power supply disturbance. Small scale wind farms tend to have higher expected hourly variation than the larger ones [53]. To reduce such a negative impact, energy storage is commonly integrated to balance the wind energy output and provide peak-hour backup. Recently there are plentiful literature studying the status, technologies and implementation of current energy storages [53-66].

Energy storage systems for wind power generation can be broadly categorized by their characteristics and technologies, such as pumped hydro-storage, compressed air energy storage, battery and flow battery energy storage, hydrogen-based energy storage system, flywheel, superconducting magnetic energy storage, supercapacitor energy storage [53, 57, 58, 60-62]. Depending on the size of energy system, energy storage is selected in terms of efficiency, cost, capacity, charge/discharge rate, and life cycle. The application with energy storage offers voltage support while maintaining grid stabilization and system reliability, mitigation of transmission curtailment at the same time smoothing renewable energy generation.

There are studies of integrating energy storage into wind energy generation to maintain good power quality and uninterruptible power supply. For example, as reviewed by Beaudin, et.al. [53] in grid scale wind power production, Iowa Stored Energy Park is expected to use wind energy and off peak electricity to store compressed air; Utility Xcel Energy in Cabin Creek, CO, upgraded a pumped hydroelectric storage to mitigate wind variability; upper Wisconsin has the largest installation of superconduction magnetic energy storage; last but not the least, wind-hydrogen hybrid energy system has been

implemented among European countries like Denmark, Norway and southern California in U.S.. For wind farm scale energy storage, the largest lead acid storage 10 MW/ 40 MWh was installed in Chino, CA; Lthium-ion battery was constructed in Kansas with capacity of 60 MWh; Tomanae wind farm in Japan integrated Vanadium redox battery with capacity of 4 MW / 6 MWh.

There are other studies proposing new energy storage integrated renewable energy systems. Aissou et.al. [55] presents hybrid wind/solar PV power system with battery storage and design of system components has been modeled. Fazeli et. al. [59] and Levron et.al. [63] propose integration of wind farm with energy storage to supply a local micro-grid. A two-level energy storage system is developed by Xi, et. al. [66]. To improve the overall performance, super capacitors are designed to meet the short term fast changing power, while Li-ion battery and Vanadium Redox are designed to meet large-scale long-term energy capacity requirement.

2.6 Renewable Energy Based Micro-Grid Applications

Fifteen years ago, micro-grid was introduced as an electric reliability technology solution, meaning to be a system that connects with generators and carries loads, converting energy from power sources and carries out correlative control. By definition, a micro-grid is a localized energy group that can perform while connected to the traditional power grid, or isolated and function as an electrical island. It operates as an active distribution network which includes distribution generators and loads. In recent years, renewable energy powered micro-grids have increasing public attention. Renewable energies such as wind power and solar PV have been commercially integrated into micro-grid systems, operating in both grid connection and standalone model. On top of that, energy storage is a good

complement to stabilize the electricity generation and provide backup to satisfy the peak demands.

There have been inspiring works in the area of micro-grid with sustainable energy systems [59, 63, 67-72]. Borhanazad et.al. [71] studies a hybrid wind/PV energy system with battery storage and diesel generator in micro-grid, and use multi-objective particle swarm optimization to find its best configuration and component sizes. Niinisto [72] simulates a micro-grid with wind, solar and gas generators and present an energy management algorithm to forecast process errors and dispatch allocation decisions. Zhang et.al. [69] presents research on hybrid wind/solar/energy storage based micro-grid technology. In this literature, renewable energy system is connected to the power grid as a supplement. The scale of the energy storage system has been configured to suppress power fluctuations, and at the same time, allocation of hybrid energy system and traditional power grid has been optimized.

2.6.1 Renewable Energy Community in Micro-grid

The Renewable Energy Community concept promoted by National Renewable Energy Laboratory (NREL) advocates innovation; meantime it changes the way we design new communities that could significantly decrease the energy use and associated emissions and climate change impacts. The renewable energy community is an innovative community in which integrated renewable energy technologies play the primary role in meeting the energy supply and demand needs of its residents, with the possibility of providing excess energy back to the grid or other communities[73]. This community is designed to have near-zero or zero-energy homes, integrated transportation modes with advanced vehicles, local renewable energy generation, and incorporate sustainable living practices. Figure 2-1 shows an example of ‘zero-energy homes’ community built in Premier Garden,

Sacramento, CA. To be considered as a renewable energy community, it needs to integrate sustainable design approach and advanced energy efficient transportation into the micro-grid or solar/zero energy buildings [73].

Figure 2-1 Zero-energy homes community, premier garden, sacramento, CA

By combining multiple distributed energy resources, micro-grids are usually intended for local production of power with islanding capabilities and capacity to sell back to macro-grids. Cost and benefit for such a system are tightly coupled with the operation of its own resources. A typical micro-grid portfolio of energy resources includes Photo-Voltaic (PV) panels, wind turbines, gas-fired generation, storage and purchase from the grid. A proper mix of power generation resources and timely investment in these resources is an important design and major operational planning decision for micro-grid development. These decisions can significantly impact micro-grids short-term and long-term objectives, such as savings from energy costs, reducing risks for grid blackouts, and the use of renewables in a generation portfolio. Therefore, it is very likely that micro-grid investors are motivated by energy and cost savings that can be realized from local energy resources, and by security and reliability that micro-grids can offer, especially at times of peak loads and rare events

due to unexpected disasters. From appropriately sizing the micro-grid and minimizing the risks of dependency on the grid, the micro-grid owners and investors will be able to maximize their savings while ensuring higher levels of energy security and reliability.

2.7 Advanced Scheduling and Maintenance Policies

Over the years, different maintenance policies and scheduling models have been researched in both onshore and offshore wind farms. According to literature by Song et al. [74], the most commonly used policies include preventive maintenance, corrective maintenance, continuous monitoring and condition-based maintenance.

Specifically, among all the studies, Jiang et al. designs two-stage multi-objective model to solve for the collaborative scheduling of wind farm and electric vehicle battery switch station (BSS), considering demand curtailment of BSS, wind curtailment of wind farm and generation schedule tracking [75]. Zhang et al. presents an optimization model to schedule power generation at a wind farm using particle swarm algorithm with small world network structure [76]. Song et al. conducts a condition-based maintenance meanwhile considered opportunistic maintenance based on geographical clusters of wind turbines [74]. Tian et al. develops a condition-based maintenance optimization model for wind farms by defining two failure probability thresholds at wind turbine level under continuous monitoring [77]. Sinha designs a condition-based prognostic maintenance plan based on failure analysis to control cost of power and make maintenance more efficient [78].

Kovacs introduces a system that performs the detailed scheduling of maintenance operations at a set of wind farms maintenance by a common crew, which constitutes an integrated framework for condition monitoring, diagnosis and maintenance of wind turbines [79]. Lei conducts a simulation-based real options analysis model to determine the optimal maintenance schedules, which are predicted based on remaining useful life prior

to failure for a wind farm maintained by power purchase agreement, at the same time, considering the operational state of turbines, the energy delivered as well as delivery target, prices and penalty [80]. Seyr et al reviews literatures in the scheduling of operations and maintenance in offshore wind farm [81]. Besnard develops an opportunistic maintenance optimization model for an offshore wind power system [82]. Asensio et al. presents a novel maintenance management method for offshore wind farm based on condition monitoring systems and the economic study of its life cycle cost [83]. Nilsson performs a life cycle cost analysis with strategies using condition monitoring systems to improve maintenance planning, the case studies include a single onshore wind turbine and an offshore wind farm [84].

Chapter 3 PROBLEM FORMULATION

3.1 Modeling Dynamic Interactions Between Turbines

Wind energy captured by a turbine in the farm varies by locations and surrounding turbines. To model such stochastic interaction between turbines, a wake loss model is needed to estimate the wind speed reduction. In this work, Jensen's model is used to quantify the wake effects among turbines. We consider following assumptions: (1) the vertex vortices effect is neglected in the near field where wind speed right behind the rotor is reduced to one third of original speed; (2) The wake radius expands linearly behind the turbine; and (3) the wake deficit is obtained by assuming linearized momentum conservation. In Jensen's wake loss model, the speed at a turbine is mainly affected by wake interactions with upwind turbines. Figure 3-1 shows the wake shadow behind an upwind turbine in the wind direction.

The wake region of an upwind turbine can be simply defined by a cone centered at its rotor centroid along the wind direction d at an angle γ=arctan(κ), where κ is the speed entrainment constant. If a downwind turbine j is inside the wake cone of an upwind turbine i, the speed reduces from u_0 to u, where u_0 is the upwind speed at i; otherwise j has the same speed u_0 as i if j is not in the wake of i.

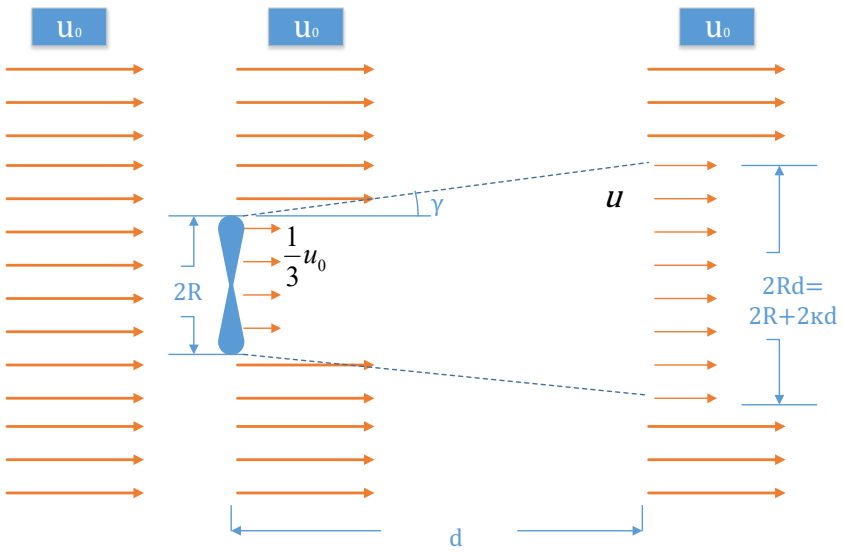

Figure 3-1 Jensen's wake loss model.

Considering the wake effect from multiple upwind turbines, a downwind turbine can have wake loss caused by multiple upwind turbines. For example, as shown in Figure 3-2, when the wind blows from west to east, both turbines T1 and T2 are upwind without any wake effect between each other; turbine T5 has the wake interaction solely with T2; and T4 is located in the combined wake loss region of T1, T2 and T3. On the other side, T3 is outside of both wake cones of its upwind turbine T1 and T2; therefore, there is no wake loss of wind power for T3, given this wind direction.

Wind power generation at a time instance for a turbine is often modeled by equation (12) with the wind speed u_i at the turbine i. Accurate evaluation of wind power generated from a turbine also needs to offset the power from wake loss caused by upwind turbines. As the wind direction and speed are highly dynamic, the wake loss zones in the farm changes in time.

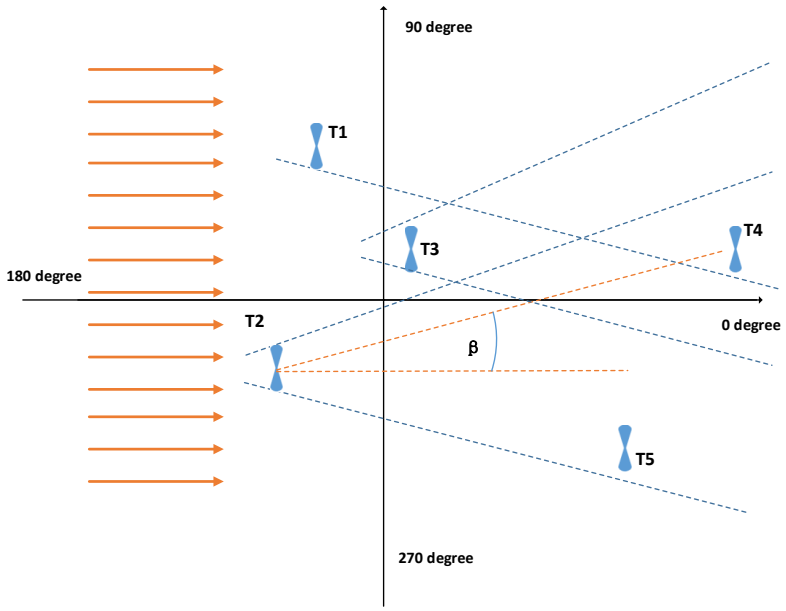

Figure 3-2 Turbines under the wake of multiple turbines (top view).

Considering the wake loss between a pair of identical turbines i and j, the Jensen's model quantifies the reduction of wind speed at j. As indicated with equation (1), the wind speed u at the downwind turbine j can be calculated by equation (2).

$$Def = 1 - \frac{u}{u_0} = \frac{2\alpha}{\left(1 + \frac{\kappa d}{R}\right)^2} \tag{1}$$

$$u = u_0\left[1 - Def\right] = u_0\left[1 - \frac{2\alpha}{\left(1 + \frac{\kappa d}{R}\right)^2}\right] \tag{2}$$

Where u_0 is the wind speed at turbine i, u is the reduced wind speed at turbine j, d is the distance between turbines i and j in the wind direction, and R is the radius of turbine rotor. The entrainment constant κ, which indicates how quickly the wake decays in distance, can be quantified with a simple model (3):

$$\kappa = \frac{0.5}{\ln\left(\frac{Z}{Z_0}\right)} \tag{3}$$

Where Z is the hub height of wind turbine, and Z_0 is the surface roughness of the terrain. In this study, identical wind turbines and a flat farmland spans with homogeneous obstructions are considered, therefore Z_0 and Z are assumed to be constant throughout the field.

In equation (1), α is the axial induction factor around a turbine, specifying the reduction rate of wind speed when the wind passes through the upwind turbine. The factor α can be calculated using the thrust coefficient C_T:

$$\alpha = \frac{1}{2}\left(1 - \sqrt{1 - C_T}\right) \tag{4}$$

Where C_T is a characteristic parameter of the turbine. Let R_d be the radius of wake cone, R_d can be calculated by equation (5).

$$R_d = R\sqrt{\frac{1-\alpha}{1-2\alpha}} \tag{5}$$

By equations (3) and (4), the reduced wind speed u in the wake zone (equation (2)) is a function of the distance d between turbines i and j. When a turbine j locates within multiple turbines' wake regions, due to the multiple wake loss effects, the total energy loss for j can be computed by equation (6) based on the kinetic energy balance. After a simple transformation by equation (1) and (6), the wind speed for turbine j can be computed by (7).

$$Vel\_def_j = \sqrt{\sum_{i=1, i\neq j}^{N_j} Vel\_def_{i,j}^2} \tag{6}$$

$$u_j = u_0 \left[1 - \sqrt{\sum_{i=1}^{N_j} \left(1 - \frac{u_{ij}}{u_i} \right)^2} \right] \quad (7)$$

In equation (7), N_j is the total number of upwind turbines that generate wake effect $Vel\_def_{i,j}$ at turbine j. Note that N_j may vary continuously as the wind direction and speed change through the time and at different locations in the farm. Here u_{ij} represents the reduced speed at turbine j affected by upwind turbine i.

3.2 Optimal Development of Wind Farm

The objective of wind farm development projects considers minimizing the Cost per Expected Power Production (CEPP). Given a layout X= [X_1, X_2, X_3, …, X_i,…,X_N], it can be formulated as follows.

$$\text{argmin}_{(N,X)} \ \text{CEPP} = \frac{\text{Annual Total Cost}}{\text{Expected Power Production}}$$

Subject to: $u_0 \geq u_i$ (8)

$$\left\| X_i - X_j \right\| \geq 200, \forall\, i \neq j \in \{1,2 \ldots N\}$$

The total development costs and expected annual energy production are evaluated and analyzed. Distance constraints for turbine layout design are included in the proposed turbine placement optimization models.

3.3 Two-stage Optimization Framework

In order to find both the optimal number of turbines and their most productive locations, a two-stage optimization framework is proposed. In the first stage of optimization, the wind farm field is discretized to a number of candidate locations for turbines placement. A binary global search optimization model is used to find the optimal number of turbines and their locations. A solution represents a layout design for the wind farm development.

In the second stage, a continuous optimization model is considered. That is, the turbines can be located anywhere in the field. In this stage, the solution returned from the first stage is used and the objective value is further improved by finding better locations for these turbines. The optimization model continuously searches the entire field until a feasible layout solution that specifies the most productive turbine locations is found.

3.3.1 Genetic Algorithm (GA) Based Two-stage Optimization Algorithm

Genetic algorithm (GA), a stochastic global search technique, has been widely applied to wind farm layout optimization [10, 11, 14, 16, 19]. It is general, evolutionary and does not require gradient estimation of the objective function. Evolving through iterations, GA, however, is often slow to converge and in some cases, terminating with premature convergence.

To design an efficient optimization algorithm, we propose a two-stage optimization framework for the optimal wind farm layout. Initially the wind farm field is discretized to a number of candidate locations where turbines are considered to install. In the first stage, the GA-based binary global search optimization model is developed to find the optimal number of turbines and their locations. As shown in Figure 3-3, the optimization in first stage searches solutions $\vec{K}$=[K_1, K_2, K_3, …, K_i,…,K_M] where $K_i \in \{0,1\}$ and M is the total number of candidate locations $K \in \{0,1\}^M$. $K_i = 1$ indicates a turbine being installed at location i and $K_i = 0$ otherwise. Thus, GA returns a solution $\vec{K}^*$ specifing a layout design for the wind farm. $N = \sum_{i=1}^{M} K_i$ is the optimized number of turbines.

In the first stage, we need to determine the parameters in GA, including the population size, number of iterations, crossover and mutation rates. The coding, reproducing and new population sampling in the search space determine the evolution of solutions in the process

of GA. The string of binary-coded decision variables identifies the possible layout of wind farm, where '1' represents turbine's placement in the candidate location while '0' represents no turbine installed. Individual solutions are evaluated in terms of objective values. The best solutions in the population are selected after ranking, as shown in Figure 3-3, then crossover and reproducing procedures are applied to generate new populations of solutions. Mutation, randomly switching selected variables in the string, is the next step to prevent the process from falling into local optima. Both crossover and mutation solutions are selected randomly, each variable has equal probability of being selected and is able to generate new sets of individuals (solutions). Objective values are evaluated in each iteration until optimal condition or terminating criteria is satisfied. The best set of solutions in the last population will be returned when GA terminates.

The second stage optimization takes the initial solution $\overrightarrow{X_0}$, which is the corresponding coordinates for turbines determined by $\vec{K}^*$. As mentioned, the continuous searching of decision variables (x_i,y_i) will be applied by a local search optimization method to locate an improved layout solution $\vec{X}^*$ that specifies the most productive locations for *N* turbines in the field. In this work, a Positive Basis Pattern Search algorithm is employed to find $\vec{X}^*$ - the optimal wind farm layout.

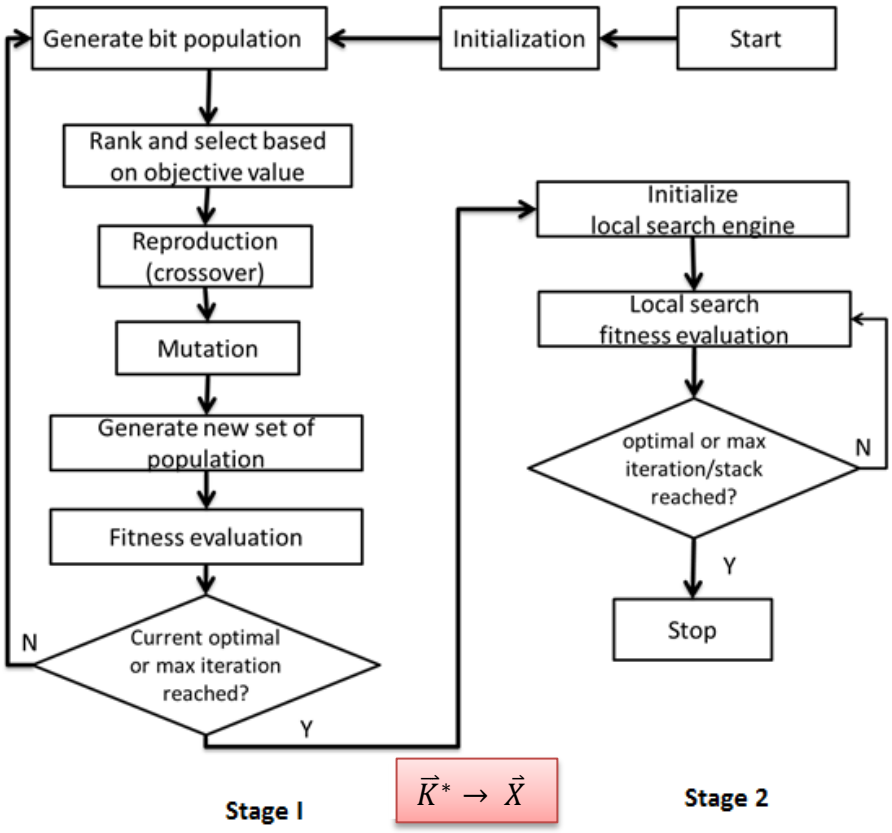

Figure 3-3 Two-stage optimization model.

3.3.2 Heuristic Algorithm for Two-stage Optimization

A heuristic model aims to produce solutions in a reasonable time frame without rigorous convergence guarantee. It sorts outcomes at each iteration based on current available information and then decides the direction of next step. Therefore, the move is predictable, and an exact solution may be reached during reevaluation.

Heuristic optimization algorithms presented in this study improves the objective values iteratively by first examining the overall power production, as shown in Figure 3-4. In each step, the value of wind power production per turbine is evaluated, and the one that generates the least power is removed after comparison. This way the layout scheme is updated by each iteration. According to wake loss model, the wake interaction between turbines is changed by the time turbine layout pattern shifts, therefore the wind speed captured by

each turbine may change too. To take such variation into account, objective values CEPP is updated by each layout scheme. At the end of evaluation, there are M objective values corresponding to each iteration, the one with the best fitness value is considered as the current optimal solution $\vec{K}^*$; this solution provides the optimal number of turbines and best layout scheme for next stage.

Same as the GA-based two-stage optimization model, during the second stage, the previous solution $\vec{K}^*$ is converted into coordinates-based solution, such that it continuously improves in the space until the most productive locations $\vec{X}^*$ is located.

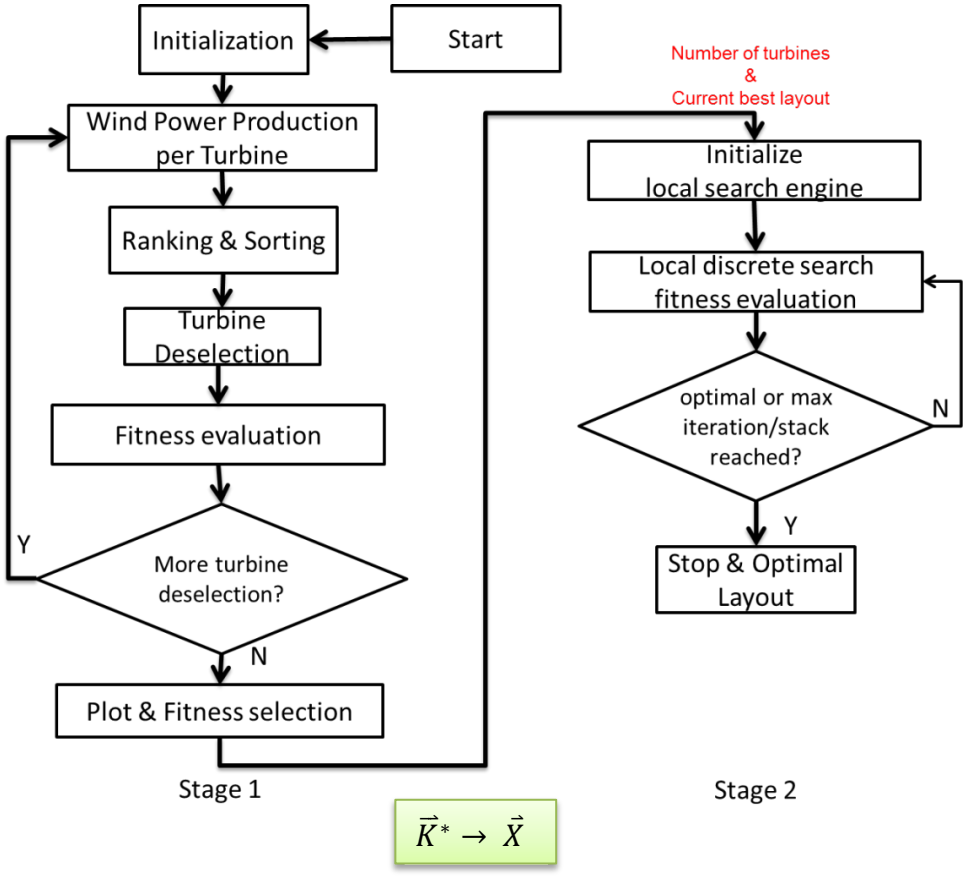

Figure 3-4 Heuristic-based two-stage optimization model

Chapter 4 PRELIMINARY RESEARCH RESULTS

To evaluate the performance of proposed wind farm development optimization model, five different applications have been studied, in terms of geometric shape of wind farm, site selection and energy system configurations with storage or other renewable sources such as bio-generator.

First, the most commonly used rectangular wind farm is studied with pre-defined cells, where the center of each cell represents the candidate turbine location. Second, the arbitrarily shaped wind farm is applied to both onshore and offshore wind farm models, which fits flexibly in various surface conditions. Then a wind farm model in Energy Storage Integrated Wind Energy System (ESIWES) is designed within micro-grid. With energy storage functioning as backup supply, the wind farm generates electricity in order to meet the demand of the micro-grid community, and at the same time, maintain the minimal CEPP cost by leveraging storage of excess wind energy. Stepping up from ESIWES, the last application expands the renewable energy system and includes biorefinery – the waste-to-energy recovery pipeline. By implementing bio-system, it generates more sustainable energy, and at the same time, tackle environmental risk problems caused by waste.

In all cases, the two-stage optimization method is applied to find the optimal layout of turbines, meanwhile considering the wind uncertainty in the design solution.

4.1 Optimal Development of Regular-shaped Onshore Wind Farm

4.1.1 Square-shaped Wind Farm Field

The wind farm model considered in this study is based on the case study used in [10]. In the first stage, the wind farm of a 2x2 km^2 squared terrain is discretized into 10x10 equal area squared cells. The center of each cell is assumed to be a candidate location of each

turbine, in total there are 100 possible turbine locations (Figure 4-1). In the published study, the wind direction is fixed from west toward east as 0 degree, counter-closewise increasing to cover the entire plane. Figure 4-1 shows the discretized field in wind direction of 0 degree. Turbines are assumed identical, therefore the same power curve function is applied to all turbines.

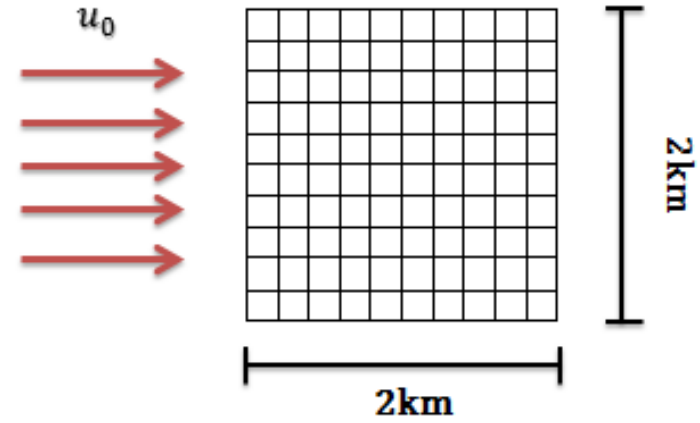

Figure 4-1 Discretized wind farm (Mosetti's [10])

4.1.2 Modeling Wind Uncertainty

Wind resources are modeled based on a wind farm in Montezuma, Kansas. Historical wind speed and direction data is collected. The data from year 2007 is used to fit the wind probabilistic models. With statistical analysis, the wind directions can be estimated with lognormal distribution with mean 5.1677 and standard deviation 0.3247. As shown in the wind rosemap in Figure 4-2, historical data indicates that the wind blows mostly in the direction from 45 degree to 320 degree, with higher probabilities in the range of (128, 200) degree.

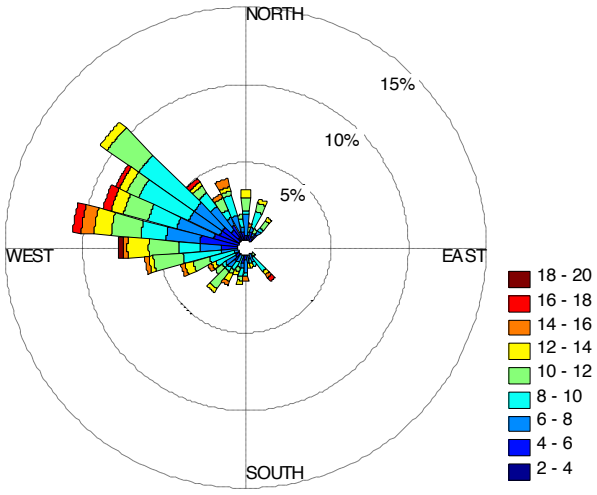

$$f_\theta(\theta) = \text{lognormal}(5.1677, 0.3247)$$

Figure 4-2 Rosemap for stochastic wind modeling

Based on wind speed data, which was retrieved in 10 minutes interval, the wind speed changes significantly in different seasons and times of the day. To account for such variations, wind models were built in four scenarios: warm season daytime, warm season nighttime, cold season daytime, and cold season nighttime. The warm season represents the dates from April 1st to Sept 30th; the cold season represents the dates before April 1st and after Sept 30th. The daytime is from 6 am to 5:50 pm and the rest of the day is considered as nighttime. The wind rosemap in Figure 4-2 shows the speed is mostly in the range of 6 m/s-12 m/s. The daily-averaged wind speed follows a Weibull distribution with fitted shape parameters and scale parameters, as shown in Table 4-1.

	Cold season (01/01-03/31, 10/01-12/31)		Warm season (04/01-09/30)	
	Shape Parameter	Scale Parameter	Shape Parameter	Scale Parameter
Daytime (06:00-17:50)	3.461	10.8764	2.9638	9.7399
Nighttime (00:00-05:50, 18:00-23:50)	3.2264	10.0686	3.069	10.4743

Table 4-1 Weibull models for stochastic wind speed in four scenarios

4.1.3 Optimal Development of Wind Farms

The objectives of wind farm development projects are to minimize the Cost per Expected Power Production (CEPP). Turbine installation costs and expected annual energy productions are considered in our economic analysis. Geographical and engineering constraints on layout design are considered in the proposed optimization models.

4.1.3.1 Installation Costs of Wind Turbines

Turbine installation cost, including the capital investment of equipment and labor costs, is considered as the major cost of wind farm development. A review by National Renewable Energy Laboratory (NREL) shows that 68% of the capital cost of onshore wind project is associated with the turbine installation [85]. In this research, we focus on minimizing the overall investment cost of wind turbines. The average cost per turbine can be reduced by additional installations in the farm. As discussed in Mosetti's and Grady's work [10, 11], the total cost of wind farm project (K$) can be estimated with the total number of turbines installed in the designated wind farm:

$$C(N) = N\left(\frac{2}{3} + \frac{1}{3}e^{-0.00174N^2}\right) \tag{9}$$

Where N is the number of turbines. From equation (9), if N is large enough, the average cost of each turbine can be reduced by about 33%.

4.1.3.2 Expected Annual Energy Production

The potential energy P_{wind} in the wind of speed U is modeled by equation (10). Considering the energy loss in power generation, a turbine can produce $P_{turbine}$, the proportion of the total wind energy with an efficiency coefficient C_p, as described by equation (11).

$$P_{wind} = \frac{1}{2}\rho A U^3 \tag{10}$$

$$P_{turbine} = \frac{1}{2}C_p \rho A U^3 \tag{11}$$

Where ρ is the air density, A is the rotor swept area, U is the spontaneous wind speed. Power coefficient C_p varies by aerodynamic and mechanical losses. According to the Betz's law, the maximum energy captured by a turbine can be no more than 59.3% of the kinetic energy in wind; that is $C_p \leq 0.593$. Similar to Grady's [11], a simple power curve function is applied as the function of wind speed u_i in a given direction θ captured by turbines i, which yields the following expression for power generation:

$$P_{turbine\,i}(u_i) = 0.3u_i^3 \tag{12}$$

In general, the power generated from a turbine is not always related to wind speed u_i by (12), particularly for borderline u_i (considerably low or high). As commonly accepted, the equation (12) is only applied to a certain range of wind speed $[u_{in}, u_{out}]$ for turbine. The minimum effective speed u_{in} is called the cut-in speed for a turbine to start generation power, while the maximum effective speed u_{out} is called the cut-out speed. In this study $u_{in} = 3\ m/s$, $u_{out} = 20\ m/s$. For any speed u in between u_{in} and u_{out}, a turbine generates energy estimated by the power curve function (12). If speed u is greater than u_{out}, the turbine will terminate operation to avoid damage. The power generation from a turbine i can be calculated as:

$$P_i(u_i) = \begin{cases} 0.3u_i^3 & 3 \leq u_i \leq 20 \\ 0 & \text{Otherwise} \end{cases} \tag{13}$$

4.1.3.3 Objective Model

Considering stochastic wind speed u_0 and direction θ_0, both can be modeled with probabilistic function $f_U(u_0)$ and $f_\Theta(\theta_0)$ respectively. The expected total wind power produced from a wind farm with *N* turbines can be computed:

$$E_{\theta_0,u_o}(u_0,\theta_0) = \sum_{i=1}^{N} \int_0^{360} \int_{u_{in}}^{u_{out}} P_i(u_i;u_0,\theta_0) f_U(u_0) f_\Theta(\theta_0) du_0\, d\theta_0 \tag{14}$$

Again u_0 is the free stream wind speed before it encounters turbines. u_i is the wind speed captured by turbine i in account of wake loss.

Given a layout $\vec{X}$=[X_1, X_2, X_3, …, X_i,…,X_N], $u_i = u_0$ if turbine i is located at a place without any upwind turbines under wind direction θ_0; otherwise, $u_i < u_0$ can be quantified by considering the wake loss from related upwind turbines:

$$u_i(X;u_0,\theta_0 \mid T(s),s) = u_0\left(1-\sqrt{\sum_{j=1}^{N_i(X;u_0,\theta_0|T(s),s)}\left(\frac{2\alpha}{\left(1+\frac{\kappa d_{ij}(X;u_0,\theta_0 \mid T(s),s)}{R}\right)^2}\right)^2}\right) \tag{15}$$

The objective function of optimization is to minimize the annual turbine installation cost per expected power production (CEPP). It can be formulated as follows.

$$\begin{aligned} \operatorname{argmin}_{(N,\vec{X})}\ \mathrm{CEPP} &= \frac{\text{Annual Installation Cost}}{\text{Expected Power Production}} \\ &= \frac{C(N)}{E_{\theta_0,u_o}} = \frac{N\left(\frac{2}{3}+\frac{1}{3}e^{-0.00174N^2}\right)}{\sum_{i=1}^{N}\int_0^{360}\int_{u_{in}}^{u_{out}} P_i(u_i;u_0,\theta_0) f_U(u_0) f_\Theta(\theta_0) du_0\, d\theta_0} \end{aligned} \tag{16}$$

Subject to: $u_0 \geq u_i$

$$\min\left\|X_i - X_j\right\| \geq 200, i \neq j \in \{1,2 \ldots N\}$$

There is no closed form solution to solve for problem with such complexity. In order to approximate numerical solutions, Monte Carlo method can be utilized to sample wind data, from there one will be able to estimate CEPP based on sample mean.

Capturing the uncertainty of wind speed and direction, due to their significant variations, four scenarios are considered: warm season daytime, warm season nighttime, cold season daytime and cold season nighttime. Specifically, one year of wind uncertainty data is studied. To approximate model (16), 10 data points are randomly sampled from each scenario, resulting in 40 wind data points for (u_0, θ_0). During optimization process, the sampled wind speed and direction data is used in function evaluation. In this case, comprehending equations (1)(2)(6)(7), CEPP in model (16) can be extended as:

$$\widehat{\mathrm{CEPP}} = \frac{\mathrm{N}(\frac{2}{3} + \frac{1}{3}\mathrm{e}^{-0.00174\mathrm{N}^2})}{\sum_{\mathrm{i}=1}^{\mathrm{N}}(0.25\sum_{\mathrm{s}=1}^{4}(0.1\sum_{\mathrm{T(s)}=1}^{10}0.3(\mathrm{u_i}(\vec{\mathrm{X}};\mathrm{u_0},\theta_0|\mathrm{T(s)},\mathrm{s}))^3))} \tag{17}$$

$$= \frac{\mathrm{N}(\frac{2}{3} + \frac{1}{3}\mathrm{e}^{-0.00174\mathrm{N}^2})}{0.0075\sum_{\mathrm{i}=1}^{\mathrm{N}}\sum_{\mathrm{s}=1}^{4}\sum_{\mathrm{T(s)}=1}^{10}\mathrm{u_i}(\vec{\mathrm{X}};\mathrm{u_0},\theta_0|\mathrm{T(s)},\mathrm{s})^3}$$

The wind speed and direction are determined by season-time index *T(s)*: $1 \leq T(s) \leq 10$ with assigned season-time scenario s ($s \in \{1, 2, 3, 4\}$). d_{ij} is the distance between turbine i and its upwind turbine j. N_i is total number of upwind turbines for turbine i, based on live wind direction.

4.1.4 Computational Results

To demonstrate the proposed two-stage optimization framework, the numerical studies with three cases of wind profiles are evaluated:

- constant wind speed in fixed wind direction: speed= $12m/s$, direction=0;
- constant wind speed in random wind directions: speed= $12m/s$, direction= $f_\Theta(\theta_0)$;

- stochastic wind speeds in random wind directions: speed $= f_U(u_0)$, direction=$f_\Theta(\theta_0)$.

Turbines are considered with following parameters: hub height Z is 60 m, thrust coefficient C_T is 0.88, and surface roughness length Z_0 is 0.3 m. The rectangular wind field has 2x2 km^2 dimensions. The rotor radius of turbines R is 20 m. For the first stage optimization, each cell width is 200 m, which equals to 10R. There is a minimum distance of 200m in between rotor center of adjacent turbines, this constraint further applied to both optimization stages to avoid speed plummet. Simple calculation by equation (3) (4) leads to the values of entrainment constant κ and the axial induction factor α: κ=0.0944, α=0.3268.

4.1.4.1 Constant Wind Speed in Fixed Wind Direction

In the first case, to demonstrate the effectiveness and accuracy of the proposed two-stage method, optimization results are compared with previous studies by Grady [11] and Marmidis [20]. A similar model is applied as in previous studies - 0 degree fixed horizontal wind direction with constant speed 12 m/s.

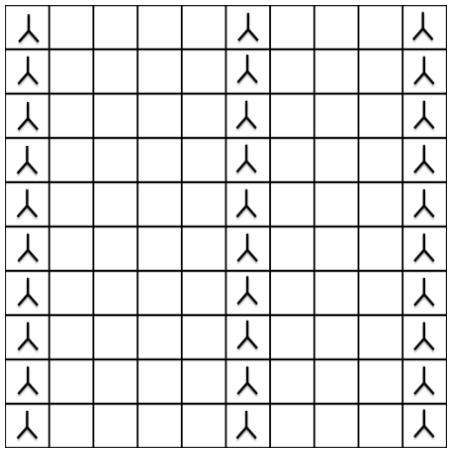

(a) Grady et al.'s

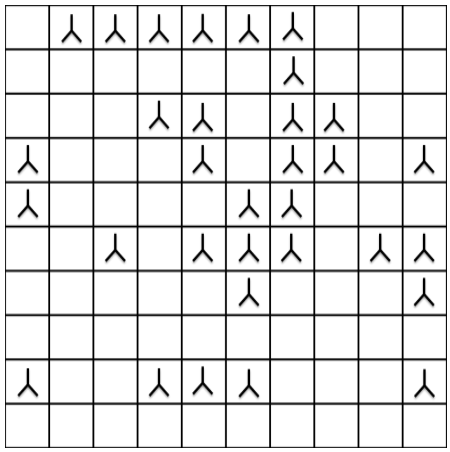

(b) Marmidis et al.'s

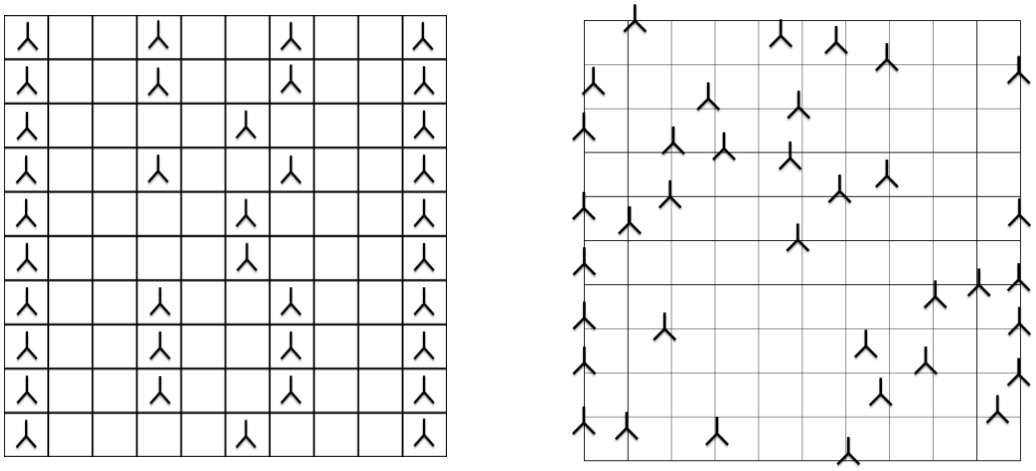

(c) Stage 1

(discrete cell-based search)

(d) Stage 2

(continuous coordinates-based search)

Figure 4-3 Turbine placement schemes from three studies

In Figure 4-3, the result generated by Grady's (4-3(a)) shows a symmetrical layout because their optimization was applied to a single row and then duplicated for 10 rows. The layout in 4-3(b) obtained by Marmidis using Monte Carlo simulation was quite scattered with no clear pattern. Our algorithm's first stage results in 4-3(c) show the layout with more turbines and lower CEPP value. Under the horizontal wind direction, there is little turbine interactions between adjacent rows and small wake effects between two horizontal rows. Mostly the turbines uniformly align at border columns of the field. This makes intuitive sense since with 1.8 km apart - the maximum horizontal distance in between turbines, the wake deficit ratio in equation (6) is reduced to approximately 0.7248%. In the result of second stage (4-3(d)), interior turbines are quite scattered along the wind direction to reduce the wake interactions. This maximizes the usage of wind farm terrain to diminish the wake loss. In our study, the number of turbines is 36, increases by 6 compared to Grady's 30, but the overall cost per production is significantly decreased with the results obtained in the second stage, as shown in Table 4-2.

Efficiency of energy production is defined as the ratio of energy production under current layout over the production with no wake loss where all turbines capture the same wind speed. In Table 4-2, it shows efficiency in Grady's is slightly better than the cell-based optimization results in this study, because fewer turbines installed help to avoid the wake interactions, thus improve the efficiency. However, allowing turbines to freely adjust in the second stage of optimization helps further reducing the overall wake interactions. By the end of second stage, coordinates-based solution shows optimized layout with improved efficiency. For the purpose of maintaining accuracy during comparison, the objective values CEPP from both previous studies are reevaluated. Additional cell-based studies are conducted in the second stage without removing the field discretization constraint, as shown in column 5. The difference from Marmidis' published result is surprisingly significant: the CEPP generated after rerun is 0.0018637, comparing to 0.0014107 in the published result. According to turbine placement in Figure 4-3(b), lower expected power production makes intuitive sense since turbines frequently align along the wind direction, causing unavoidable wake interactions.

The objective function, CEPP, trades off the cost and energy production. The results shown in Table 4-2 indicate that the optimized layout from the two-stage algorithm has more turbines, thus produces more power relative to higher installation costs, as a result a lower CEPP value. By implementing cell-based local search in stage 2, it slightly improves the objective function and efficiency around 1.4% and 1.3%. Further with proposed coordinates-based continuous search method, the objective function and efficiency are significantly improved by 8.26% and 5.85%.

	Grady et al.	Marmidis et al.	Present study stage 1	Present study stage 2 (cell-based)	Present study stage 2 (coordinates-based)
Number of turbines	30	32	36	36	36
Total power (kW/year)	14,801	12,410	17,103	17,125	18,514
Objective value CEPP (k$/kW.year)x10^{-3}	1.492	1.864	1.477	1.475	1.364
Efficiency (%)	95.17	74.81	91.64	91.76	97

Table 4-2 Optimization results compare to previous studies

4.1.4.2 Constant Wind Speed in Random Wind Directions

In this section, the case with constant wind speed u_0=12 m/s and stochastic wind directions $f_\Theta(\theta_0)$ is considered. The random wind directions θ_0 is modeled with Lognormal distribution, i.e. $\log(\theta_0) \sim N(5.1677, 0.3247^2)$, such that CEPP becomes the expected value of a random function in wind uncertainty. To study turbine performance in the farm, the expected energy production is estimated by computer sampling thought one year. Accounting for uncertainty wind direction, four scenarios: warm season daytime, warm season nighttime, cold season daytime, and cold season nighttime are modeled.

The randomly sampled four day-time intervals totals up to 40 days and forms a subset of wind data. The wind frequency rosemap in Figure 4-4(a) illustrates that wind blows mostly in the range of (110, 270) degree, the optimized wind farm layout at stage 1, shown in Figure 4-4(b), indicates most of turbines are located near the boundary of wind farm to eliminate the wake effect. If not avoidable, the distance between turbines increases to reduce wake loss. The result is improved by applying continuous coordinates-based search in second stage (Figure 4-4(c)). From the rosemap, due to the frequent shift of wind directions, turbine layout tends to intensively lay along horizontal and vertical directions

where the magnitude of wind is weakening. In addition, because of higher wind frequency in (180, 270) degree range, turbines tend to be scattered in the diagonal direction. Similar results are obtained in the case of (100, 180) degree range.

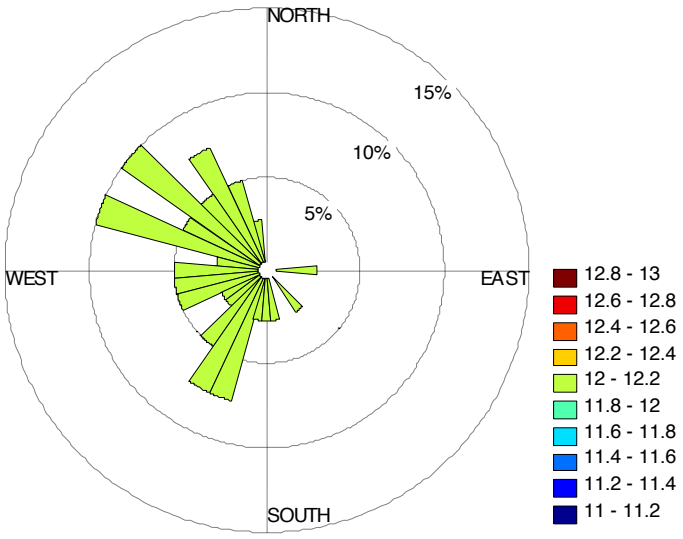

(a) 40 days Wind rosemap

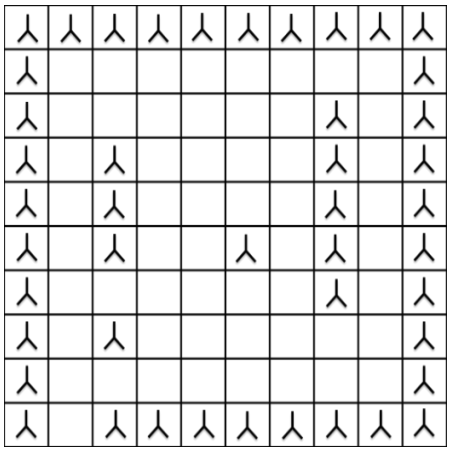

(b) Stage 1

(discrete cell-based search)

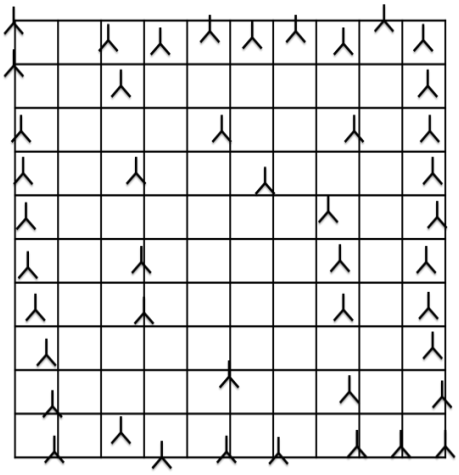

(c) Stage 2

(continuous coordinates-based search)

Figure 4-4 Wind rosemap and optimal layout in scenario 2

Table 4-3 illustrates the results of wind farm layout design in scenario 2, which indicates by continuously refining the turbine layout with local search in second stage, the annual expected power production potentially increases by 5.11%. Improved farm layout mitigates turbine interactions by extending turbine distance or cross installation along high probabilistic wind direction. This strategy reduces the speed loss caused by wake interactions, whereas obtaining the optimal layout design with minimized CEPP value.

	Stage 1 Genetic Algorithm	Stage 2 (discrete cell-based)	Stage 2 (continuous coordinates-based)
Number of turbines	45	45	45
Expected power (kW/year)	21,545	21,571	22,646
Objective value CEPP (k$/kW.year) x$10^{-3}$	1.413	1.411	1.390
Efficiency (%)	96.71	96.98	97.08

Table 4-3 Optimization results in scenario 2

4.1.4.3 Stochastic Wind Speeds in Random Wind Directions

The third case is more realistic in wind modeling. The wind direction model follows a lognormal distribution ($\log(\theta_0) \sim N(5.1677, 0.3247^2)$), same as the previous case, and stochastic wind speed follows a Weibull distribution with parameters shown in Table 4-1. In this extensive study, to demonstrate the effectiveness of turbine dynamic interaction model and proposed two-stage optimization framework, the wind farm dimension is scaled up from previously introduced 10x10 to 12x12 equal size cells, with 44 more candidate locations. Figure 4-5(b)(c) shows the optimized turbine placement scheme obtained by the two-stage optimization approach.

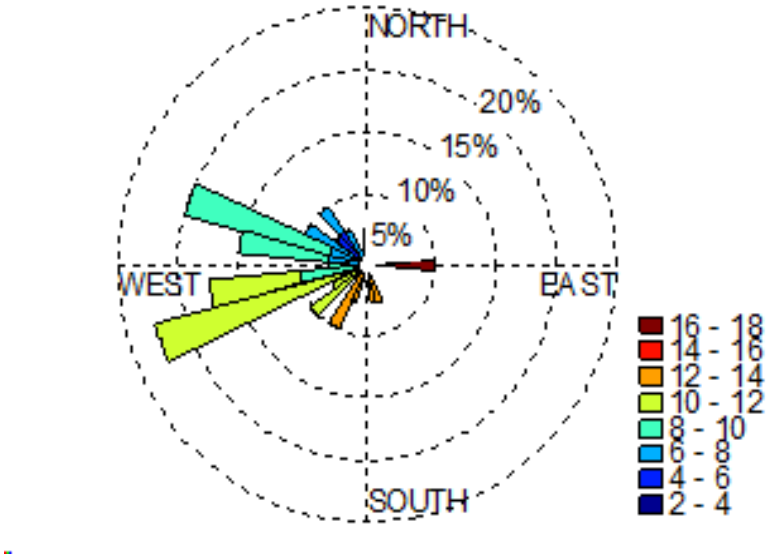

(a) 40 days Wind rosemap

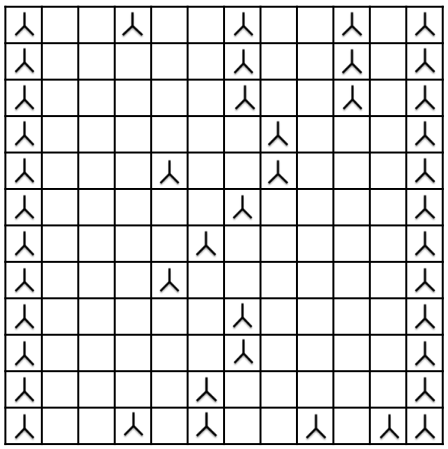

(b) Stage 1

(discrete cell-based search)

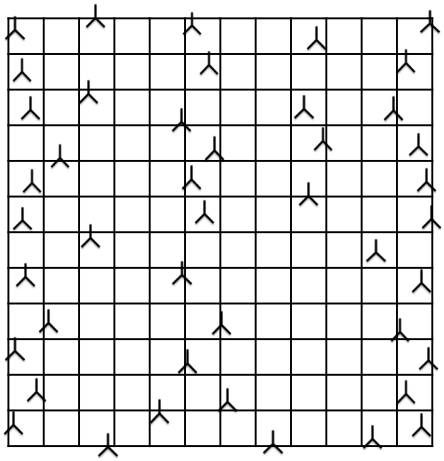

(c) Stage 2

(continuous coordinates-based search)

Figure 4-5 Wind rosemap and optimal layout in scenario 3

Corresponding to the wind rosemap shown in Figure 4-5(a), the wind directions lie mostly in the ranges of (140, 170) and (190, 215) degrees and the major wind speed are between 8m/s and 12m/s. The optimized layouts in 4-5(b) and 4-5(c) maintain extensive space in the high probabilistic diagonal direction, in the meantime closely aligning along low frequency wind direction (in current case, with lower wind speed as well). Since

turbines are allowed to freely move in the field, the pattern from stage 2, in Figure 4-5(c), shows optimized adjustment in prevailing wind directions.

From Table 4-4, the objective value CEPP in current scenario is higher than ones reached from previous cases, because wake interactions are dynamic and potentially increased due to wind variation. The optimal results demonstrate the improvement by local search algorithms. In terms of efficiency, the result obtained by coordinates-based search in stage 2 is 3.8% higher than the one obtained from stage 1, while 2.3% higher than the cell-based local search one.

	Stage 1 Genetic Algorithm	Stage 2 (discrete cell-based)	Stage 2 (continuous coordinates-based)
Number of turbines	44	44	44
Expected power (kW/year)	14,677	14,721	14,809
Objective value CEPP (k$/kW.year) x$10^{-3}$	2.033	2.027	2.015
Efficiency (%)	91.15	92.69	94.96

Table 4-4 Optimization results in scenario 3

4.2 Optimal Development of Arbitrary-shaped Onshore Wind Farm

4.2.1 Arbitrary-shaped Wind Farm Field

In reality, wind farms are designated either on the mountain ridge or surrounded by existed structures, such as community, airport, main roads, forests, reservoirs, restriction zones and so on. Terrains can be complicated, with various topology and different obstruction. In this section of study, flat terrain is considered as shown in Figure 4-6(a), surrounded by trees, restriction zone (i.e., wild birds protection area) and water reservoir.

Because of this particular structure, the designated wind farm has an irregular-shaped boundary.

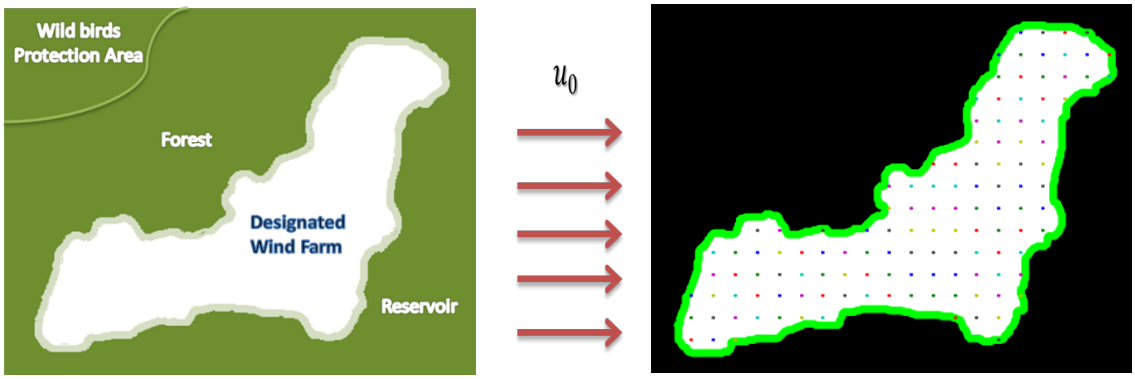

(a) Wind farm model in complex terrain (b) Wind farm with candidate turbine locations

Figure 4-6 Arbitrary shaped wind farm model in complex terrain

At the first stage, the wind farm is divided into 123 blocks that are 150m apart. The wind direction is assumed from west toward east as 0 degree, counterclockwise covering all directions. Identical turbines and uniform terrain condition are considered in this case, therefore the same power curve function is applied to all turbines. Figure 4-6(b) shows the discretized field in the wind direction of 0°.

The same wind uncertainty model and optimization model from regular-shaped wind field are applied in the arbitrary-shaped wind farm, with distant constraint (150m) as mentioned above. To demonstrate the proposed two-stage optimization framework, the computational study with dynamic wind profile is evaluated using both the GA-based two-stage optimization algorithm and the heuristic-based two-stage optimization algorithm.

4.2.2 Computational Results

The GA-based optimized layouts design and heuristic-based optimized layout are shown in Figure 4-7 and Figure 4-8 respectively. According to results from first stage by both optimization approaches, large space between adjacent turbines helps to mitigate the

wake loss interaction. During the second stage without predefined location constraint, pattern search algorithm allows the turbine locations to change in the field, therefore the pattern tends to scatter in the major wind direction. It helps to capture greater wind speeds by reducing the wake loss interactions between turbines, thus improves energy production.

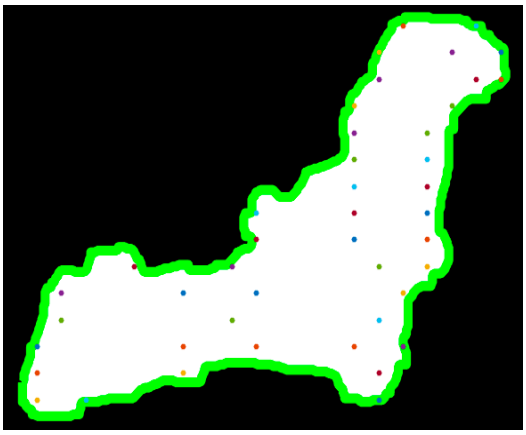

(a) Stage 1 Layout
(discrete location-based search)

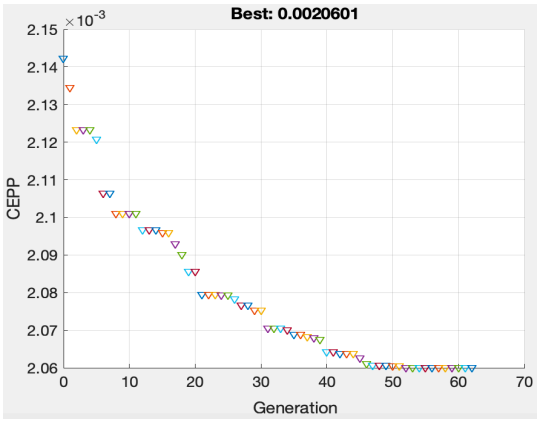

(b) Stage 1 Convergence
(discrete location-based search)

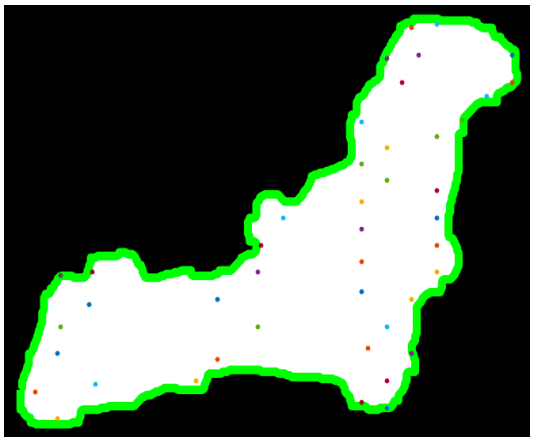

(c) Stage 2 Layout
(continuous coordinates-based search)

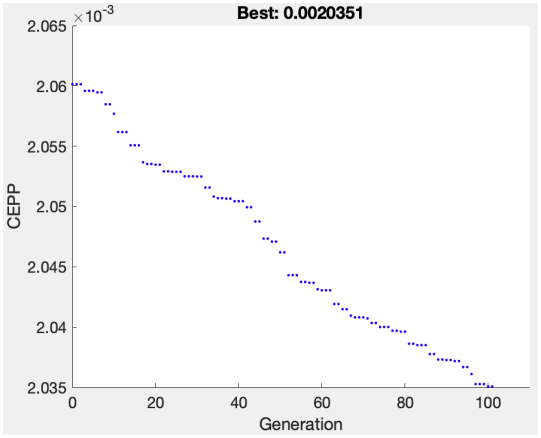

(d) Stage 2 Convergence
(continuous coordinates-based search)

Figure 4-7 GA-based two-stage optimal layouts and convergence diagrams

Comparing to GA-based first stage layout (Figure 4-7(a)), layout from heuristic-based first stage (Figure 4-8(a)) is less dominant because of its close alignment in the major wind direction. In this case GA is expected with better fitness value, which can be confirmed in

column 2 and 4 of Table 4-5. However, by extending the number of iterations in continuous search during stage 2 of heuristic-based optimization, the fitness value is improving iteratively and the difference between both algorithms is narrowed down. The objective value CEPP solved by heuristic-based shows slightly better than the one obtained by GA-based method.

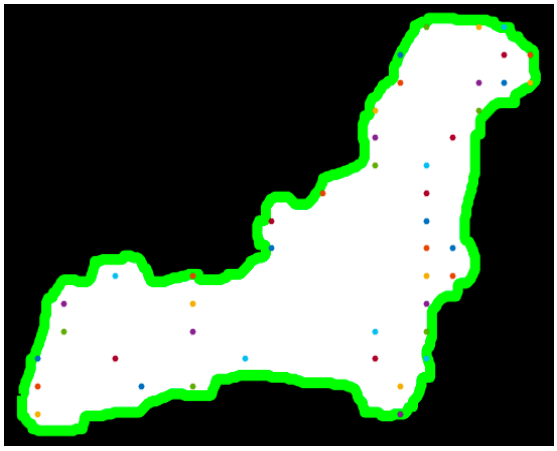

(a) Stage 1 Layout
(discrete location-based search)

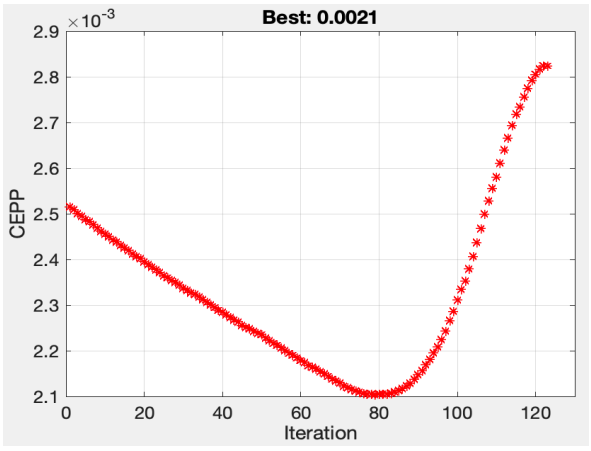

(b) Stage 1 Convergence
(discrete location-based search)

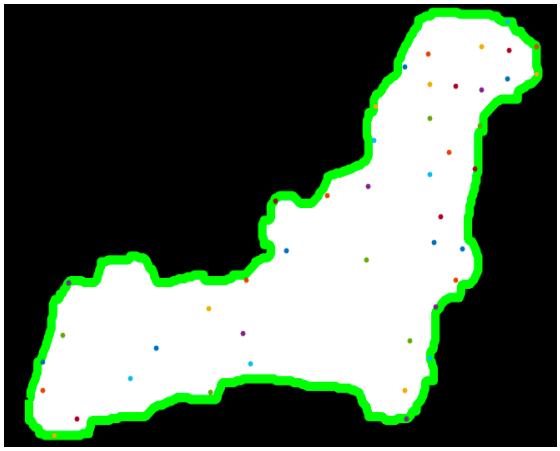

(c) Stage 2 Layout
(continuous coordinates-based search)

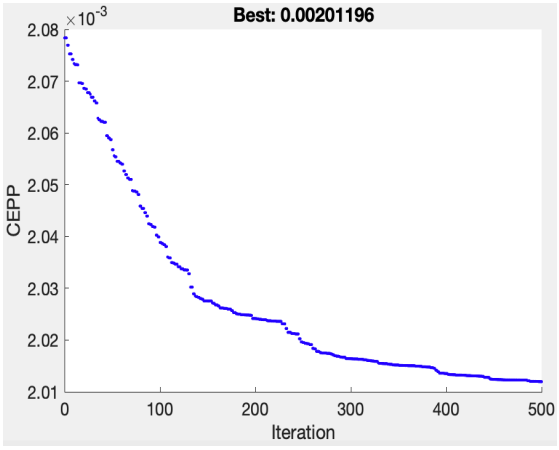

(d) Stage 2 Convergence
(continuous coordinates-based search)

Figure 4-8 Heuristic-based two-stage optimal layouts and convergence diagrams

One thing worth mentioning is that the statement - 'heuristic-based optimization method's result is better' is not always guaranteed. On one side, straightforward heuristic-based method is less computationally intensive in terms of running cycle and computing time. Because of its simplicity and step-dependent searching path, heuristic-based method improves the efficiency by saving almost 80% of computing time, which is a promising feature in solving large scale optimization problems within limited timespan. On the other side, due to its constructive nature in approximating solution algorithm by making deterministic moves, proposed heuristic-based search method only searches the adjacent hyperplane, therefore it can only guarantee local optimality. On the contrast, GA-based approach avoids falling into local optima by stepwise evolving and mutating, from this point of view it is highly possible to locate a global solution. Therefore, heuristic method is frequently used when either there is no known solution algorithm or solving straightforward problem within narrow timeframe; in cases of refining solutions while encountering multiple local optima, global optimality may not be satisfied. In order to overcome such limitation, additional algorithm is suggested for continuous improvement.

	GA based Two-stage Optimization		**Heuristic based Two-stage Optimization**	
	Stage 1 Genetic algorithm	Stage 2 Positive basis Pattern Search	Stage 1 Heuristic algorithm	Stage 2 Positive basis Pattern Search
Number of turbines	44	44	45	45
Expected power (kW/year)	14,485	14,663	14,496	15,131
CEPP (k$/kW.year) $x10^{-3}$	2.060	2.035	2.100	**2.012**

Table 4-5 Optimization results for arbitrary-shaped wind farm

4.3 Optimal Development of Offshore Wind Farms

4.3.1 An Offshore Wind Farm at New Jersey Coast

The wind farm case studied in this work is based on an on-going offshore wind power project in New Jersey. The considered region off the coast of New Jersey is shown in Figure 4-9(a). During the first stage, 132 candidate locations are pre-determined for possible turbines as shown in Figure 4-9(b). The farm is about 7km x 3km and adjacent turbine locations are about 400m apart. Different from onshore wind farm, offshore wind field (particular for wind speed) is heterogeneous; wind decreases significantly towards coastline due to change of tide and terrain conditions. To take this into account, a linear reduction term is added to the wind speed model. A 20% reduction is assumed as wind flows through the farm from its east side (ocean) to west side (coastline).

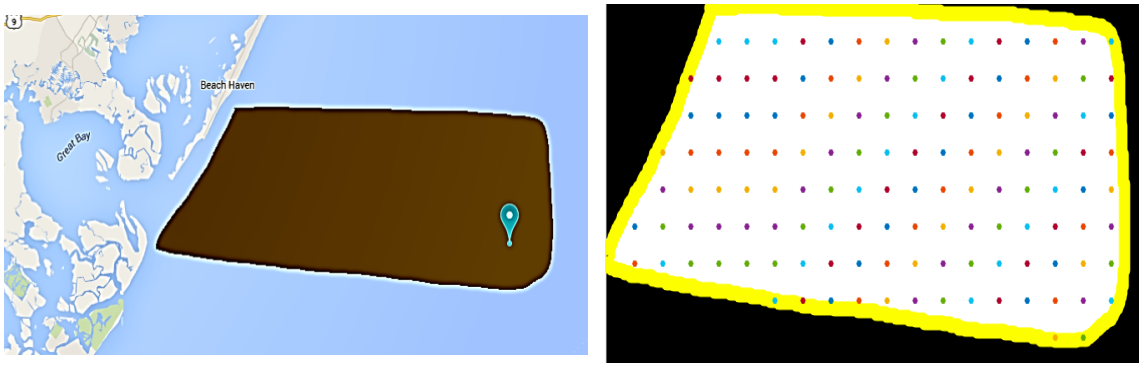

(a) Offshore wind farm in New Jersey

(b) Wind farm with 132 candidate turbine locations

Figure 4-9 an NJ coast offshore wind farm

4.3.2 Modeling Wind Uncertainty

The wind uncertainty along the NJ coast is studied and historical wind speed and direction data in this area is collected once every 10 minutes at the measuring location. The one-year wind data of 2014 is used to fit the wind probabilistic models.

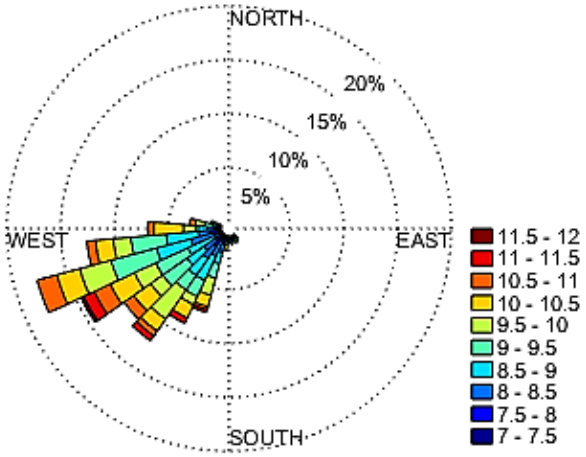

Figure 4-10 Rosemap for stochastic wind modeling

Based on the wind rosemap shown in Figure 4-10, historical data indicates wind mainly blows in the direction from 162° to 267°, with higher probabilities falling in the range of (181°, 267°). With some distribution analysis, the wind direction θ_0 at measuring location can be estimated by a lognormal distribution $\log(\theta_0) \sim N(5.3566, 0.1184^2)$). Wind speed varies significantly at different times of a day.

In this section of study, different wind speeds are modeled considering two dayparts scenarios: (12pm,22pm], (22pm,12pm]. Figure 4-10 indicates the wind speed is mostly in the range of 9 m/s - 11 m/s. With some statistical fitting analysis, two Weibull distributions are determined for the two scenarios respectively with parameters shown in Table 4-6.

	T(1) (22:10pm~12pm)	**T(2) (12:10pm~22pm)**
Shape Parameter	3.0523	2.5042
Scale Parameter	10.5787	9.6388

Table 4-6 Weibull models for stochastic wind speed considering two dayparts scenarios

4.3.3 Optimization of Offshore Wind Farm Design

4.3.3.1 Costs of Wind Turbines

The costs for offshore wind farm development include the capital investment of equipment, cable and devices installation, as well as the labor costs. In this research, it aims

to minimize unit development cost. The average installation cost for each turbine can be reduced by installing more turbines in the field. Same as the installation cost in the previous two applications, the total cost of a wind farm project (K$) can be estimated by *N*, the total number of turbines installed in the wind farm.

$$C_{ins}(N) = N\left(\frac{2}{3} + \frac{1}{3}e^{-0.00174N^2}\right) \tag{18}$$

The farther a turbine installed from the coast, the more it will cost due to increasing consumption of cables materials and associated installation costs. Such cable costs can be estimated by a linear cost function:

$$C_{cable}(D_i) = c_0 + c_d * D_i \tag{19}$$

Where D_i is the distance of a turbine away from the coast, c_0 is fixed cost for major cable structure installation and c_d is the cable installation cost per unit distance from the shoreline. The total wind farm cost is modeled as:

$$C(N, D_i) = C_{ins}(N) + \sum_{i=1}^{N} C_{cable}C(D_i) \tag{20}$$

4.3.3.2 Expected Annual Energy Production

The same energy production equation (12) as in the previous two applications is applied in this case study. $u_{in} = 3\ m/s$, $u_{out} = 22m/s$. For any speed u in between u_{in} and u_{out}, a turbine generates energy E_{θ_0,u_o} estimated by (12).

4.3.3.3 Objective Model

A slight modification from previous applications will provide objective model as follows:

$$\operatorname{argmin}_{(N,X)}\ \mathrm{CEPP} = \frac{\text{Annual Total Cost}}{\text{Expected Power Production}}$$

$$= \frac{C\,(N, D_i)}{E_{\theta_0,u_o}} = \frac{N\left(\frac{2}{3} + \frac{1}{3}e^{-0.00174N^2}\right) + (c_0 + c_d * D_i)}{\sum_{i=1}^{N} \int_0^{360} \int_{u_{in}}^{u_{out}} P_i(u_i; u_0, \theta_0) f_U(u_0) f_\Theta(\theta_0) du_0\, d\theta_0} \tag{21}$$

Subject to: $u_0 \geq u_i$

$$\left\|X_i - X_j\right\| \geq 200, \forall\, i \neq j \in \{1,2 \ldots N\}$$

To account for significant variations of wind during a day, two daypart scenarios *s* ($s \in \{1, 2\}$) are considered: (22pm,12pm], (12pm,22pm]: *s*=1 when wind energy is produced during (22pm,12pm]; *s*=2 otherwise. To approximate (21), twenty data points from each scenario *s* are randomly sampled, resulting in 40 wind data points for (u_0, θ_0). CEPP in model (21) can be approximated by the following sampling technique:

$$\widehat{\mathrm{CEPP}} = \frac{N\left(\frac{2}{3} + \frac{1}{3}e^{-0.00174N^2}\right) + (c_0 + c_d * \sum_{i=1}^{N} D_i)}{\sum_{i=1}^{N}(0.25 \sum_{s=1}^{2}(0.1 \sum_{T(s)=1}^{20} 0.3(u_i(X; u_0, \theta_0 | T(s), s))^3))} \tag{22}$$

$$= \frac{N(\frac{2}{3} + \frac{1}{3}e^{-0.00174N^2}) + (\$10{,}000 + \$500 * D_i)}{0.0075 \sum_{i=1}^{N} \sum_{s=1}^{2} \sum_{T(s)=1}^{20} u_i(X; u_0, \theta_0 | T(s), s)^3}$$

Where building the cable structure has a fixed cost $c_0 = \$10\text{k}$ and installation cost is about \$500/m.

4.3.4 Computational Results

Based on the one-year wind data at the measurement location, the wind direction is modeled with a lognormal distribution $\log(\theta_0) \sim N(5.3566, 0.1184^2)$, and the wind speed is modeled as a Weibull distribution with parameters shown in Table 4-6. Figure 4-10 shows that the wind directions lie mostly in the range of (181°, 267°) and the wind speeds are mainly between 9m/s and 11m/s. The offshore wind often blows from the ocean

towards the coast and the speed reduces when it approaches the coastline. A 20% linear speed reduction is used when wind hits the coastline.

The two-stage simulation optimization is applied to this case. The optimized layouts in Figure 4-11 show that turbines tend to locate at the farthest places from the coast where the wind is strongest, even though the cable costs will be higher. Figure 4-11(a) presents the optimized layout by the first stage of optimization, where the 98 turbines are located at the predetermined cells.

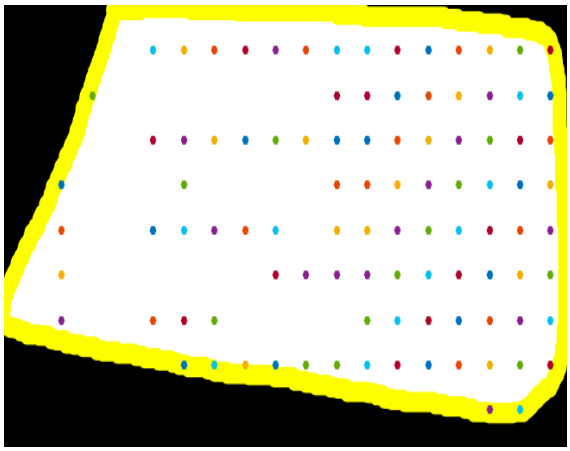

(a) Stage 1 Layout

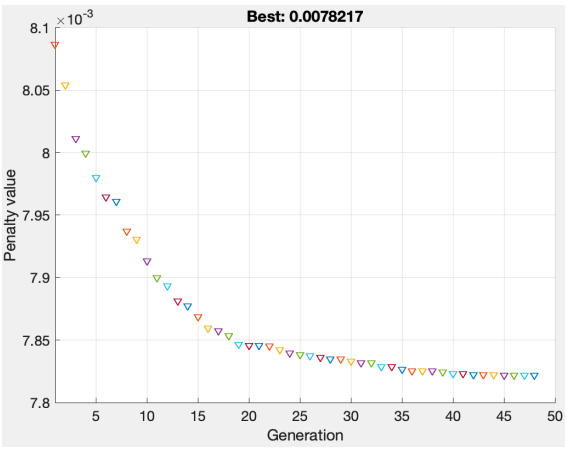

(b) Stage 1 Convergence

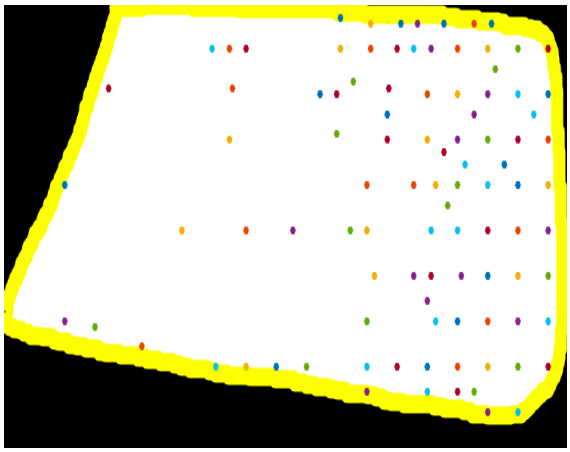

(c) Stage 2 Layout

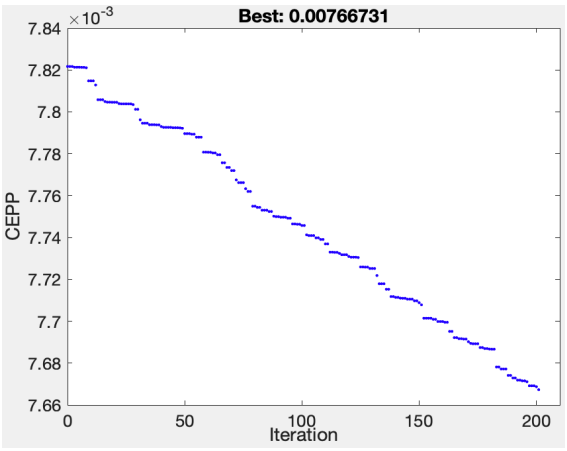

(d) Stage 2 Convergence

Figure 4-11 Optimal layouts and optimization progresses

The optimization results of this case are summarized in Table 4-7. The first stage optimization determines that 98 turbines to be built in the farm with objective value 0.007822. The second stage further reduces CEPP by changing the locations of those 98 turbines; the CEPP value is decreased to 0.007667. With the same amount of turbin installations, the power production at the end of second stage has increased almost 5,000 kW/year.

	Stage 1 (discrete location-based search)	Stage 2 (continuous coordinates-based search)
Number of turbines	98	98
Expected power (kW/year)	18,550	20,319
Objective value CEPP (k$/kW.year) x10^{-3}	7.822	7.667

Table 4-7 Optimization results for developing the NJ offshore wind farm

4.4 Optimal Layout Design of Wind Farm with Energy Storage system in Micro-grid

4.4.1 Energy Storage Integrated Wind Energy System (ESIWES) in Micro-grid

Wind power has been widely used in micro-grids for community energy consumptions. While it is clean, sustainable and low operational cost, in reality wind power is highly fluctuating. A practical solution to maintain reliable supply is using energy storage. In this application an Energy Storage Integrated Wind Energy System (ESIWES) is proposed as wind farms equipped with electrochemical battery energy storage. To best meet the electricity demand of an interconnected micro-grid community, the CEPP is minimized for optimal turbine layout. To demonstrate the idea, the ESIWES is applied to a typical micro-grid community including residential households; the optimal design of wind farm layout in ESIWES is illustrated to maintain 100% service level and meet the fluctuating demand.

Electrochemical battery is a type of energy storage technology using chemical reactions within battery cells, which converts electrical energy into chemical energy while charging, and facilitates the flow of electrons to generate electric current when discharging [86]. Lithium-ion battery, for example, has important features such as high energy density thus portable, fast charge / discharge capability, relatively high efficiency with low standby losses, etc. Lithium-ion battery is commonly used for wind energy systems where the service time and weight are important [57]. There have been applications using Lithium-ion battery to demonstrate voltage support as well as reserve capacity and renewable integration. Figure 4-12 shows the map of planned and existing Lithium-ion battery usage by the year of 2009 [87]. The size of star indicates the size of project; yellow stars indicate auto major contracts while red stars mean no auto contract.

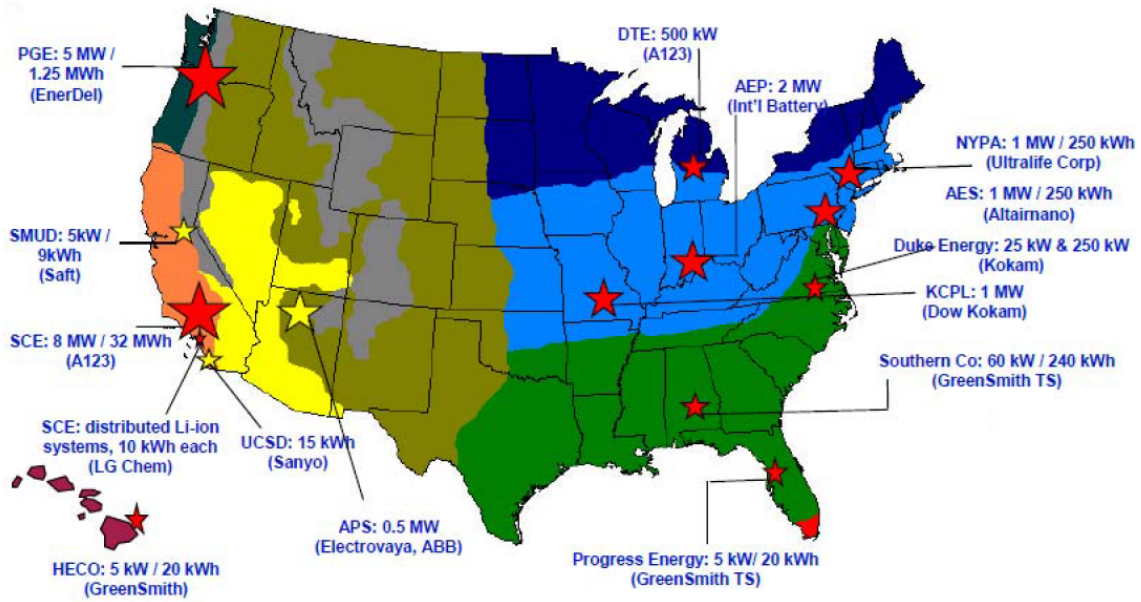

Figure 4-12 Map of planned and existing lithium ion battery demonstrations (2009)

In this case study, as shown in Figure 4-13, the problem of energy system is boiled down to planning the generation assets – wind farm and energy storage. A model of daily micro-grid operation is under implementation and its function form is defined. The

proposed ESIWES in micro-grid is designed to sufficiently respond to local community's daily demands, and the optimal layout of wind farm to sustainably support such demand is developed.

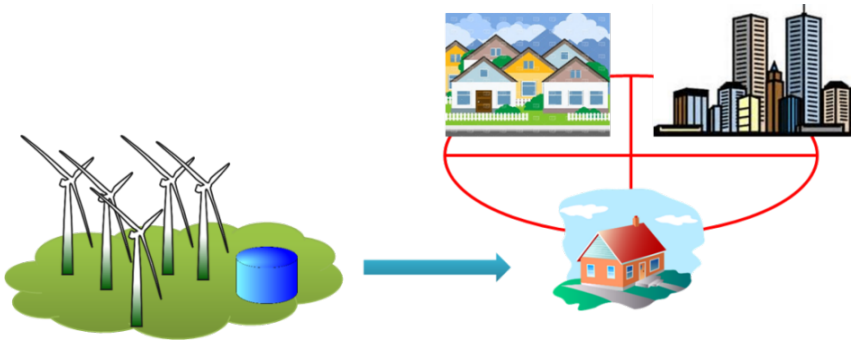

Figure 4-13 Development of ESIWES in micro-grid community

The technique in the ESIWES model is shown in Figure 4-14. The wind farm is considered as the primary energy supplier for the micro-grid community's electricity demand, the power generated from turbines is directly transmitted to the consumer end for daily consumption. At night times when wind reaches its maximum while demand is low, the excess energy can be stored in energy storage as the secondary energy supplier. If demand exceeds supply, the electricity will be discharged from the energy storage to satisfy the excess usage and maintain power quality.

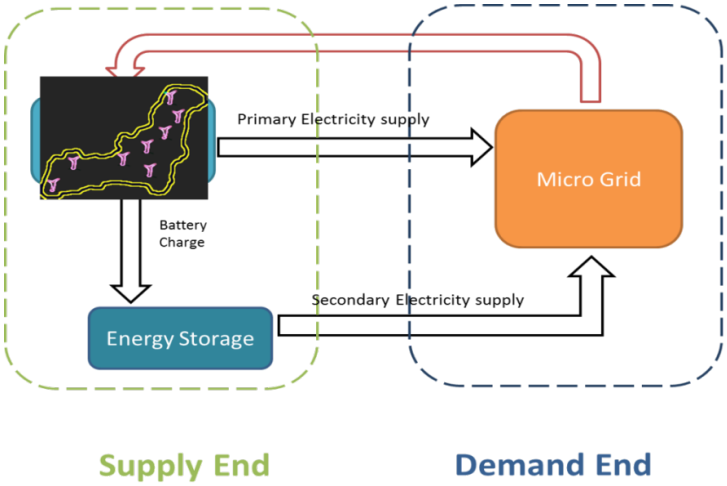

Figure 4-14 Sustainable energy system feedback loop

4.4.2 Demand from Local Community

In the current scenario, the demand side includes 10 residential buildings. The hourly energy consumption data (1/1/2000 to 12/10/2019) from Pacific Gas & Electric (PG&E) are used [88]. The boxplots for daily loads in Residential building is shown in Figure 4-15, which demonstrates median and corresponding $25^{th}/75^{th}$ percentiles of daily loads for demands.

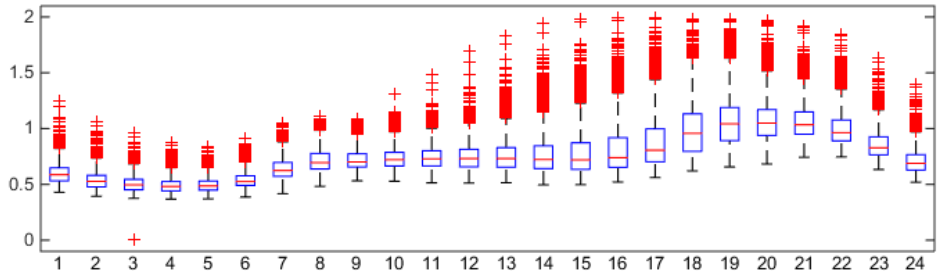

Figure 4-15 Historical data of Residential hourly energy consumption (2000-2019)

The historical data on demand of 10 residential units is added and fitted to a lognormal distribution, which is used to generate random daily demands in a sampled year as indicated in Figure 4-16.

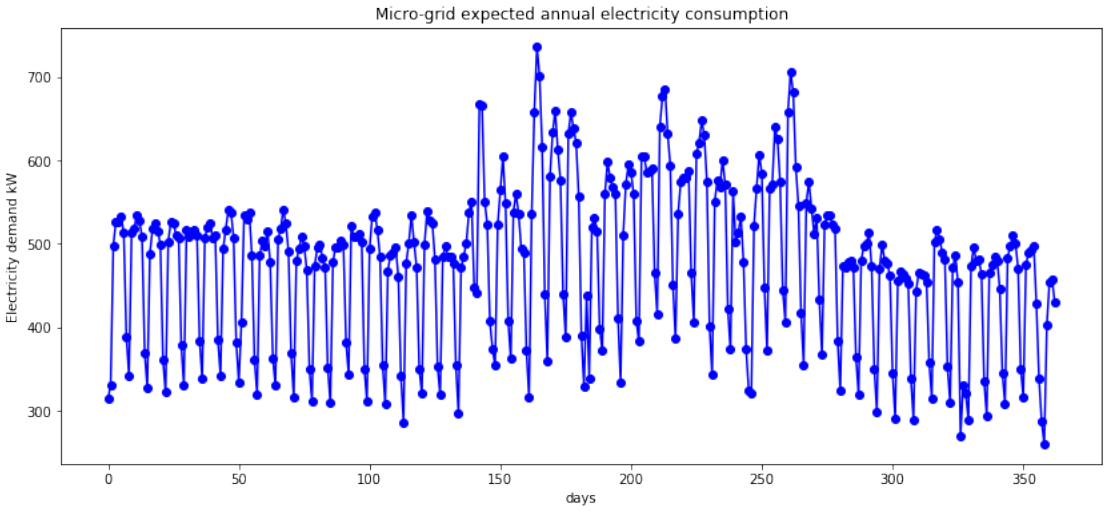

Lognormal (6.1423, 0.2118)

Figure 4-16 Annual electricity consumption in micro-grid community

4.4.3 Optimal Development of Wind Farm in ESIWES

4.4.3.1 Investment costs of ESIWES

The investment costs of ESIWES proposed in this case study including two parts: installation cost of wind turbine and investment cost for Lithium-ion battery. The same turbine installation cost model from previous case studies is used in this section:

$$C_{WF}(N) = N(\frac{2}{3} + \frac{1}{3}e^{-0.00174N^2}) \tag{23}$$

The investment cost model for Lithium-ion battery is:

$$C_{ES|S_d} = c_{ES} * E_{ES|S_d} \tag{24}$$

Where c_{ES} is the cost per energy usage. In this case, the charge cycle of battery at night is assumed to be short enough for it to fully function by the next morning.

Based on [87], the Levelized Cost (LCOE) for the 1 MW Lithium-ion battery ranges approximately from $400/KW-year to $1,700/KW-year. This study used 1 MW Lithium-ion battery, $c_{ES} = \$600$/kW year.

S_d is a variable associated with energy supplied from the wind farm, which represents the status of discharge in energy storage on day *d*. It will be further introduced in equation (28).

Given S_d, the total energy system cost is modeled as:

$$C(N) = C_{WF}(N) + C_{ES|S_d} \tag{25}$$

4.4.3.2 Expected Annual Energy Production

The same wind farm energy production model is applied in this session. Averaged to daily electricity generation, equation (12) is transformed into:

$$E_{i,d|(u_0,\theta_0)} = 0.000822{u_i}^3 \qquad 3 \le u_i \le 20 \tag{26}$$

$$E_{WF|(u_0,\theta_0)} = \sum_{d=1}^{365} E_{WF,d|(u_0,\theta_0)} = \sum_{d=1}^{365}\sum_{i=1}^{N} E_{i,d|(u_0,\theta_0)} \quad (27)$$

Again S_d is the energy supplied from energy storage on daily basis. Specifically, in day d:

$$S_d = \min\left(Cap_{ES}, \max\left(0, Demand_d - E_{WF,d|(u_0,\theta_0)}\right)\right) \quad (28)$$

Where Cap_{ES} is the capacity of energy storage and in this application with Lithium-ion battery, $Cap_{ES} = 1\ MW$. The power function of energy storage and overall energy power function are respectively as:

$$E_{ES|S_d} = \sum_{d=1}^{365} S_d \quad (29)$$

$$E_{(u_0,\theta_0)} = E_{WF|(u_0,\theta_0)} + E_{ES|S_d} \quad (30)$$

4.4.3.3 Objective Function

Same as in the previous applications, the objective function for minimizing CEPP can be transformed as:

$$\text{argmin}_{(N,X)}\ \text{CEPP} = \frac{\text{Annual Total Cost}}{\text{Expected Power Production}} = \frac{C\ (N)}{E_{(u_0,\theta_0)}} \quad (31)$$

$$= \frac{N\left(\frac{2}{3} + \frac{1}{3}e^{-0.00174N^2}\right) + \sum_{d=1}^{365}\min\left(Cap_{ES}, \max\left(0, Demand_d - E_{WF,d|(u_0,\theta_0)}\right)\right) * c_{ES}}{\sum_{d=1}^{365}\left[\sum_{i=1}^{N}\int_1^{360} f_\Theta \int_3^{27} E_{i,d|(u_0,\theta_0)} f_U(u_0) du_0\, d\theta_0 + \min\left(Cap_{ES}, \max\left(0, Demand_d - E_{WF,d|(u_0,\theta_0)}\right)\right)\right]}$$

Subject to:

$$E_{WF,d|(u_0,\theta_0)} + S_d \geq Demand_d$$

$$u_0 \geq u_i$$

$$\left\|X_i - X_j\right\| \geq 200, \forall\ i \neq j \in \{1,2 \ldots N\}$$

4.4.4 Computational Results

The objective model (31) is optimized by GA-based and heuristic-based two-stage algorithms. Optimized layouts are shown below in Figure 4-17. In this case the layouts from both stages of GA-based results are better than the ones obtained by heuristic-based methods. According to the layout from first stage of heuristic-based model in Figure 4-17(c), most of turbines are distributed uniformly in the wind farm, which does not make much progress in reducing turbine interactions. In stage two (Figure 4-17(d)), the result is improved by local search algorithm, however it still contains clusters of turbines in the same area which does not gain much advantage in captured maximum wind speed, thus the objective solution by this model is expected to be suboptimal. This finding is confirmed by the CEPP value, as listed in Table 4-8.

On the other side, the GA-based model shows its advantages in continuous improving objective values. Figure 4-17(a) represents the first stage layout by GA optimization method, with turbines divergently align facing major wind directions, and it becomes even more so after the local search optimization (Figure 4-17(b)). In this way, turbines are able to effectively reduce wake loss effect and further maximize power generation.

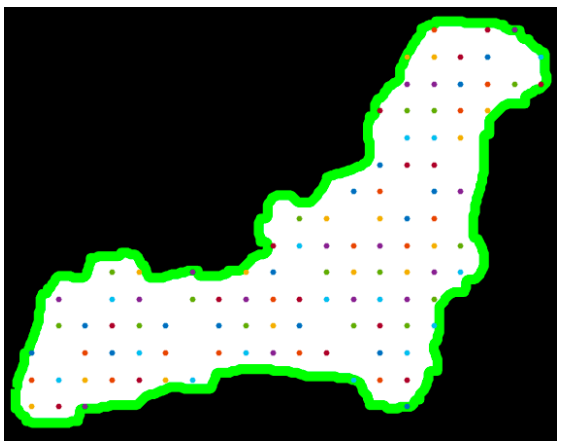

(a) Layout from GA-based first stage

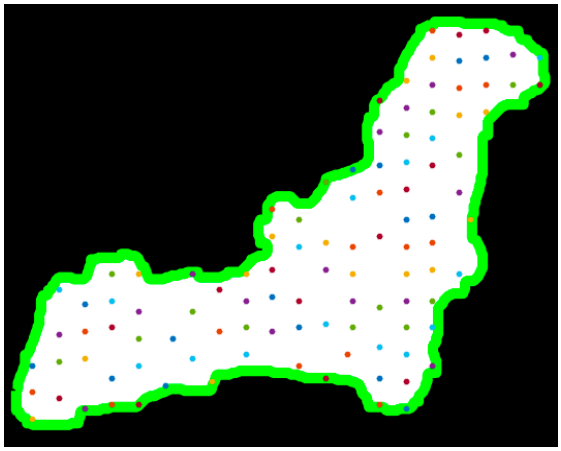

(b) Layout from GA-based second stage

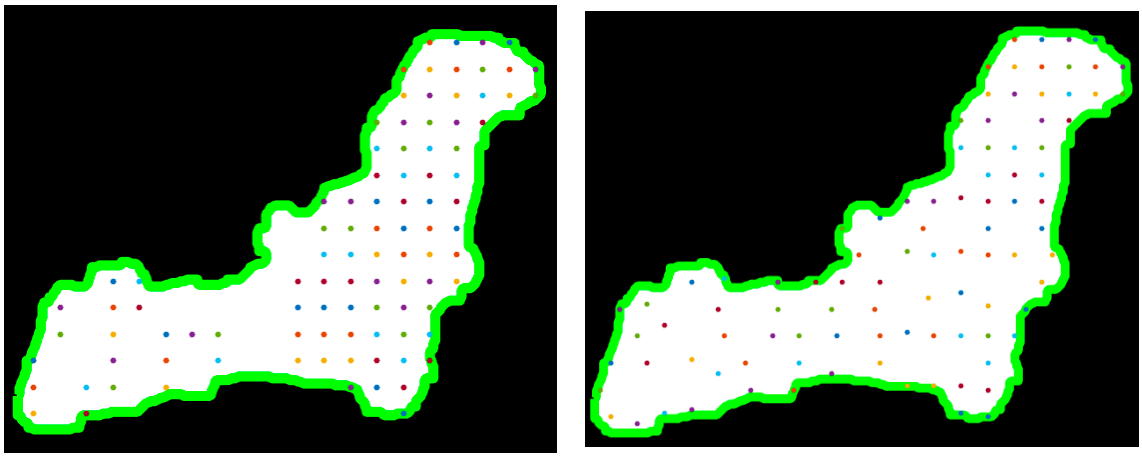

(c) Layout from Heuristic-based first stage (d) Layout from Heuristic-based second stage

Figure 4-17 Two-stage optimal layouts for wind farm in ESIWES

Results shown in Table 4-8 indicate that ESIWES with fewer turbines can actually provide better power supply to the micro-grid community with more energy support at lower costs. The wind farm is able to optimize energy generation and maintain energy efficiency. Furthermore, the optimization solution successfully integrates the usage of energy storage with wind farm operation, thus increases the service availability. The capacity of the 1 MW Lithium-ion battery can meet a fair amount of daily electricity demand when needed, which gives ESIWES leverage to maintain power sustainability for the micro-grid community without overspending on turbine installations.

	GA based Two-stage Optimization		**Heuristic based Two-stage Optimization**	
	Stage 1 Genetic algorithm	Stage 2 Positive basis Pattern Search	Stage 1 Heuristic algorithm	Stage 2 Positive basis Pattern Search
Number of turbines	105	105	96	96
Expected power (kW year)	173,280	174,780	132,729	153,983
CEPP (k$/kW year)	0.498	**0.493**	0.623	0.529

Table 4-8 Optimization results in ESIWES

4.5 Optimize Wind Farm Layout in Hybrid Wind/Biorefinery/Energy-Storage Energy System

The project in Section 4.4 presents the studies of a wind farm based renewable energy system (ESIWES) to meet small micro-grid community's electricity demand. In reality, renewable energy generation has greatly expanded so that it is able to meet demand from both locally owned sustainable community and larger-scale grid-wise energy consumption. In order to do so, high capacity power generators such as gas turbine, hydro-electricity generator and bio-generation system, are better sources in energy compensation providing baseload in energy system. In this section, stepping up from the ESIWES model, the wind farm model will be integrated into Hybrid wind / biorefinery / energy-storage based renewable energy system (HWBRES) to support energy consumption in the micro-grid community. Such hybrid energy systems can be easily expanded to large-scale city-wise energy generation.

The work is inspired by the increase of public awareness towards environmental sustainability such as waste decomposition and renewable production. Global municipality, especially in densely populated regions, generates thousands of tons of municipal solid waste (MSW) – food waste plays a major role, which raises multiple environmental risks, such as greenhouse gas leakage and underground waste contamination. Now the question of concern is: instead of targeting them separately, what is the most efficient method to tackle both those issues together? Among all the possibilities, the most effective answer to the question is "biorefinery".

The development of biorefineries represents the key for access to an integrated production of food, feed, chemicals, goods, and fuels of the future. A wide variety of biomass is available depending on local geographic conditions – traditional agricultural

crops, forestry waste, food waste, etc. During the process of biorefineries, biomass is converted into value-added products such as biogas, specialty chemicals, and pharmaceuticals. Therefore, to explicitly respond to the aforementioned question: by the access and treatment to MSW, particularly food waste (sugar, starch, vegetable oils and animal fats, etc.), MSW can be effectively synthesized to various renewable end products, including biogas and further converted electricity. The new addition of this research will concentrate on the conversion of biogas and then further to electricity, by the function of the biorefinery system, specifically with the feedstock from micro-grid residence's food waste.

4.5.1 Waste-To-Energy Recovery System

Food waste, including pre- and post-consumption leftovers from both residence and commercial establishments, contains great amount of rapid degradable components such as protein, carbohydrates and short chain fat etc. Hall et al. [89] estimated the energy content of food waste by comparing the U.S. food supply data to the estimated food consumption, finding that approximately 1400 kcal were wasted by one person per day, which adds up to 150 trillion kcal per year. To produce 1 kcal of food it requires 3 kcal of fossil fuel on average, therefore the annual food waste accounts for approximately 300 million barrels of oil or about 4% of U.S. oil consumption.

To generate eco-friendly energy by utilizing the most common solid waste, there are four waste-to-energy recovery scenarios: direct combustion, landfill-to-gas, composting and anaerobic digestion.

4.5.1.1 Direct Combustion

Direct combustion is the most conventional thermochemical conversion technology to generate electricity on a large scale. The feedstock is not required to be processed before

incineration, which makes it popular on countries where land is a scarce resource. The energy efficiency of the process is not overly high, per Bosmans et.al. in waste-to-energy technology review, the net electrical efficiency of the current advanced combustion plants ranges between 22-26% [90].

The main stages of the combustion process include drying, degassing, pyrolysis, gasification and oxidation [90]. Waste is combusted at a temperature of 850° C and transformed to carbon dioxide, vapor and non-combustible incinerator bottom ash. Since combustion is normally applied to mechanically dewatered wastes, the high moisture content in food waste makes it less promising in net electricity generation. During the pretreatment, a significant amount of energy is consumed to dry or dewater the combined waste stream. Additionally, combustion with energy recovery may also raise potential environmental problems, especially the abundance of dust and ash (25-30% by weight of the solid waste input) and the toxicity of the flue gases [91]. In order to meet strict emission standards, waste gas treatment equipment needs to be installed to eliminate those harmful substances, but the associated cost will drive up the price of final products such as heat or electricity.

Although the low generating efficiency along with costly treatment facility make direct combustion limited in practice, there are also possible options that can maximize its economic benefits. For example, the bottom ash in an incinerator can be collected and sold as the raw content on the production of building materials, such as cement and bricks, for their application in construction.

4.5.1.2 Landfill-to-gas

Traditional landfills have a long history to be the extensively used technologies for solid waste management. There has been growing interest in upgrading traditional landfills

with gas recovery facilities. At this point the modern managed landfills become the most commonly used method to dispose solid waste globally.

Wastes in the landfill sites can be converted into bioenergy through phases including initial adjustment, pyrolysis, liquefaction and gasification. The initial steps are aerobic, but later turn into anaerobic when oxygen is running out. While the organic fractions, such as food and garden waste, paper, wastewater, etc., slowly decompose, the landfills gas is formed containing a mixture of methane (45-60%), carbon dioxide (40-55%) and a trace amount of other components [91]. In practice, the moisture content of waste compound, the temperature inside the reactor, the size of disposed waste, the air flows can affect the degradation process in landfills. Every kWh energy generated from biogas would avoid 1.1000952 kg CO_2 emission as oppose to the power generation at a landfill. Biogas in this scenario can be collected for a variety of end uses including electricity generation, bio-diesel fuels of transportation, or upgrading to biomethane gas. A common treatment is to burn biogas which can give out a significant amount of energy (50.2 GJ/ton waste). When it is directly converted to electricity, over 50% of energy would be lost as heat, which is assumed to be partly used in maintaining digesters at optimal temperature level and partly transported to the local heating system [91].

While landfilling is an economic method of waste disposal, the environmental contribution of landfills with gas recovery facility may be minimized if it is not managed property [92]. The major problems include the surface and ground waste contamination, methane leakage and odor emission. Therefore, landfill leachates need proper post-treatments before being released to the environment. After 1996 federal regulations, the

amount of methane recovered grows and is expected to continue increasing in the next decades.

4.5.1.3 Composting

Composting, or aerobic digestion, is a bio-oxidative process. During the process, a large portion of the degradable organic carbon is converted into carbon dioxide and water [93]. Comparing to other processes, composting produces less odor and a considerable amount of heat, which brings the temperature of the pile to more than 60 ° C and helps to reduce the concentration of pathogens inside the composter [94]. Being able to supply stable pathogen free source of organic nutrients makes composting a feasible option for waste management.

Organic solid wastes, such as food waste, yard waste and sludge, are commonly treated in a composter. After the process, compost can be used as fertilizer or disposed of in landfills, which contains approximately 8.3 kilograms of nitrogen per dry ton waste and 2.0 kilograms of phosphorus per dry ton waste [95, 96]. For farmlands that are depleted through agricultural practice over multiple years, compost with a large amount of organic matter is an ideal soil amendment.

Furthermore, the two common methods to utilize the energy from the composter are self-circulating warm water for heating and converting biogas for electricity generation. The generated electricity can be used on-site or sold to the local grid as income. The energy consumption during the composting process, to some extent, diminish the advantage of composting. A study found that the composting process requires about 0.5-0.75 KWh of aeration energy per kg of chemical removed, and about 54.4 megajoules electricity are needed for digestion per dry ton of food waste [97]. In addition, the other drawback of using composts/digestates as fertilizer is that large amount of nitrogen being in the form of

ammonia/ammonium, which is prone to be released to the atmosphere after surface land application [94]. More expensive land application methods, such as shallow injection, are therefore recommended to reduce ammonia loss to air. Overall, the economic benefit to operate a composting plant with full-scale energy recovery facility is unfortunately insignificant.

4.5.1.4 Anaerobic Digestion

Anaerobic digestion is a fermentation process that breaks down organic matter in the absence of oxygen to produce biogas and a digestate. Because of its high energy recovery ability and less negative environment impact, anaerobic digestion is considered as the most cost-effective green technology among all the biological waste-to-energy treatments, which results in less energy consumption, fewer greenhouse gas emissions and few pollutants released.

The process of anaerobic digestion is composed of three phases: hydrolysis, fermentation and methanogensis. Zhang's study calculated the methane yield from different mixtures of food waste and manure based on a first-order kinetic model [98]. Two prediction models have been developed, indicating a positive linear relationship between the food waste and final methane yield in 20 - 30 days, further proved food waste can make positive contribution on methane production using an anaerobic batch digester. The content of methane can reach 60 - 70% while the content of carbon dioxide reached 30 - 40%, and a trace of other gases including hydrogen sulfide. The digestate byproduct can be used as an organic fertilizer after certain post-treatment process or as the raw material for further composting.

Comparing to other waste management methods, anaerobic digestion has several merits [91]: First, anaerobic digestion is better in treating waste with high wet content than direct

combustion and landfilling, and cooking oil is better treated in an anaerobic digestion process than through composting process. Second, the emission of CO_2 from anaerobic digestion tends to be 25 - 67% less than that from composting [99]. Because of all these advantages, the anaerobic digestion is employed as the main waste-to-energy biorefinery process in HWBRES to simulate the food waste to biogas converted electricity process.

4.5.2 Biorefinery

4.5.2.1 Biorefinery and Energy Generation

By producing multiple products, a biorefinery takes advantage of the various components in biomass and their intermediates therefore maximizing the value derived from the biomass feedstock – food waste in particular. A biorefinery could, for example, produce one or several low-volume, but high-value, chemical or nutraceutical products and a low-value, but high-volume liquid transportation fuel such as biogas, at the same time, generating electricity and process heat, through combined heat and power (CHP) technology, for its own use and perhaps enough for sale of electricity to the local utility. The power production helps to lower energy costs and reduce greenhouse gas emissions from traditional power plant facilities. Figure 4-18 presents a list of integrated biorefinery project locations by the end of 2016, while it was in pilot / demonstration / pioneer scale or under design [100].

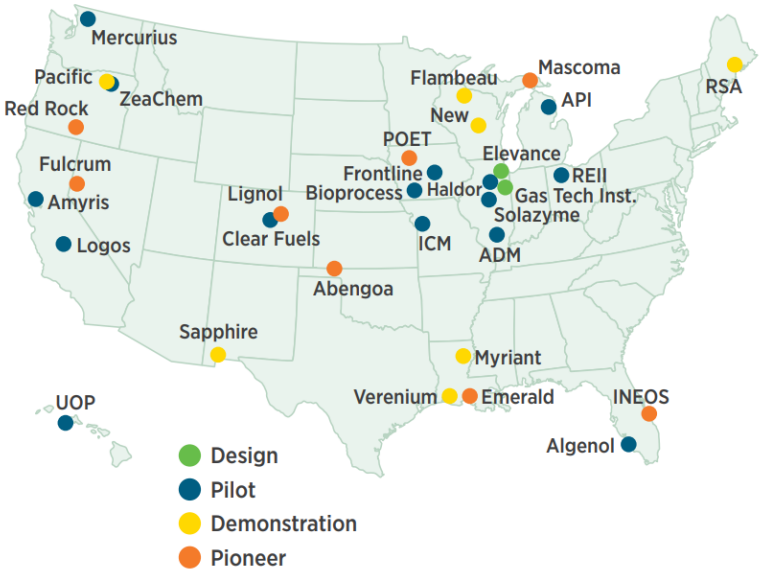

Figure 4-18 Integrated biorefinery project locations

4.5.2.2 Food Waste to Biogas Generation

Biogas is a methane rich gas produced by the degradation of organic materials. The two main sources for biogas production are organic wastes and harvested biomass. The biogas, which is roughly about half methane, and half carbon dioxide, with small contributions from other gases such as H_2S and NH_3, can be used in a number of ways. Post-digestion treatment depends upon the selected end use. With minimal post treatment, namely some drying and desulphurization, the biogas can be combusted to provide local heat or, with more extensive desulphurization, heat and power for use on-site. For use away from the generating facility, the gas must be more thoroughly treated to remove corrosives and other contaminants. The overall energy balances and economics that dictate which use will be most efficient are strongly dependent upon the complete process parameters, including feedstock production and usage.

In this study, food waste generated from household becomes the major feedstock. Since the food waste contains 70% moisture, anaerobic digestion is more preferred. Among all

biological treatments to convert waste to energy, anaerobic digestion is frequently the most cost-effective green technology due to its high energy recovery ability and less negative impact on the environment. It is a fermentation process that breaks down organic matter in the absence of oxygen to produce biogas and digestate. Based on a lifecycle analysis, anaerobic digestion results in less energy consumption, fewer greenhouse gas emissions, and fewer pollutants released. Moreover, the process also results in sterilization, as certain pathogenic bacteria present in the feedstock are eliminated [101]. By reducing existing waste, the process results in a by-product that can be used as an organic fertilizer.

The simplest use of biogas is for heat and power at the conversion site, domestic supply or collocated industry; facilities can provide municipal heat and electricity. Conversion of biogas to electricity and heat by internal combustion engines is usually accomplished at about 60% efficiency but can range from 45 - 90%. Typically, losses are less for integrated biorefinery system. The general anaerobic digestion based food waste to electricity generate process is shown in Figure 5-2, and conceptual framework is explained in [94, 101].

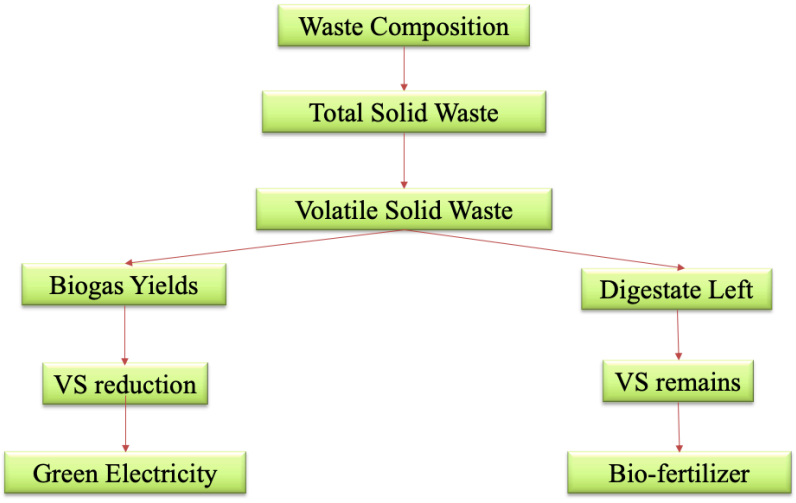

Figure 4-19 Anaerobic digestion for electricity generation from food waste

4.5.2.3 Electricity Generation by Anaerobic Digestion

The key focus of this section is to combine simple and computationally efficient anaerobic digestion model into integrated energy system (ESIWES) to estimate the green electricity generation from food waste disposal. In the process to determine the technical feasibility of biorefinery with food waste as input material, it is assumed the combined waste stream is constant across the micro-grid community.

Biogas is consumed on-site for power generation with the residual electricity sold to the grid. Gross energy generated (P_{AD}, measured in kJ/yr.) can be calculated based on the volume of methane generated ($V_{CH_{4,yr}}$) using the following equation:

$$P_{AD} = V_{CH_{4,yr}} * 35{,}846 * \theta_p \quad (32)$$

where $V_{CH_{4,yr}}$ is the volume of methane generated from combined waste in a whole year. The net heating energy of methane (35,846 KJ/m3) was obtained from an EIA report [102]. With 50 - 60% methane content in biogas, the net heating energy of biogas is approximate 23 MJ per cubic meters. The total efficiency of power generation (θ_p) - the sum of electrical and thermal efficiencies – ranges from 70% to 80% [10], in this study $\theta_p = 75\%$ with 50% methane concentration are used.

The efficiency of the internal combustion engine (θ_e) is 35% [10]. Thus, the final electricity generation (KWh) can be expressed as following:

$$E_{AD} = P_{AD} * 0.35 * (1/3{,}600) \quad (33)$$

Greenhouse gas emission from transportation to the processing facilities is neglected. For simplicity and brevity, the location of the community and power generation facilities is assumed as the same.

Anaerobic digester is a great source to treat various waste stream with different solid composition. Except partial released as heat, most of degraded energy is stored as a form as methane molecule, which is one of major advantages in energy recovery. Then the biogas can be used to drive the turbine engine to generate electricity. This way, with methane as the intermediate product, it is convenient to control the schedule and amount of electricity generation.

As mentioned previously, there are three stages during the anaerobic digestion process, including hydrolysis, fermentation and methanogensis, as shown in the chemical equation [91]. During the first stage, the degradable organic solids are broken down into monosaccharides, amino acids and fatty acids, then the product is converted into short chain fatty acids in the fermentation phase. By the activity of methanogens, methane and carbon dioxide are produced in the final stage.

$$organic\ solids \xrightarrow{hydrolysis} C_xH_yO_z \xrightarrow{fermentation} \frac{x}{2}CH_3COOH \xrightarrow{methanogensis} \frac{x}{2}CH_4 + \frac{x}{2}CO_2 \tag{34}$$

There have been decades of work in mathematical models to describe anaerobic digestion of organic waste. Due to its simplicity and compatibility with other energy models, Zhang's first-order kinetics model [98] and its synchronized equations are applied to simulate the food waste anaerobic digestion process. The total solids (TS) and volatile solids (VS) of the food waste is measured according to standard methods [103]. The TS total for food is 25%; and the volatile solids content, especially the degradable VS, is 21%, considered as the main source for methane emission from inflow feedstocks [91]. Therefore, the estimation of methane is derived from the VS consumption. The chemical composition in the current biorefinery model is the same as the one in Li's thesis. From Table 5-1 [91],

VS/TS ratio for food waste is 93%, biodegradable COD concentration is approximately 291 kg/m^3 when food waste density is chosen to be 496.57 kg/m^3.

	Food Waste		
	Value	**Reference**	**Current**
TS (%)	30.90±0.1	Zhang et al.(2007)	25
VS (%)	26.35	Zhang et al.(2007)	21
VS/TS ratio	0.853	Zhang et al.(2007)	0.93
C:N	14.8	Zhang et al.(2007)	21.53
COD (kg/m3)	238.5±3.8	Zhang et al.(2010)	291
Density (kg/m3)	496.57	Parry (2013)	496.57
Moisture content (w/w %)	50-80	Tchbanoglous (1993)	75
Biogas yields ($m^3/kg\ VS$)	0.5	Gebrezgabher (2009)	0.353-0.5
Heat Content (MJ/kg)	21-25	EIA (2005)	22.36

Table 4-9 Chemical properties of food waste

The degradation rate of the feedstock is calculated by Equation (35) and the methane yield is assumed to be proportional to the predicted VS decomposition as Equation (36). Then the volumetric methane production rate can be derived from kinetic model in Equation (39) [104]. The first two differentiation equations are solved to get VS_t. The maximum specific growth rate of microorganisms $\mu_m(day^{-1})$ is linearly dependent on temperature (T) between 20 and 60 ºC [104]. Parlom and Speeces also claim that solids retention time (SRT) or microbial generation time is inversely related to growth rate and substrate utilization rate. The kinetic parameter K_{ds} in Equation (39) is exponentially related with influent VS concentration TS (%) [91, 105].

$$\frac{dVS_t}{dt} = \frac{-k_{FW} * VS_t}{K + VS_t} \tag{35}$$

$$M_{end} = (VS_o - VS_t) * \beta_{FW} \tag{36}$$

$$\mu_m = 0.013 \cdot T - 0.129 \quad (20 < T < 60\ ℃) \tag{37}$$

$$K_{ds} = 0.8 + 0.0016 \cdot e^{0.06 \cdot TS_{total}} \tag{38}$$

$$M_V = \frac{M_{end} \cdot VS_{total}}{SRT}[1 - \frac{K_{ds}}{SRT \cdot \mu_m - 1 + K_{ds}}] \tag{39}$$

where:

t = digestion time (days)

VS_t = volatile food waste at digestion time t

K = saturation constant (kg/m^3)

k_{FW} = first order biodegradation kinetics constant for food waste

β_{FW} = substrate utilization rate for food waste

K_{ds} = kinetic paramter, dimensionless

M_{end} = ultimate methane yield (m^3)

M_V = volumetric methane production rate per day (m^3/day)

SRT = solids retention time (days)

μ_m = The maximum specific growth rate of microorganisms

The biodegradation kinetics constants for food waste remains the same as the one in Zhang's model, $k_{FW} = 0.118\ kg/m^3 \cdot day$. For anaerobic bio-refinery, β_{FW} is assumed to be in the range of 0.353 to 0.5 m^3/kg VS consumed.

There are also a few limitations that can affect the accuracy of the designed biorefinery system. First, the actual waste composition of food waste in the proposed micro-grid community is unavailable. The strict assumption about constant waste generation, production efficiency and non-transportation method could potentially cause the overestimation of the overall economic benefit. Additionally, electricity is taken as the primary energy product from the food waste-to-energy process. The heat generation and

recycling during the process, on the other side, is not specified in the current simulation process.

4.5.3 Hybrid Wind / Biorefinery / Energy-Storage Based Renewable Energy System (HWBRES)

There have been research studies about the process of bioenergy generation [94, 101, 106-113], it is mainly fed from agricultural residues, algae, woods, energy crops, MSW, vegetative and yard waste, as well as primary product includes bioproducts, renewable hydrocarbons and biogas upgraded fuels. To integrate biorefinery into the current study, the anaerobic digestion process is simulated from municipal food waste to biogas generation and then convert it into electricity.

The scheme of hybrid wind / biorefinery / energy-storage based renewable energy system (HWBRES) is presented below in Figure 4-20. Generally speaking, wind farm and biorefinery are both primary power suppliers for community-wise power usage, while energy storage plays as secondary resource to maintain power quality. Biorefinery is fed from food waste collected from the community, in turns producing and transmitting electricity back. Overall it functions as base load and works with wind farm to provide power in order to meet general demand.

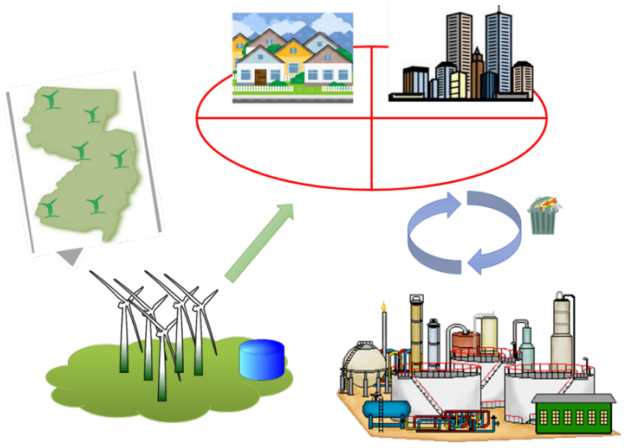

Figure 4-20 Development of wind farm in HWBRES

Under an assumption the food waste is collected from local and fed into biorefinery as raw materials. The same two-stage optimization will be applied to minimize CEPP and the optimized wind farm layout in HWBRES will be presented.

4.5.4 Optimal Development of Wind Farm in HWBRES

4.5.4.1 Investment Costs of HWBRES

In this proposed HWBRES application, the total costs will include investment costs for all three parts: wind farm, energy storage and biorefinery. The cost model for the first two parts is presented in section 4.4.3.1. The general cost for the biorefinery system is comprised of plant capital cost, operations and maintenance cost, and tipping fee saving from MSW recycle, which is shown as:

$$C_{Bio}(W) = (c_b + c_m - s_{tip}) * W \tag{40}$$

The first two segment costs relate to the combined MSW disposal in community level, where c_b is the unit capital cost ($/ton) for waste-to-energy recovery, c_m is the unit operations and maintenance cost ($/ton) for recovery, W (tons) is the total food waste collected from residential community. The last term is tipping fee saving, where in the equation (40), s_{tip} is the unit tipping fee earned ($/tons).

The information of candidate biorefinery is summarized from a variety of databases, the primary source of data comes from EPA's database. Population and land area are captured based in New Jersey, and the data is collected from US Census Bureau's FactFinder. Generally speaking, the bio waste-to-energy recovery technology is more capital intensive then traditional non-renewable electricity generation technology, in this analysis Wang's economic analysis model [91] is used to compute the total cost of biorefinery process.

The first cost term, total annual capital cost, is calculated as the product of average capital cost per ton and the amount of combined waste disposed in the recovery system. Based on the micro-grid community with residential buildings, it is assumed the biorefinery's capacity is sufficient and the unit capital cost $c_b = \$50$/ton [114].

The second cost term, fixed operations and maintenance cost, includes labor salary, equipment maintenance and materials, overhead, tax, etc. Using the traditional definition, transportation makes up one of the important cost factors; fuel consumption and transportation distance are considered key inputs in determining overall operations cost. Due to lack of real cost parameters, transportation cost will be combined as a component of operations and maintenance cost. According to EIA's annual report [114], operations and maintenance cost of full scale biorefinery ranges from \$60 - 100/ton, here in equation (40), $c_m = \$80$ is used.

The tipping fee is the charge levied on waste disposal to offset the cost of landfill site maintenance, nowadays the shortage of landfill space is contributing to the escalation in tipping fee. For waste-to-energy recovery plants, tipping fee is one of their primary income sources, especially when energy sales revenue is not overly high [91]. In the current study, tipping fee is considered as cost savings, because the waste-to-energy recovery process recycles MSW at the same time, which brings off waste disposal site usage. Under this assumption, the total tipping fee saving is positively related to the amount of total waste collected from the community. Based on data collected in New Jersey (Dec 2019), $s_{tip} = \$97.85$/ton.

Extend from equation (25), the total energy system cost is modeled as:

$$C(N, W) = C_{WF}(N) + C_{ES|S_d} + C_{Bio}(W) \tag{41}$$

4.5.4.2 Expected Annual Energy Production

The expected annual energy production in HWBRES includes three parts: expected wind farm energy production and energy storage power function, which were introduced in 4.4.3.2, as well as annual biorefinery energy production E_{Bio}.

In this application, anaerobic digestion is used as a waste recovery method under proposed biorefinery, Zhang's first kinetics model [98] is applied to predict methane yield based on the micro-grid community's food waste inputs. Specifically, in equations (35) - (36): biodegradation kinetics constant $k_{FW} = 0.118$, saturation constant $K = 0.63, \text{VS}$ concentration in food waste $VS_0 = 21\%$, SRT=30, utilization rate β_{FW} is in the range of 0.353 to 0.5, and efficiency of methane to electricity generation β_e is 35%.

Extended from equation (30), the updated expected annual energy production equation in HWBRES is:

$$E_{(u_0,\theta_0,W)}=E_{WF|(u_0,\theta_0)} + E_{ES|S_d} + E_{Bio}(W) \tag{42}$$

Where $E_{Bio}(W) = \sum_{d=1}^{365} E_{bio,d}(W_d) = \sum_{d=1}^{365} \mathrm{M}_{\mathrm{end},\,d}(W_d) * \beta_e$.

4.5.4.3 Objective Function

Similar to the one in ESIWES, objective function for minimizing CEPP in HWBRES model can be shown as:

$$\mathrm{argmin}_{(\mathrm{N,X})}\ \mathrm{CEPP} = \frac{\text{Annual Total Cost}}{\text{Expected Power Production}} = \frac{\mathrm{C\ (N, W)}}{\mathrm{E}_{(u_0,\theta_0,\mathrm{W})}} \tag{43}$$

$$= \frac{\mathrm{N}\left(\frac{2}{3} + \frac{1}{3}\mathrm{e}^{-0.00174\mathrm{N}^2}\right) + S_d * \mathrm{c_{ES}} + (\mathrm{c_b} + \mathrm{c_m} - \mathrm{s_{tip}}) * \mathrm{W}}{\sum_{\mathrm{d}=1}^{365}[\sum_{\mathrm{i}=1}^{\mathrm{N}} \int_1^{360} \mathrm{f}_\Theta \int_3^{27} \mathrm{E}_{\mathrm{i,d}|(u_0,\theta_0)} \mathrm{f_U}(\mathrm{u_0})\mathrm{du_0}\,\mathrm{d}\theta_0 + S_d + \mathrm{M}_{\mathrm{end},\,\mathrm{d}}(W_d) * \beta_\mathrm{e}]}$$

Subject to:

$$\mathrm{E}_{\mathrm{WF,d}|(u_0,\theta_0)} + \mathrm{E}_{\mathrm{bio,d}} + \mathrm{S_d} \geq \mathrm{Demand_d}$$

$$\mathrm{u_0} \geq \mathrm{u_i}$$

$$\left\|\mathrm{X_i} - \mathrm{X_j}\right\| \geq 200, \forall\, \mathrm{i} \neq \mathrm{j} \in \{1,2 \ldots \mathrm{N}\}$$

Where $S_d = \min\left(Cap_{ES}, \max\left(0, \text{Demand}_{\text{d}} - \text{E}_{\text{WF,d}|(\text{u}_0,\theta_0)} - \text{E}_{\text{Bio}}\right)\right)$.

4.5.5 Computational Study Results

Extended based on the ESIWES model, the cost and energy function of biorefinery have been added into HWBRES' optimization model, as indicated in equation (43), to evaluate the economic benefit of the waste-to-energy recovery process. Generally, the cost of electricity generation from food waste in the biorefinery can be impacted by various factors such as bio-generator investment and maintenance cost, feedstock quality and quantity, technology and location, etc. Concentrating on the renewable energy system and optimization model development, total investment costs are simplified as a combination of initial capital cost of waste-to-energy recovery process and operations and maintenance cost minus tipping fee revenue. Furthermore, all cost and benefits are scaled on an one-year basis, without considering account inflation and money value across the plant's life span. The unit cost and sale price are drawn from actual markets and prior studies [91].

Table 4-10(a) shows the total cost and overall electricity recovered from residentials' food waste in the micro-grid community. Based on the data from EPA, total annual food waste collected from community containing 10 residential buildings is about 4.32 tons. This amount of waste is transferred and inputted into the biorefinery for energy recovery, resulting in capital and operations and maintenance related costs $56.16 and electricity generation 2,414 kW per year. On the other side with tipping fee $97.85/ton in selected counties, the total tipping saving of $42.27 offsets major portion of prementioned cost, reducing the overall investment cost to $13.89/ton. Although in reality, the development of energy recovery system in particular area also relies on regulatory environment, market specification and its waste steam, the trade-off between costs and benefits in proposed

waste-to-energy recovery model indicates that the biorefinery is a great option for localized communities who are seeking sustainable source for green electricity supply.

	Capital, O&M costs ($/ton)	Tipping saving ($/ton)	Total investment cost ($/ton)	power generation (kW year)
WTE recovery	130	97.85	32.15	2,414

(a) Economic benefit of biorefinery

	GA based Two-stage Optimization	
	Stage 1 Genetic algorithm	Stage 2 Positive basis pattern search
Number of turbines	100	100
Expected power (kW year)	171,213	173,610
CEPP (k$/kW year)	0.494	**0.487**

(b) Optimization results

Table 4-10 Computational results in HWBRES

With biorefinery and energy storage serving as baseline suppliers for electricity consumption, the GA-based two stage optimization algorithm is implemented to locate the best wind farm layout scenario for the objective of minimizing CEPP. According to the layout in Figure 4-22, during the GA-based first stage, turbines are spread quite uniformly among the wind farm except in couple central zones. The scatter around those spots were likely due to the aggravated wake interaction among turbines caused by frequent wind direction (162° - 267° as shown in Figure 4-10). During the second stage, turbines are allowed to continuously move around, in this case the line-up of turbines scatters to alleviate the wake interactions, by doing so power generation is maximally improved.

The optimization results are listed in Table 4-10(b). Comparing to the results from ESIWES in Table 4-8, with the support of energy recovered from biorefinery, the total number of turbines proposed decreased from 105 to 100. By the end of stage two, even with 5 turbines less the expected total power production is fairly maintained, at the same

time, the objective value CEPP is improved from ESIWES' 0.493 to 0.487. It proves adding a biorefinery to the renewable energy system provides better support to the micro-grid community with less unit cost per production.

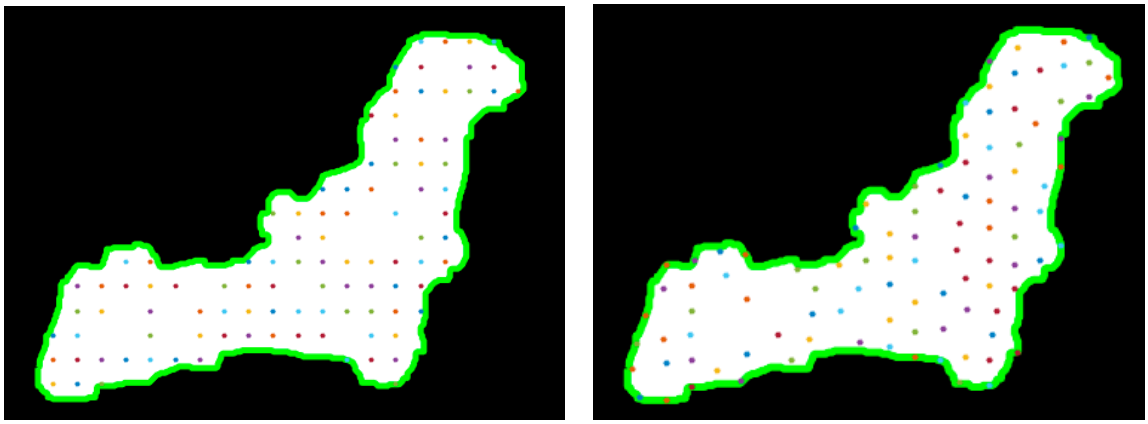

(a) Layout from GA-based first stage (b) Layout from PSO-based second stage

Figure 4-21 Two-stage optimal layouts for wind farm in HWBRES

In the current technology, the development of biorefinery is rapidly expanding in the states, which consists the sustainable exploitation of biomass and transfers them into a wide range of value-added products, bio-energy is only one of them. Taking advantages of its additional capacity and high efficiency in use of energy and materials, it is wise to extend single stream biorefinery into multi-product processes, to synthesize intermediates (carbohydrates, proteins) into platform bio-chemicals such as Polylactic Acid or ethanol, at the same time maintain bio-energy production. As a part of revenue to alleviate the cost of biorefinery investment, these bio-chemicals are ready to be commercialized and the digestate to be sold as fertilizer, both productions are expected to increase substantially in the coming years with an expanding market share. On the other side, due to its large capacity, significant capital investment and utility expense, a biorefinery is commonly suggested to work with high volume of raw inputs, therefore based on the MSW collection, the energy support it provides can easily go beyond city level. With the stimulation from

the increasing production of organic wastes and reduced landfill capacity, the future research can scale up the development of wind farm and integrated it into HWBRES for city-wise energy generation.

Chapter 5 ADVANCED OPERATION SCHEDULING AND MAINTENANCE POLICY IN WIND FARM

With the development of wind energy generation system, wind farm monitor and system control technology have also been advanced. The old traditional manual-inspection-based management stays in the past, many current wind farms establish the control center, real-time monitoring turbine operation and status through sensor, and developing plan to dispatch manual inspection when necessary.

Nowadays, the well-operating turbines are not always on. There are several reasons for turning off operating turbines, such as curtailment, maintenance, power requirement, complain from nearby neighborhoods (very rare), etc. The curtailment happens when excess energy exists in the power system, wind speed at the turbines is not strong enough, or a much larger swath of wake effect due to wind direction change that causes speed disruption and rotor harm by turbulence. In such cases, the control room sends out the signal to turbine sensors and turn offs the turbine in the short-term. Additionally, when a fault or degradation related to the major components is detected, or there is an on-going maintenance scheduled, the system is shutting down for further inspection. The shutting down due to maintenance is much more common than the others.

5.1 Advanced Scheduling and Maintenance Policy for HWBRES

Inspired by current technology behind the wind farm control center, scheduling models are further explored to evaluate wind farm performance and advanced maintenance policy on daily turbine operation. There have been some researches in the area of wind farm production and maintenance scheduling, as reviewed in section 2.7. The optimal maintenance policy and optimal wind farm development plan are inter-dependent. Therefore, to optimize the maintenance schedule in this particular HWBRES energy

system, first, the wind farm has to be optimized at its most productive layout, and at the same time, satisfy the electricity demand of the local residential-based micro-grid community. The optimization in section 4.5 suggests the layout design of a wind farm with 100 turbines, for the purpose of assignment maintenance schedules each turbine is labeled with a numeric index, as shown in Figure 5.1.

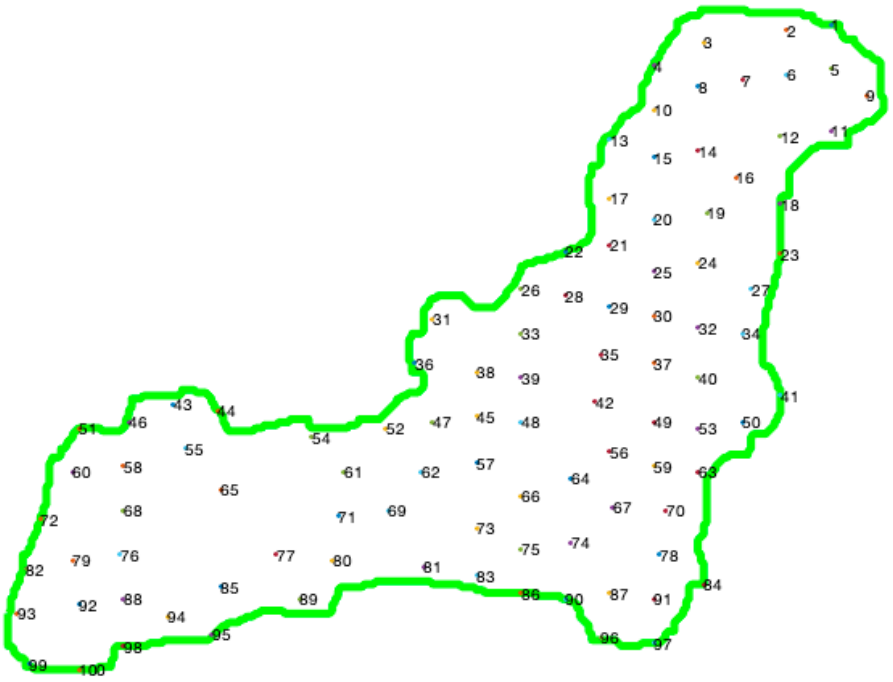

Figure 5-1 Wind turbine placement with labels

Next with enough power to meet the average daily demand, an advanced ON/OFF operation schedule is designed to save energy from excess production while maintaining the reliability of each turbine. Two simplified maintenance policies are considered in this case: age-based preventive maintenance and opportunistic maintenance. It is decided the wind farm is under inspection and maintenance periodically. Meanwhile under an advanced operation schedule, if there are enough switched-off turbines, a same day opportunistic maintenance is assigned by control center, and crews will be dispatched to

perform inspection and maintenance to those down turbines that have not been recently inspected.

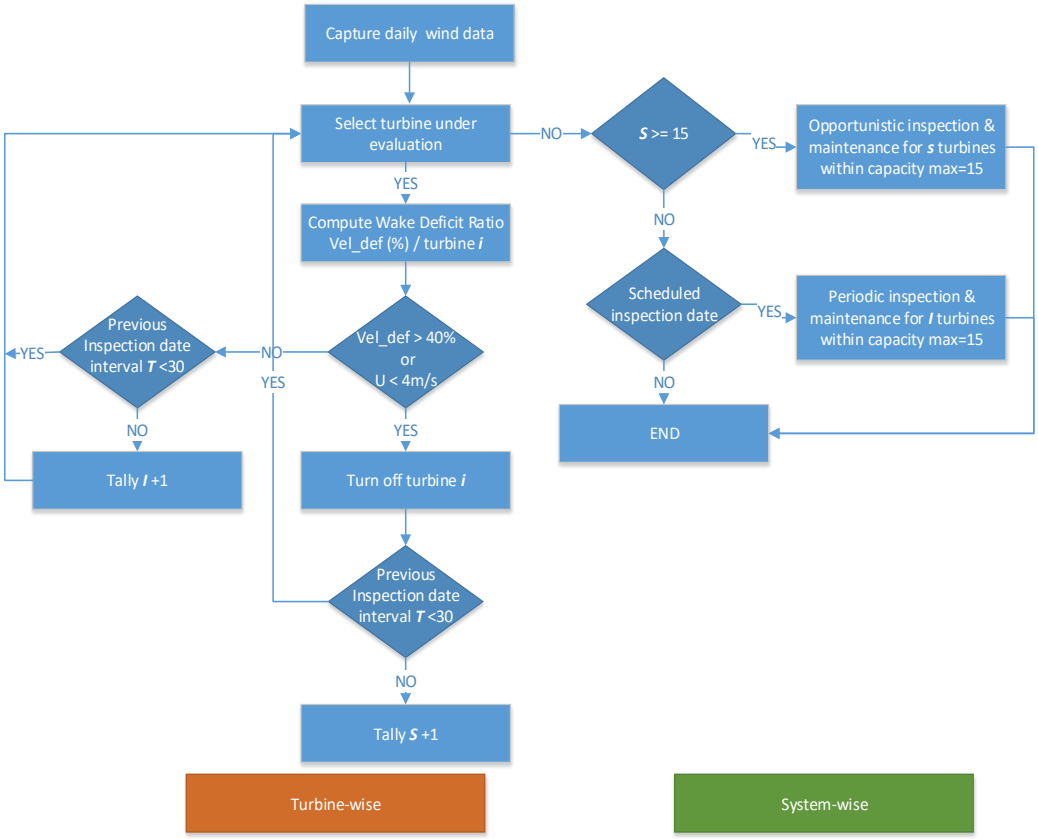

Figure 5-2 Operation and maintenance scheduling

Figure 5-2 represents the flow chart for proposed operations and maintenance scheduling. Given wind speed and directional data, information such as the wake effect and captured speed (thus energy generation) at every single turbine is evaluated. It is designated to be switched off if the wake deficit ratio at the turbine point is greater than 40% (comparing to original wind speed), or speed captured is less than 4 m/s. The periodic maintenance cycle for a single turbine is defined as 36 days, with 10 turbines maintained during each scheduled day. There is a 15-turbine daily maintenance capacity per crew team. If more than 15 turbines are switched off on particular non-periodic maintenance day, a same-day inspection will be scheduled to the ones that have not been inspected in 30 days.

With the possibility of more than 15 down turbines in the candidate pool, the top 15 turbines will be selected based on distances and captured wind speed (lowest). If there are less than 15 down turbines during a particular day but the farm is scheduled to perform periodic maintenance, the inspection and maintenance will be proceeded to the assigned turbines as scheduled, as well as the down turbines that have not been inspected in 30 days, within daily capacity.

The completed periodic maintenance schedules for the wind farm is addressed in Appendix 7.1. As previous mentioned, the maintenance cycle is defined as 36 days with 10 turbines scheduled during each inspection day. Additionally, based on wind speed and direction conditions, there are 35 days having turbine switched off due to significant wake effect, as shown in Table 5-1, 15 of which are non-periodic days with more than 15 down turbines, thus the opportunity maintenance is scheduled. With all decision criteria taken into consideration, the updated maintenance schedules are analyzed with daily capacity 15 turbines, the complete list is addressed in Appendix 7.2.

Days	4	**18**	**85**	**86**	**88**	91	**98**	**106**	110
Total TB Off	15	15	15	15	15	1	15	15	3
Days	**120**	121	**128**	**131**	139	148	151	156	**167**
Total TB Off	15	8	15	15	10	15	13	3	15
Days	181	190	206	214	222	228	**229**	**247**	252
Total TB Off	15	15	5	9	15	3	15	15	6
Days	270	**273**	278	**287**	291	**306**	330	331	
Total TB Off	10	15	2	15	4	15	1	4	

Table 5-1 Wind farm opportunistic maintenance dates

5.2 Updated Levelized Costs Model to Minimize Levelized Cost per Expected Power Production (LCEPP)

Based on advanced scheduling and maintenance policy mentioned in section 5.1, a new optimization model will be developed including wind farm maintenance management costs to minimize Levelized Cost per Expected Power Production (LCEPP). Generally speaking, all individual parts in LCEPP are considered based upon daily operation, summing up through the year to get annual objective values. The updated optimization model is shown below in equation (44).

$$\operatorname{argmin}_{(\mathrm{N_d},\mathrm{X})}\ \mathrm{LCEPP} = \frac{\text{Annual Total Cost}}{\text{Expected Power Production}} = \frac{\sum_{\mathrm{d}=1}^{365} \mathrm{C}\ (\mathrm{N_d}, \mathrm{W})}{\sum_{\mathrm{d}=1}^{365} \mathrm{E}_{(\mathrm{N_d},\mathrm{u_0},\theta_0,\mathrm{W})}} \tag{44}$$

$$= \frac{\sum_{d=1}^{365}[\frac{N_d}{365}\left(\frac{2}{3}+\frac{1}{3}e^{-0.00174{N_d}^2}\right) + S_d\, c_{ES} + c_{wm}(100-N_d)] + (c_b + c_m - s_{tip})W}{\sum_{d=1}^{365}[\sum_{i=1}^{N_d}\int_1^{360} f_\Theta \int_3^{27} E_{i,d|(u_0,\theta_0)} f_U(u_0)du_0\, d\theta_0 + S_d + \mathrm{M_{end,\,d}} * \beta_e]}$$

Subject to:

$$\mathrm{E_{WF,d|(u_0,\theta_0)}} + \mathrm{E_{bio,d}} + \mathrm{S_d} \ \geq\ \mathrm{Demand_d}$$

$$100 \geq N_d \geq 85$$

$$u_0 \geq u_i$$

$$\left\|X_i - X_j\right\| \geq 200, \forall\ i \neq j \in \{1,2 \ldots N\}$$

Where $S_d = \min\left(Cap_{ES}, \max\left(0, Demand_d - E_{WF,d|(u_0,\theta_0)} - \mathrm{E_{Bio}}\right)\right)$.

The wind farm maintenance cost $c_{wm} = \$1{,}037$ per turbine [74]. In regards to the wind farm cost, the main difference between the newly developed LCOE model and previous cost model is the use of variable N_d - the number of turbine in operation at given day *d*, instead of a general variable – total number of turbines *N*. Due to wind uncertainty, N_d varies by day and ranges from 100 to 85 with 15 turbines maintained maximally.

On the other side, the expected energy production shifts on daily basis as well. It is not only because of wind fluctuantions, but also from the switched-off turbines under newly

developed operations schedule. The bottom line is, the daily power production shall always satisfy the demand of the community. With energy storage and biorefinery provided baseline power support, the occasion of turbine switching off should not have significant impact on the overall power generation.

Wind Farm		Storage & Bio	Total		
Invest. Cost (k$)	**Maint. Cost (k$)**	**Supply Cost (k$)**	**LCOE (k$)**	**EPP (kW year)**	**LCEPP (k$/kW year)**
64.711	1,110.60	85,447.59	86,622.90	173,593	0.499

Table 5-2 Updated objective values

Based on the advanced scheduling and maintenance policy developed in section 5.1, a wind farm maintenance cost model can be developed. Formulated into LCEPP, objective model is updated according to equation (44), and the results are exhibited above in Table 5-2. Comparing to the original HWBRES wind farm cost model with 100 turbines in section 4.5, the updated investment cost reduces slightly from $66,667 to $64,711 due to occasional turbine switch-offs. At the meantime, the expected power production (EPP) is maintained well, only 17 kW less than the production with no down turbines. The annual maintenance cost is $1,110,600 for 115 days, with slightly elevated energy storage cost due to extra power support. The levelized HWBRES system cost LCEPP reaches $499 per kW year, which is approximately 5.7 cents per kWh after breaking down. This price is significantly lower than the current national average electricity price - 15.72 cents per kWh. Combined with other factors such as clean and renewable energy sources, grid stabilization, waste reduction, self-sustainable, one can draw the conclusion that based on the current economy, it is more advantageous to implement proposed integrated renewable energy system than purchasing from the grid as the energy support to small community.

Chapter 6 CONCLUSIONS

In conclusion, this research presents stochastic models and optimization methods for optimal development of wind farms in various applications. A new two-stage optimization framework is developed to optimize wind farm layout, and at the same time, satisfy the cost per expected energy production. In the first stage of optimization, a wind farm is predefined with a number of candidate locations. A binary variable is associated with each location to determine whether a turbine is installed at given point. The first stage of global search optimization process finds the optimal number of turbines needed and their corresponding locations. In the second stage of optimization, binary solutions from previous stage are converted into continuous decision variables before being introduced in a local search algorithm to further improve the turbine placement. By opting out of the assumption such as predefined turbine total or locations as did in previous literature, it thoroughly evaluates possible scenarios until the best layout design is located. As a general framework, this model can be implemented on logistic, transportation and facility planning-based combinatorial problems, where a large number of decision variables included. In addition, the heuristic algorithm is developed and applied in the first stage of the proposed optimization framework. It simplifies the searching process by branching out using current existing objective information at each iteration; this way it bypasses the complex function evaluations in solving combinatorial problems.

Secondly, stochastic wind speed and direction are considered in this study. With real data captured in the U.S., wind uncertainty is modeled by probabilistic models: lognormal distributions for wind direction and Weibull distributions for wind speed. Based on speed variation, day-parting scenarios are introduced to divide each day into subgroups before

fitting into distributions. By implementing ‘real data’ based wind model, it reflects the real time pattern shifts by scenarios, which is more practical in evaluating the intermittency of wind energy generation.

Third, the optimization model is highly application related. In this research, the wind farm project broadly covers five major topics. Specifically, regular shaped wind farm design can be placed where flat plain or ranch is used for site. Arbitrarily shaped wind farm design is suitable for more realistic cases, such as located on the ridgeline of mountain, or surrounded by existed structure and restriction zones. The offshore wind farm layout development considers ocean / shoreline conditions into wind farm model, at the same time, adding cable cost into investment cost model. This innovated research helps planning the site selection for the wind farm, assessing the viability of arbitrary-shaped offshore wind farm layout design and demonstrating the advantages in offshore wind energy generation.

The fourth application is the hybrid wind / energy storage renewable energy system in the micro-grid community. By the backup of Lithium-ion battery-based energy storage, the wind farm is designed as primary electricity supplier to meet the demand of residential building-based community, in such a way that the CEPP is minimized. The optimal design of wind farm layout in ESIWES is illustrated to maintain 100% service level and satisfy the fluctuated demand. In addition to using energy storage as a secondary energy support to the local community, the fifth application expands the renewable energy system HWBRES to include biorefinery – the waste-to-energy recovery pipeline. This work is inspired by the increase of public awareness towards environmental sustainability. With biorefineries, the HWBRES system is developed to generate more sustainable energy, and at the same time, tackle environmental risk problems caused by waste. By adding

biorefinery to convert local food waste to energy as the baseline electricity support to the community, the results from HWBRES indicate alleviated unit cost per production with less turbine installations.

Last but not the least, a computational tool for advanced scheduling and maintenance policy is developed on top of the HWBRES system, in which the turbine operation scheduling and periodic inspection are both taken into consideration to save energy from excess production while maintaining the reliability of each turbine. In addition, opportunistic maintenance is scheduled occasionally for the cluster of switched-off turbines, by implementing this model it ensures the reliable energy production with limited maintenance costs.

In the future research, it is of great interest to expand the HWBRES system to support larger populations. Generally, because of its capacity and significant capital investment, biorefinery is suggested to work with heavy volume of raw materials, thus the energy support it provides can easily go beyond city level. With the stimulation from the increasing production of organic wastes and reduced landfill capacity, the future research can scale up the size of biorefinery as well as wind farm, and integrated it into HWBRES for city-wise energy generation.

Chapter 7 APPENDIX

7.1 Periodic Inspection and Maintenance Dates of Turbines

Turbine number	Periodic Inspection and Maintenance days									
1	1	37	73	109	145	181	217	253	289	325
2	1	37	73	109	145	181	217	253	289	325
3	1	37	73	109	145	181	217	253	289	325
4	1	37	73	109	145	181	217	253	289	325
5	1	37	73	109	145	181	217	253	289	325
6	1	37	73	109	145	181	217	253	289	325
7	1	37	73	109	145	181	217	253	289	325
8	1	37	73	109	145	181	217	253	289	325
9	1	37	73	109	145	181	217	253	289	325
10	1	37	73	109	145	181	217	253	289	325
11	2	38	74	110	146	182	218	254	290	326
12	2	38	74	110	146	182	218	254	290	326
13	2	38	74	110	146	182	218	254	290	326
14	2	38	74	110	146	182	218	254	290	326
15	2	38	74	110	146	182	218	254	290	326
16	2	38	74	110	146	182	218	254	290	326
17	2	38	74	110	146	182	218	254	290	326
18	2	38	74	110	146	182	218	254	290	326
19	2	38	74	110	146	182	218	254	290	326
20	2	38	74	110	146	182	218	254	290	326
21	3	39	75	111	147	183	219	255	291	327
22	3	39	75	111	147	183	219	255	291	327
23	3	39	75	111	147	183	219	255	291	327
24	3	39	75	111	147	183	219	255	291	327
25	3	39	75	111	147	183	219	255	291	327
26	3	39	75	111	147	183	219	255	291	327
27	3	39	75	111	147	183	219	255	291	327
28	3	39	75	111	147	183	219	255	291	327
29	3	39	75	111	147	183	219	255	291	327
30	3	39	75	111	147	183	219	255	291	327
31	4	40	76	112	148	184	220	256	292	328
32	4	40	76	112	148	184	220	256	292	328
33	4	40	76	112	148	184	220	256	292	328
34	4	40	76	112	148	184	220	256	292	328
35	4	40	76	112	148	184	220	256	292	328
36	4	40	76	112	148	184	220	256	292	328

37	4	40	76	112	148	184	220	256	292	328
38	4	40	76	112	148	184	220	256	292	328
39	4	40	76	112	148	184	220	256	292	328
40	4	40	76	112	148	184	220	256	292	328
41	5	41	77	113	149	185	221	257	293	329
42	5	41	77	113	149	185	221	257	293	329
43	5	41	77	113	149	185	221	257	293	329
44	5	41	77	113	149	185	221	257	293	329
45	5	41	77	113	149	185	221	257	293	329
46	5	41	77	113	149	185	221	257	293	329
47	5	41	77	113	149	185	221	257	293	329
48	5	41	77	113	149	185	221	257	293	329
49	5	41	77	113	149	185	221	257	293	329
50	5	41	77	113	149	185	221	257	293	329
51	6	42	78	114	150	186	222	258	294	330
52	6	42	78	114	150	186	222	258	294	330
53	6	42	78	114	150	186	222	258	294	330
54	6	42	78	114	150	186	222	258	294	330
55	6	42	78	114	150	186	222	258	294	330
56	6	42	78	114	150	186	222	258	294	330
57	6	42	78	114	150	186	222	258	294	330
58	6	42	78	114	150	186	222	258	294	330
59	6	42	78	114	150	186	222	258	294	330
60	6	42	78	114	150	186	222	258	294	330
61	7	43	79	115	151	187	223	259	295	331
62	7	43	79	115	151	187	223	259	295	331
63	7	43	79	115	151	187	223	259	295	331
64	7	43	79	115	151	187	223	259	295	331
65	7	43	79	115	151	187	223	259	295	331
66	7	43	79	115	151	187	223	259	295	331
67	7	43	79	115	151	187	223	259	295	331
68	7	43	79	115	151	187	223	259	295	331
69	7	43	79	115	151	187	223	259	295	331
70	7	43	79	115	151	187	223	259	295	331
71	8	44	80	116	152	188	224	260	296	332
72	8	44	80	116	152	188	224	260	296	332
73	8	44	80	116	152	188	224	260	296	332
74	8	44	80	116	152	188	224	260	296	332
75	8	44	80	116	152	188	224	260	296	332
76	8	44	80	116	152	188	224	260	296	332
77	8	44	80	116	152	188	224	260	296	332

78	8	44	80	116	152	188	224	260	296	332
79	8	44	80	116	152	188	224	260	296	332
80	8	44	80	116	152	188	224	260	296	332
81	9	45	81	117	153	189	225	261	297	333
82	9	45	81	117	153	189	225	261	297	333
83	9	45	81	117	153	189	225	261	297	333
84	9	45	81	117	153	189	225	261	297	333
85	9	45	81	117	153	189	225	261	297	333
86	9	45	81	117	153	189	225	261	297	333
87	9	45	81	117	153	189	225	261	297	333
88	9	45	81	117	153	189	225	261	297	333
89	9	45	81	117	153	189	225	261	297	333
90	9	45	81	117	153	189	225	261	297	333
91	10	46	82	118	154	190	226	262	298	334
92	10	46	82	118	154	190	226	262	298	334
93	10	46	82	118	154	190	226	262	298	334
94	10	46	82	118	154	190	226	262	298	334
95	10	46	82	118	154	190	226	262	298	334
96	10	46	82	118	154	190	226	262	298	334
97	10	46	82	118	154	190	226	262	298	334
98	10	46	82	118	154	190	226	262	298	334
99	10	46	82	118	154	190	226	262	298	334
100	10	46	82	118	154	190	226	262	298	334

7.2 Advanced Inspection and Maintenance Scheduled of Turbines

Turbine number	Inspection and maintenance days									
1	1	37	73	109	145	181	217	253	287	325
2	1	37	73	106	145	181	217	253	289	325
3	1	37	73	109	145	181	217	253	289	325
4	1	37	73	109	145	181	217	253	289	325
5	1	37	73	106	145	181	217	253	289	325
6	1	37	73	106	145	181	217	253	289	325
7	1	37	73	109	145	181	217	253	289	325
8	1	37	73	109	145	181	217	253	287	325
9	1	37	73	109	145	181	217	253	289	325
10	1	37	73	106	145	181	217	253	289	325
11	2	38	74	106	146	182	218	254	287	326
12	2	38	74	110	146	182	218	254	290	326
13	2	38	74	110	146	182	218	254	290	326
14	2	38	74	110	146	182	218	254	290	326
15	2	38	74	106	146	182	218	254	290	326
16	2	38	74	110	146	182	218	254	290	326
17	2	38	74	106	146	182	218	254	290	326
18	2	38	74	106	146	182	218	254	287	326
19	2	38	74	110	146	181	218	254	290	326
20	2	38	74	110	146	182	218	254	290	326
21	3	39	75	106	147	183	219	255	291	327
22	3	39	75	106	147	183	219	255	287	327
23	3	39	75	106	147	183	219	255	291	327
24	3	39	75	106	147	181	219	255	291	327
25	3	39	75	106	147	183	219	255	291	327
26	3	39	75	106	147	183	219	255	287	327
27	3	39	75	106	147	183	219	255	287	327
28	3	39	75	111	147	183	219	255	287	327
29	3	39	75	111	147	183	219	255	287	327

30	3	39	75	111	147	183	219	255	287	327
31	4	40	76	112	148	184	220	256	287	328
32	4	40	76	112	148	184	220	256	287	328
33	4	40	76	112	148	184	220	256	287	328
34	4	40	76	112	148	181	220	256	287	328
35	4	40	76	112	148	184	220	256	287	328
36	4	40	76	112	148	184	220	256	292	328
37	4	40	76	112	148	184	220	256	292	328
38	4	40	76	112	148	184	220	256	292	328
39	4	40	76	112	148	184	220	256	292	328
40	4	40	76	112	148	184	220	256	292	328
41	5	41	77	113	149	185	221	257	293	329
42	5	41	77	113	149	185	221	257	293	329
43	5	41	77	113	149	185	221	257	293	329
44	5	41	77	113	149	185	221	257	293	329
45	4	41	77	113	148	185	221	257	293	329
46	5	41	77	113	149	185	221	257	293	329
47	5	41	77	113	149	181	221	257	291	329
48	5	41	77	113	149	185	221	257	293	329
49	5	41	77	113	149	185	221	257	293	329
50	5	41	77	113	149	185	221	257	293	329
51	6	42	78	114	150	186	222	258	294	330
52	6	42	78	114	150	181	222	258	294	330
53	6	42	78	114	150	186	222	258	294	330
54	6	42	78	114	148	186	222	258	294	330
55	6	42	78	114	150	186	222	258	294	330
56	6	42	78	114	150	186	222	258	294	330
57	6	42	78	114	150	186	222	258	294	330
58	6	42	78	114	150	186	222	258	294	330
59	6	42	78	114	150	186	222	258	294	330
60	4	42	78	114	150	186	222	258	291	330
61	7	43	79	115	151	187	223	259	295	331

62	7	43	79	115	151	187	223	259	295	331
63	7	43	79	115	148	187	223	259	295	331
64	7	43	79	110	151	187	223	259	295	331
65	7	43	79	115	151	187	223	259	295	331
66	4	43	79	115	151	187	223	259	295	331
67	7	43	79	115	148	187	223	259	291	331
68	4	43	79	115	151	187	222	259	295	331
69	7	43	79	115	151	187	223	259	295	331
70	4	43	79	115	151	187	223	259	295	331
71	8	44	80	116	152	188	224	260	296	332
72	8	44	80	116	152	188	224	260	296	332
73	8	44	80	116	152	188	224	260	296	332
74	8	44	80	116	152	188	224	260	296	332
75	8	44	80	116	152	188	224	260	296	332
76	8	44	80	116	152	188	222	260	296	332
77	8	44	80	116	152	188	224	260	296	332
78	8	44	80	116	152	188	224	260	296	332
79	8	44	80	116	152	188	224	260	296	332
80	8	44	80	116	152	188	222	260	296	332
81	9	45	81	117	148	189	225	261	297	333
82	9	45	81	117	153	189	222	261	297	331
83	9	45	81	117	153	189	225	261	297	333
84	9	45	81	117	153	189	225	261	297	333
85	9	45	81	117	153	189	222	261	297	333
86	9	45	81	117	153	189	225	261	297	333
87	9	45	81	117	153	189	225	261	297	333
88	9	45	81	117	153	189	225	261	297	333
89	9	45	81	117	153	189	225	261	297	333
90	9	45	81	117	151	189	225	261	297	333
91	10	46	82	118	154	190	226	262	298	334
92	10	46	82	118	154	190	226	262	298	334
93	10	46	82	118	154	190	226	262	298	334

94	10	46	82	118	154	190	226	262	298	334
95	10	46	82	118	154	190	226	262	298	334
96	10	46	82	118	154	190	226	262	298	334
97	10	46	82	118	154	190	226	262	298	334
98	10	46	82	118	154	190	226	262	298	334
99	10	46	82	118	154	190	226	262	298	334
100	10	46	82	118	154	190	226	262	298	334

Chapter 8 BIBLIOGRAPHY

[1] "Renewable 2016 - Global Status Report," Renewable Energy Policy Network, 2016.

[2] Fossil fuel energy consumption [Online] Available: http://data.worldbank.org/indicator/EG.USE.COMM.FO.ZS

[3] Benefits of Renewable Energy Use [Online] Available: http://www.ucsusa.org/clean-energy/renewable-energy/public-benefits-of-renewable-power

[4] "New Record in Worldwide Wind Installations," World Wind Energy Association, 2015.

[5] "Annual Wind Industry Report, Year Ending 2013," American Wind Energy Association, 2014.

[6] "Renewable Energy Technologies - Wind Power," International Renewable Energy Agency, 2012.

[7] S. P. Breton and G. Moe, "Status, plans and technologies for offshore wind turbines in Europe and North America," *Renewable Energy,* vol. 34, no. 3, pp. 646-654, 2009.

[8] "A Framework for Offshore Wind Energy Development in the United States," Massachusetts Technology Collaborative, US Department of Energy, GE, 2005.

[9] "Technology White Paper On Wind Energy Potential On The U.S.. United States," Department of Interior, 2006.

[10] G. Mosetti, C. Poloni, and B. Diviacco, "Optimization of wind turbine positioning in large windfarms by means of a genetic algorithm," *Journal of Wind Engineering and Industrial Aerodynamics,* Article vol. 51, no. 1, pp. 105-116, 1994.

[11] S. A. Grady, M. Y. Hussaini, and M. M. Abdullah, "Placement of wind turbines using genetic algorithms," *Renewable Energy,* Article vol. 30, no. 2, pp. 259-270, 2005.

[12] O. Aytun, U. and B. A. Norman, "Heuristic methods for wind energy conversion system positioning," *Electric Power Systems Research,* Article vol. 70, no. 3, pp. 179-185, 2004.

[13] X. Chen and R. Agarwal, "Optimal placement of horizontal - and vertical - axis wind turbines in a wind farm for maximum power generation using a genetic algorithm," *International Journal of Energy & Environment,* Article vol. 3, no. 6, pp. 927-938, 2012.

[14] Y. Chen, H. Li, K. Jin, and Q. Song, "Wind farm layout optimization using genetic algorithm with different hub height wind turbines," *Energy Conversion and Management,* vol. 70, pp. 56-65, 2013.

[15] T. G. do Couto, B. Farias, A. C. G. Diniz, and M. V. G. de Morais, "Optimization of Wind Farm Layout Using Genetic Algorithm," in *10th World Congress on Structural and Multidisciplinary Optimization*, 2013.

[16] A. Emami and P. Noghreh, "New approach on optimization in placement of wind turbines within wind farm by genetic algorithms," *Renewable Energy,* Article vol. 35, no. 7, pp. 1559-1564, 2010.

[17] C. M. Ituarte-Villarreal and J. F. Espiritu, "Optimization of wind turbine placement using a viral based optimization algorithm," in *Procedia Computer Science*, 2011, vol. 6, pp. 469-474.

[18] A. Kusiak and Z. Song, "Design of wind farm layout for maximum wind energy capture," *Renewable Energy,* vol. 35, no. 3, pp. 685-694, 2010.

[19] X. Li, J. Wang, and X. Zhang, "Equilateral-triangle mesh for optimal micrositing of wind farms," in *14th WSEAS international conference on computers*, 2010, pp. 187-95.

[20] G. Marmidis, S. Lazarou, and E. Pyrgioti, "Optimal placement of wind turbines in a wind park using Monte Carlo simulation," *Renewable Energy,* Article vol. 33, no. 7, pp. 1455-1460, 2008.

[21] A. Mittal, "Optimization of the layout of large wind farms using a genetic algorithm," Case Western Reserve University, 2010.

[22] C. Wan, J. Wang, G. Yang, X. Li, and X. Zhang, "Optimal micro-siting of wind turbines by genetic algorithms based on improved wind and turbine models," in *Proceedings of the IEEE Conference on Decision and Control*, 2009, pp. 5092-5096.

[23] C. Wan, J. Wang, G. Yang, and X. Zhang, "Optimal siting of wind turbines using real-coded genetic algorithms," in *Proceedings of European wind energy association conference and exhibition*, 2009.

[24] C. Wan, J. Wang, G. Yang, H. J. Gu, and X. Zhang, "Wind farm micro-siting by Gaussian particle swarm optimization with local search strategy," *Renewable Energy,* vol. 48, pp. 276-286, 2012.

[25] T. Ishihara, A. Yamaguchi, and Y. Fujino, "Development of a new wake model based on a wind tunnel experiment," *Global Wind Power,* 2004.

[26] S. Frandsen, "On the wind speed reduction in the center of large clusters of wind turbines," *Journal of Wind Engineering and Industrial Aerodynamics,* Article vol. 39, no. 1-3, pp. 251-265, 1992.

[27] J. S. González, J. R. Santos, M. B. Payan, A. G. Gonzalez Rodriguez, and J. C. Mora, "Optimization of wind farm turbines layout using an evolutive algorithm," *Renewable Energy,* Article vol. 35, no. 8, pp. 1671-1681, 2010.

[28] M. Abbes and J. Belhadj, "Wind resource estimation and wind park design in El-Kef region, Tunisia," *Energy,* Article vol. 40, no. 1, pp. 348-357, 2012.

[29] N. J. Choi, S. Hyun Nam, J. Hyun Jeong, and K. Chun Kim, "Numerical study on the horizontal axis turbines arrangement in a wind farm: Effect of separation distance on the turbine aerodynamic power output," *Journal of Wind Engineering and Industrial Aerodynamics,* Article vol. 117, pp. 11-17, 2013.

[30] A. Crespo, J. Hernandez, and S. Frandsen, "Survey of modelling methods for wind turbine wakes and wind farms," *Wind Energy,* vol. 2, no. 1, pp. 1-24, 1999.

[31] A. Makridis and J. Chick, "Validation of a CFD model of wind turbine wakes with terrain effects," *Journal of Wind Engineering and Industrial Aerodynamics,* Article vol. 123, pp. 12-29, 2013.

[32] M. Rezaei Mirghaed and R. Roshandel, "Site specific optimization of wind turbines energy cost: Iterative approach," *Energy Conversion and Management,* Article vol. 73, pp. 167-175, 2013.

[33] B. Sanderse, S. Pijl, and B. Koren, "Review of computational fluid dynamics for wind turbine wake aerodynamics," *Wind Energy,* vol. 14, no. 7, pp. 799-819, 2011.
[34] M. X. Song, K. Chen, Z. Y. He, and X. Zhang, "Bionic optimization for micro-siting of wind farm on complex terrain," *Renewable Energy,* Article vol. 50, pp. 551-557, 2013.
[35] M. X. Song, K. Chen, Z. Y. He, and X. Zhang, "Optimization of wind farm micro-siting for complex terrain using greedy algorithm," *Energy,* Article vol. 67, pp. 454-459, 2014.
[36] N. O. Jensen, "A note on wind generator interaction," 1983.
[37] B. Pérez, R. Mínguez, and R. Guanche, "Offshore wind farm layout optimization using mathematical programming techniques," *Renewable Energy,* vol. 53, pp. 389-399, 2013.
[38] Y.-K. Wu, C.-Y. Lee, C.-R. Chen, K.-W. Hsu, and T. Huang-Tien, "Optimization of the Wind Turbine Layout and transimission system planning for a large-scale offshore wind farm by AI technology," *IEEE Transactions On Industry Applications,* vol. 50, no. 3, pp. 2071-2080, 2014.
[39] P. Hou, W. Hu, M. Soltani, and Z. Chen, "Optimized Placement of Wind Turbines in Large-Scale Offshore Wind Farm Using Particle Swarm Optimization Algorithm," *IEEE Transactions On Sustainable Energy,* vol. 6, no. 4, pp. 1272-1282, 2015.
[40] S. F. Rodrigues, R. Teixeira Pinto, M. Soleimanzadeh, P. A. N. Bosman, and P. Bauer, "Wake losses optimization of offshore wind farms with moveable floating wind turbines," *Energy Conversion and Management,* vol. 89, pp. 933-941, 2015.
[41] X. Gao, H. Yang, L. Lin, and P. Koo, "Wind turbine layout optimization using multi-population genetic algorithm and a case study in Hong Kong offshore," *Journal of Wind Engineering and Industrial Aerodynamics,* vol. 139, pp. 89-99, 2015.
[42] L. Amaral and R. Castro, "Offshore wind farm layout optimization regarding wake effects and electrical losses," *Engineering Applications of Artificial Intelligence,* vol. 60, pp. 26-34, 2017.
[43] P. Fuglsang and K. Thomsen, *Cost optimization of wind turbines for large-scale offshore wind farms*. 1998.
[44] J. Serrano González, M. Burgos Payán, and J. M. Riquelme Santos, "An improved evolutive algorithm for large offshore wind farm optimum turbines layout," in *2011 IEEE Trondheim PowerTech*, 2011, pp. 1-6.
[45] P. D. Hopewell, F. Castro, and D. I. Bailey, "Optimising the Design of Offshore Wind Farm Collection Networks," in *Proceedings of the 41st International Universities Power Engineering Conference*, 2006, vol. 1, pp. 84-88.
[46] M. A. Lackner and C. N. Elkinton, "An analytical framework for offshore wind farm layout optimization," *Wind Engineering,* Article vol. 31, no. 1, pp. 17-31, 2007.
[47] M. Nandigam and S. K. Dhali, "Optimal design of an offshore wind farm layout," in *2008 International Symposium on Power Electronics, Electrical Drives, Automation and Motion*, 2008, pp. 1470-1474.

[48] Q. Li and H. Wang, "Two-stage simulation optimization for optimal development of offshore wind farm under wind uncertainty," in *2016 Winter Simulation Conference (WSC)*, 2016, pp. 2891-2902.

[49] S. Salcedo-Sanz, D. Gallo-Marazuela, A. Pastor-Sánchez, L. Carro-Calvo, A. Portilla-Figueras, and L. Prieto, "Evolutionary computation approaches for real offshore wind farm layout: A case study in northern Europe," *Expert Systems with Applications,* vol. 40, no. 16, pp. 6292-6297, 2013.

[50] G. Van Bussel and M. Zaaijer, *Reliability, availability and maintenance aspects of large-scale offshore wind farms, a concepts study*. Institute of marine engineers, 2003.

[51] F. Liu and Z. Wang, "Offshore Wind Farm Layout Optimization Using Adapted Genetic Algorithm: A different perspective," *arXiv preprint arXiv:1403.7178,* 2014.

[52] S. Chowdhury, J. Zhang, A. Messac, and L. Castillo, "Optimizing the arrangement and the selection of turbines for wind farms subject to varying wind conditions," *Renewable Energy,* vol. 52, pp. 273-282, 2013.

[53] M. Beaudin, H. Zareipour, A. Schellenberglabe, and W. Rosehart, "Energy storage for mitigating the variability of renewable electricity sources: An updated review," *Energy for Sustainable Development,* vol. 14, no. 4, pp. 302-314, 2010.

[54] C. Abbey and G. Joos, "Supercapacitor Energy Storage for Wind Energy Applications," *IEEE Transactions on Industry Applications,* vol. 43, no. 3, pp. 769-776, 2007.

[55] S. Aissou, D. Rekioua, N. Mezzai, T. Rekioua, and S. Bacha, "Modeling and control of hybrid photovoltaic wind power system with battery storage," *Energy Conversion and Management,* vol. 89, pp. 615-625, 2015.

[56] N. Bigdeli, "Optimal management of hybrid PV/fuel cell/battery power system: A comparison of optimal hybrid approaches," *Renewable and Sustainable Energy Reviews,* vol. 42, pp. 377-393, Modeling and control of hybrid photovoltaic wind po 2015.

[57] F. Díaz-González, A. Sumper, O. Gomis-Bellmunt, and R. Villafáfila-Robles, "A review of energy storage technologies for wind power applications," *Renewable and Sustainable Energy Reviews,* vol. 16, no. 4, pp. 2154-2171, 2012.

[58] A. Evans, V. Strezov, and T. J. Evans, "Assessment of utility energy storage options for increased renewable energy penetration," *Renewable and Sustainable Energy Reviews,* vol. 16, no. 6, pp. 4141-4147, 2012.

[59] M. Fazeli, G. M. Asher, C. Klumpner, L. Yao, and M. Bazargan, "Novel Integration of Wind Generator-Energy Storage Systems Within Microgrids," *IEEE Transactions on Smart Grid,* vol. 3, no. 2, pp. 728-737, 2012.

[60] N. S. Hasan, M. Y. Hassan, M. S. Majid, and H. A. Rahman, "Review of storage schemes for wind energy systems," *Renewable and Sustainable Energy Reviews,* vol. 21, pp. 237-247, 2013.

[61] S. Koohi-Kamali, V. V. Tyagi, N. A. Rahim, N. L. Panwar, and H. Mokhlis, "Emergence of energy storage technologies as the solution for reliable operation of smart power systems: A review," *Renewable and Sustainable Energy Reviews,* vol. 25, pp. 135-165, 2013.

[62] T. Kousksou, P. Bruel, A. Jamil, T. El Rhafiki, and Y. Zeraouli, "Energy storage: Applications and challenges," *Solar Energy Materials and Solar Cells,* vol. 120, Part A, pp. 59-80, 2014.

[63] Y. Levron, J. M. Guerrero, and Y. Beck, "Optimal Power Flow in Microgrids With Energy Storage," *IEEE Transactions on Power Systems,* vol. 28, no. 3, pp. 3226-3234, 2013.

[64] A. Rabiee, H. Khorramdel, and J. Aghaei, "A review of energy storage systems in microgrids with wind turbines," *Renewable and Sustainable Energy Reviews,* vol. 18, pp. 316-326, 2013.

[65] S. Sundararagavan and E. Baker, "Evaluating energy storage technologies for wind power integration," *Solar Energy,* vol. 86, no. 9, pp. 2707-2717, 2012.

[66] X. Xiao, H. Yi, Q. Kang, and J. Nie, "A Two-level Energy Storage System for Wind Energy Systems," *Procedia Environmental Sciences,* vol. 12, pp. 130-136, 2012.

[67] P. Mathema, "Optimization Of Integrated Renewable Energy System - Micro Grid," Bachelor of Engineering in Electrical Engineering, Tribhuvan University, 2011.

[68] T. Shinji, "Operation of dispersed power systems including wind farm in micro grid," in *2009 CIGRE/IEEE PES Joint Symposium Integration of Wide-Scale Renewable Resources Into the Power Delivery System*, 2009, pp. 1-6.

[69] J. Zhang, M. Ma, J. Zhan, and Y. Zhao, "Research on Renewable Energy Power Based Microgrid Technology," in *2012 Asia-Pacific Power and Energy Engineering Conference*, 2012, pp. 1-4.

[70] Z. Zhang, J. Wang, and X. Wang, "An improved charging/discharging strategy of lithium batteries considering depreciation cost in day-ahead microgrid scheduling," *Energy Conversion and Management,* vol. 105, pp. 675-684, 2015.

[71] H. Borhanazad, S. Mekhilef, V. Gounder Ganapathy, M. Modiri-Delshad, and A. Mirtaheri, "Optimization of micro-grid system using MOPSO," *Renewable Energy,* vol. 71, pp. 295-306, 2014.

[72] A. Niinisto, "Simulation of the Management of a Micro Grid with Wind, Solar and Gas Generators," Master of Science in Engineering, Aalto University School Of Science And Technology, 2009.

[73] N. Carlisle, J. Elling, and T. R. Penney, *A Renewable Energy Community: Key Elements: a Reinvented Community to Meet Untapped Customer Needs for Shelter and Transportation with Minimal Environmental Impacts, Stable Energy Costs, and a Sense of Belonging*. National Renewable Energy Laboratory, 2008.

[74] S. Song, Q. Li, F. A. Felder, H. Wang, and D. W. Coit, "Integrated optimization of offshore wind farm layout design and turbine opportunistic condition-based maintenance," *Computers & Industrial Engineering,* vol. 120, pp. 288-297, 2018.

[75] Z. Jiang, X. Han, Z. Li, W. Li, M. Wang, and M. Wang, "Two-Stage Multi-Objective Collaborative Scheduling for Wind Farm and Battery Switch Station," *Energies,* vol. 9, no. 11, p. 886, 2016.

[76] Z. Zhang, A. Kusiak, and Z. Song, "Scheduling electric power production at a wind farm," *European Journal of Operational Research,* vol. 224, no. 1, pp. 227-238, 2013.

[77] Z. Tian, T. Jin, B. Wu, and F. Ding, "Condition based maintenance optimization for wind power generation systems under continuous monitoring," *Renewable Energy,* vol. 36, no. 5, pp. 1502-1509, 2011.

[78] Y. Sinha and J. Steel, "A progressive study into offshore wind farm maintenance optimisation using risk based failure analysis," *Renewable and Sustainable Energy Reviews,* vol. 42, pp. 735-742, 2015.

[79] A. Kovács, G. Erdős, Z. J. Viharos, and L. Monostori, "A system for the detailed scheduling of wind farm maintenance," *CIRP Annals - Manufacturing Technology,* vol. 60, no. 1, pp. 497-501, 2011.

[80] X. Lei and P. A. Sandborn, "Maintenance scheduling based on remaining useful life predictions for wind farms managed using power purchase agreements," *Renewable Energy,* vol. 116, no. PB, p. 188, 2018.

[81] H. Seyr and M. Muskulus, "Decision Support Models for Operations and Maintenance for Offshore Wind Farms: A Review," *Applied Sciences,* vol. 9, no. 2, 2019.

[82] F. Besnard, M. Patriksson, A.-B. Strömberg, A. Wojciechowski, and L. Bertling, "An optimization framework for opportunistic maintenance of offshore wind power system," in *PowerTech, 2009 IEEE Bucharest*, 2009: IEEE, pp. 1-7.

[83] E. S. Asensio, J. P. Pérez, and F. G. Márquez, "Economic Viability Study for Offshore Wind Turbines Maintenance Management," in *Proceedings of the Ninth International Conference on Management Science and Engineering Management*, 2015: Springer, pp. 235-244.

[84] J. Nilsson and L. Bertling, "Maintenance management of wind power systems using condition monitoring systems—life cycle cost analysis for two case studies," *Energy Conversion, IEEE Transactions on,* vol. 22, no. 1, pp. 223-229, 2007.

[85] C. Mone, A. Smith, B. Maples, and M. Hand, ""2013 Cost of Wind Energy Review"," National Renewable Energy Laboratory, 2014.

[86] R. Carnegie, D. Gotham, D. Nderitu, and P. V. Preckel, "Utility Scale Energy Storage Systems, Benefits, Application, and Technologies," Purdue University, 2013.

[87] D. Raslter, A. Akhil, D. Gauntlett, and E. Cutter, "Energy Storage System Costs 2011 Update Executive Summary," *EPRI,* 2012.

[88] P. G. E. (PG&E). Energy Uses and Prices [Online] Available: https://www.pge.com/tariffs/energy_use_prices.shtml

[89] K. D. Hall, J. Guo, M. Dore, and C. C. Chow, "The progressive increase of food waste in America and its environmental impact," *PLoS One,* vol. 4, no. 11, p. e7940, 2009.

[90] A. Bosmans, I. Vanderreydt, D. Geysen, and L. Helsen, "The crucial role of Waste-to-Energy technologies in enhanced landfill mining: a technology review," *Journal of Cleaner Production,* Article vol. 55, pp. 10-23, 2013.

[91] S. Wang, "Modeling and analysis of utilizing food waste and manure in New Jersey," Rutgers University, 2014.

[92] N. S. Bolan *et al.*, "Landfills as a biorefinery to produce biomass and capture biogas," *Bioresource technology,* 2012.

[93] J. Berger, L. V. Fornés, C. Ott, J. Jager, B. Wawra, and U. Zanke, "Methane oxidation in a landfill cover with capillary barrier," *Waste management,* vol. 25, no. 4, pp. 369-373, 2005.
[94] G. Hochman, S. Wang, Q. Li, P. D. Gottlieb, F. Xu, and Y. Li, "Cost of organic waste technologies: A case study for New Jersey," *AIMS Energy,* vol. 3, no. 3, pp. 450-462, 2015.
[95] G. Finnveden, J. Johansson, P. Lind, and Å. Moberg, "Life cycle assessment of energy from solid waste—part 1: general methodology and results," *Journal of Cleaner Production,* vol. 13, no. 3, pp. 213-229, 2005.
[96] G. Finnveden, Å. Moberg, J. Johansson, and P. Lind, "Life cycle assessment of energy from solid waste—part 2: landfilling compared to other treatment methods," *Journal of Cleaner Production,* vol. 13, no. 3, pp. 231-240, 2005.
[97] A. v. Haandel and G. Lettinga, *Anaerobic sewage treatment: a practical guide for regions with a hot climate*. John Wiley & Sons, 1994.
[98] R. Zhang and H. M. El-Mashad, "Biogas production from co-digestion of dairy manure and food waste," *Bioresource technology,* vol. 101, no. 11, pp. 4021-4028, 2010.
[99] J. Mata-Alvarez, S. Mace, and P. Llabres, "Anaerobic digestion of organic solid wastes. An overview of research achievements and perspectives," *Bioresource technology,* vol. 74, no. 1, pp. 3-16, 2000.
[100] "Integrated Biorefineries: Reducing Investment Risk in Novel Technology," in "Energy Efficiency & Renewable Energy," 2014.
[101] S. Wang, Q. Li, P. Gotlieb, H. Gal, F. Xu, and Y. Li, "A sustainable waste to energy path: The benefits from organice waste and manure in New Jersey," in *Proceedings of Dairy Environmental Systems and Climate Adaptation Conference and Tours*, Cornell University, 2015.
[102] EIA, "State Profile and Energy Estimates, New Jersey," www.eia.gov/state/data.cfm?sid=NJ, 2010.
[103] A. Awwa, "Standard methods for the examination of water and wastewater," *Washington, DC Standard Methods for the Examination of Water and Wastewater,* vol. 20, 1998.
[104] A. G. Hashimoto, Y. R. Chen, and V. H. Varel, "Theoretical aspect of anaerobic fermentation: State-of-Art," *Livestock Wastes: A Renewable Resource,* pp. pp.86-91, 1981.
[105] A. G. Hashimoto, "Conversion of straw–manure mixtures to methane at mesophilic and thermophilic temperatures," *Biotechnology and Bioengineering,* vol. 25, no. 1, pp. 185-200, 1983.
[106] C. Taylor and H. Youngs, "Biogas-Potential for Deployment inTransportaion," University of California, Berkley, Energy Biosciences Institute, 2009.
[107] T. Scheper, *Biofuels* (Advances in Biochemical Engineering/Biotechnology). Springer, 2007.
[108] D. K. S. Ng, "Automated targeting for the synthesis of an integrated biorefinery," *Chemical Engineering Journal,* no. 162, pp. 67-74, 2010.
[109] R. Ulber and D. Sell, *White biotechnology*. Springer, 2007.

[110] A. M. MARGINEAN, V. TRIFA, and C. MARGINEAN, "Simulation of Fermentation Bioreactor Control for Ethanol Production," *Development and Application Systems,* p. 3.
[111] Z. K. Nagy, "Model based control of a yeast fermentation bioreactor using optimally designed artificial neural networks," *Chemical Engineering Journal,* vol. 127, pp. 95-109, 2007.
[112] T. De Mes, A. Stams, J. Reith, and G. Zeeman, "Methane production by anaerobic digestion of wastewater and solid wastes," in *Environmental Science*, 2003, pp. 58-102.
[113] C. Valkenburg, M. Gerber, C. Walton, S. Jones, B. Thompson, and D. Stevens, "Municipal Solid Waste (MSW) to liquid fuels synthesis," 2008.
[114] EIA, "Annual energy outlook 2010," 2010.